APPLICATIONS OF LEVEL SET AND FAST MARCHING METHODS IN RESERVOIR CHARACTERIZATION

A Dissertation

by

JIANG XIE

Submitted to the Office of Graduate Studies of
Texas A&M University
in partial fulfillment of the requirements for the degree of

DOCTOR OF PHILOSOPHY

August 2012

Major Subject: Petroleum Engineering

Applications of Level Set and Fast Marching Methods in Reservoir Characterization

APPLICATIONS OF LEVEL SET AND FAST MARCHING METHODS IN RESERVOIR CHARACTERIZATION

A Dissertation

by

JIANG XIE

Submitted to the Office of Graduate Studies of
Texas A&M University
in partial fulfillment of the requirements for the degree of

DOCTOR OF PHILOSOPHY

Approved by:

Co-Chairs of Committee,	Akhil Datta-Gupta
	Yalchin R. Efendiev
Committee Members,	Michael J. King
	Ding Zhu
Head of Department,	A. Daniel Hill

August 2012

Major Subject: Petroleum Engineering

ABSTRACT

Applications of Level Set and Fast Marching Methods in Reservoir Characterization.

(August 2012)

Jiang Xie, B.S., University of Science and Technology of China, Hefei, China;

M.S., Texas A&M University

Co-Chairs of Advisory Committee, Dr. Akhil Datta-Gupta

Dr. Yalchin R. Efendiev

Reservoir characterization is one of the most important problems in petroleum engineering. It involves forward reservoir modeling that predicts the fluid behavior in the reservoir and inverse problem that calibrates created reservoir models with given data. In this dissertation, we focus on two problems in the field of reservoir characterization: depth of investigation in heterogeneous reservoirs, and history matching and uncertainty quantification of channelized reservoirs.

The concept of depth of investigation is fundamental to well test analysis. Much of the current well test analysis relies on analytical solutions based on homogeneous or layered reservoirs. However, such analytic solutions are severely limited for heterogeneous and fractured reservoirs, particularly for unconventional reservoirs with multistage hydraulic fractures. We first generalize the concept to heterogeneous reservoirs and provide an efficient tool to calculate drainage volume using fast marching methods and estimate pressure depletion based on geometric pressure approximation. The applicability of

proposed method is illustrated using two applications in unconventional reservoirs including flow regime visualization and stimulated reservoir volume estimation.

Due to high permeability contrast and non-Gaussianity of channelized permeability field, it is difficult to history match and quantify uncertainty of channelized reservoirs using traditional approaches. We treat facies boundaries as level set functions and solve the moving boundary problem (history matching) with the level set equation. In addition to level set methods, we also exploit the problem using pixel based approach. The reversible jump Markov Chain Monte Carlo approach is utilized to search the parameter space with flexible dimensions. Both proposed approaches are demonstrated with two and three dimensional examples.

DEDICATION

To my parents

ACKNOWLEDGEMENTS

This dissertation would not have been possible without the guidance and the help of several individuals who in one way or another contributed and extended their valuable assistance in the preparation and completion of this study.

First and foremost, I would express my utmost gratitude to my advisor, Dr. Datta-Gupta, whose sincerity and encouragement I will never forget. Dr. Datta-Gupta has been my inspiration as I hurdle all the obstacles in the completion of this research work.

I am heartily thankful to another advisor of mine, Dr. Efendiev, whose guidance and support from the initial to the final level enable me to develop an understanding of the subject.

I am grateful to Dr. King for his inspiring ideas, encouragement and support through the upscaling course, meetings and individual discussions. His remarkable knowledge and vision make the research challenging and his personality makes life enjoyable.

I would like to thank my committee member, Dr. Zhu for her valuable comments and suggestions that shaped this dissertation.

I would like to show my gratitude to Chevron Energy Technology Company for the internship opportunities. Special thanks to my mentors and supervisor, Xian-Huan Wen, Pallav Sarma, Zhiming Wang and Wen Chen. Also, thanks to alumni of MCERI, Xianlin Ma.

I would like to thank my colleagues of MCERI and friends in TAMU. The list of names is too long for here, but I will always remember you guys and enjoyable life together in College Station.

NOMENCLATURE

A_0	=	Zero order pressure amplitude in Fourier domain
$A(r)$	=	Surface area, ft^2
C_E	=	EPA compaction factor, psi^{-1}
C_F	=	Fracture compaction factor, psi^{-1}
C_M	=	Matrix compaction factor, psi^{-1}
c_t	=	Total compressibility, psi^{-1}
d_{obs}	=	Observation data
$g(\cdot)$	=	Reservoir simulation model
k	=	Permeability, mD
k_E	=	EPA permeability, mD
k_F	=	Fracture permeability, mD
k_M	=	Matrix permeability, mD
P	=	Pressure, psi
$\tilde{P}$	=	Pressure in Fourier domain
$\bar{P}$	=	Average pressure inside drainage volume, psi
$P(\cdot)$	=	Probability distribution function
ΔP	=	Pressure drop, psi
$\Delta P'$	=	Pressure derivative, psi/day
Q	=	Darcy flux, bbl/day

Q_w	=	Well rate, bbl/day
$q(\cdot \mid \cdot)$	=	Transitional probability
r	=	Radius, ft
t	=	Time, day
$v(\mathbf{x})$	=	Velocity function in level set equation
V_p	=	Pore volume
X_{F1}	=	Fracture 1 half long axis
X_{F2}	=	Fracture 2 half long axis
X_{F3}	=	Fracture 3 half long axis
X_{F4}	=	Fracture 4 half long axis
$\mathbf{x}$	=	Space, ft
$\alpha(\mathbf{x})$	=	Hydraulic diffusivity
μ	=	Viscosity, cp^{-1}
$\pi(\cdot)$	=	Posterior distribution function
$\rho(\cdot,\cdot)$	=	Probability to accept a proposal
$\tau(\mathbf{x})$	=	Diffusive time of flight
$\phi(\mathbf{x})$	=	Porosity, %
ϕ	=	Level set function
ϕ_0	=	Initial facies function
ϕ^u	=	Updated level set function
ω	=	Frequency in Fourier domain

TABLE OF CONTENTS

Page

Page

Page

LIST OF FIGURES

Page

Page

Page

Page

Page

LIST OF TABLES

Page

CHAPTER I
INTRODUCTION AND STUDY OBJECTIVES

1.1 Introduction

In this dissertation, we focus on two problems in petroleum reservoir characterization: depth of investigation and drainage volume calculation in unconventional wells, history matching and uncertainty quantification of channelized reservoirs. After that, we will discuss the well-known numerical techniques in mathematics – the level set and fast marching methods and explore the way to solve petroleum reservoir problems using the numerical techniques.

1.1.1 Depth of Investigation

Unconventional resources are playing an increasingly important role in energy supply worldwide, especially in the United States. To estimate reservoir properties and optimize hydraulic fracture design in unconventional reservoirs, well test analysis (pressure transient and rate transient analysis) is widely used (Gringarten 1984, 2010; Ehlig-Economides 1992). The concept of radius of investigation (Lee 1982; Raghavan 1993) is fundamental to well test analysis and is routinely used to design well tests and to understand the reservoir volume investigated. The radius of investigation can also be useful in identifying new well locations (Kang et al. 2011) and planning, designing and

---

This dissertation follows the style of *SPE Journal*.

optimizing hydraulic fractures in unconventional reservoirs (Sehbi et al. 2011). It has additional implications in estimating reserves and understanding stimulated reservoir volumes. There are many definitions of radius of investigation in the literature and Kuchuk (2009) summarized them recently. Although these definitions vary in detail, they all relate to the propagation of a pressure disturbance or impose thresholds on detectable pressure or rate changes. In this work we will focus on the definition proposed by Lee (1982). Lee defines the radius of investigation as the propagation distance of the 'peak' pressure disturbance for an impulse source or sink. For simplified flow geometries and homogeneous reservoir conditions, the radius of investigation can be calculated analytically. However, such analytic solutions are severely limited for heterogeneous and fractured reservoirs, particularly for unconventional reservoirs with multistage hydraulic fractures. Thus, the purpose of this work is to generalize the concept of radius of investigation to depth of investigation to account for reservoir heterogeneity and efficiently estimate drainage volume and pressure depletion behavior.

1.1.2 History Matching of Channelized Reservoirs

Subsurface is complex geological formation encompassing a wide range of physical and chemical heterogeneities. The goal of stochastic models is to characterize its different attributes such as permeability, porosity, fluid saturation etc. Flow in the subsurface is primarily controlled by the connectivity of the extreme permeability (high and low) which is generally associated with geological patterns that create preferential flow paths/barriers.

In many geologic environments, the distribution of subsurface properties is closely associated with the location and distribution of distinct geologic facies with sharp contrasts in properties across facies boundaries (Weber 1982). For example in a fluvial setting, high permeability channel sands are often embedded in a nearly impermeable background causing the dominant fluid movement to be restricted within these channels. Under such conditions, the orientation of the channels and channel geometry determine the flow behavior in the subsurface rather than the detailed variations in properties within the channels. Traditional geostatistical techniques for subsurface characterization have typically relied on variograms that are unable to reproduce the channel geometry and the facies architecture (Haldorsen and Damsleth 1990; Koltermann and Gorelick 1996; Dubrule 1998). Discrete Boolean or object-based models can reproduce geologically realistic shapes and have been successfully used to model fluid flow and transport in many fluvial type environments (Egeland et al. 1993). The success of these object-based models, however, is heavily dependent on the parameters to specify the object size, shapes, proportion and orientation. Typically, these parameters are highly uncertain, particularly in the early stages of subsurface characterization (Dubrule 1998; Caumon et al. 2004). For example, in a channel type environment, the channel sands may be observed at only a few well locations. There are many plausible channel geometries that will satisfy the channel sand and well intersections. Thus, the stochastic models for channels will require specification of random variables that govern the channel principal direction, its horizontal and vertical sinuosity, channel width to thickness ratio etc. All these parameters have considerable uncertainty associated with

them and will profoundly impact fluid flow in the subsurface.

A considerable amount of prior information is typically available for building the facies models for fluid flow simulation (Weber 1982). These include well logs and cores, seismic data and geologic conceptualization based on outcrops and analogues. Although the prior information play a vital role in reducing uncertainty and preserving geologic realism, it is imperative that the geologic models reproduce the dynamic response based on the flow and transport data. These include pressure measurements at the wells, tracer concentration histories and in the case of multiphase flow, the production of individual phases at the wells. The reproduction of dynamic data is a necessary step to have credibility in our geologic and flow modeling and confidence in any performance forecasting.

The representation and history matching of channelized reservoirs are challenging because of the difficulties to reproduce the large-scale continuity of the channel structure and identify the channel geometry and its orientation. The traditional two-point geostatistical techniques for reservoir characterization are unable to reproduce the channel geometry and the facies architecture (Haldorsen and Damsleth 1990; Koltermann and Gorelick 1996; Dubrule 1998). As an alternative, object-based modeling (Deutsch and Wang 1996) and more recently, multi-point geostatistical methods (Caers and Zhang 2004; Strebelle and Journel 2001) have been used to represent the channel structure for dynamic data history matching. The object-based

modeling is dependent on the parameters to specify the object size, shape, and orientation. The method is usually limited to simple channel geometry and it can be difficult to condition the generated objects to dynamic production data and well observations. The multi-point geostatistical methods use training images to generate geologic realizations conditioned to the well observations. However, the success of the multi-point geostatistical methods depends on the appropriate selection of the training image.

1.2 Level Set and Fast Marching Methods

Level Set and Fast Marching Methods are two fundamental numerical techniques that can track the evolution of interfaces (Sethian and Vladimirsky 2000). They have been applied to many disciplines, such as computational geometry, medical imaging, optimization, computational fluid dynamics, and seismic analysis. These two techniques are different, but complementary to each other.

Fast Marching Method is an extremely efficient method introduced by Sethian (1999) to solve Eikonal equation, **Eq. (1.2),** while Level Set Method (Osher and Sethian 1988; Osher and Fedkiw 2002) solves a more general equation called level set equation, **Eq. (1.1)**. The following are two equations with their initial conditions.

$$\frac{\partial \phi(\mathbf{x}, t)}{\partial t} + v(\mathbf{x}) \cdot \nabla \phi(\mathbf{x}, t) = 0 \tag{1.1}$$

Initial condition: $u(\mathbf{x}, t = 0) = f(\mathbf{x})$

$$F(\mathbf{x})|\nabla T(\mathbf{x})| = 1 \tag{1.2}$$

Initial condition: $T|_{f(\mathbf{x})=0} = 0$

In level set equation, $\phi(\mathbf{x}, t)$ denotes the level set function, $v(\mathbf{x})$ is velocity vector. The level set equation can be obtained by taking derivative of $\phi(\mathbf{x}, t)$ with respect to time and adding definition $v(\mathbf{x}) = \mathrm{d}\mathbf{x}/\mathrm{d}t$.

In Eikonal equation, $T(\mathbf{x})$ is the arrival time of the front propagation ($\phi(\mathbf{x}, t = T) = 0$) and $F(\mathbf{x})$ is velocity scalar and can be defined as

$$F(\mathbf{x}) = v(\mathbf{x}) \cdot n = v(\mathbf{x}) \cdot \nabla\phi(\mathbf{x}, t)/|\nabla\phi(\mathbf{x}, t)|.$$

Both techniques are designed to track the front propagation and the difference is that velocity function $F(\mathbf{x})$ in Eikonal equation is always non negative, which ensures the front always moves forward or backward. Thus, the fast marching problem can be converted to a stationary formulation and solved very efficiently because the front crosses each grid block only once. However, the velocity function $v(\mathbf{x})$ in level set equation can be positive and negative at different locations. So the front can move forward and backward at different locations. Therefore, Level Set Method solves a more

general equation, but significantly slower compared to Fast Marching Method.

1.3 Applications in Reservoir Characterization

In recent year, Level Set and Fast Marching Methods attract a lot attention when Fast Marching Method was successfully used in geophysics to estimate seismic velocity and travel time computation (Popovici and Sethian 1998; Sun and Fomel 1998; Karrenbach 2000; Cameron et al. 2006). In the area of reservoir characterization, Karlsen et al. (2000) first presented a fast marching level set method for reservoir simulation based on fractional flow formulation of two-phase, incompressible, immiscible flow. Lie and Juanes (2005) presented a numerical simulation of first-contact miscible gas injection using a front-tracking method. They assumed that the injection gas and the residual oil mix in all proportions to form a single hydrocarbon phase. Prodanovic et al. (2010) investigated the flow between fracture and adjacent matrix using a level set method for drainage and imbibition. Their progressive quasi-static (PQS) algorithm based on the level set method finds detailed, pore-level fluid configurations satisfying the Young-Laplace equation at a series of prescribed capillary pressures. The method automatically handles topological changes of the fluid volumes as capillary pressure varies.

More specifically, one advantage of the level set method is that it is very easy to perform computations involving curves and surfaces, which is a good fit for reservoir modeling and history matching of channelized systems. Recently, level set approaches have been applied to reservoir modeling and history matching to preserve channel structure.

Mondal et al. (2010) focused on parameterizing channel structure with a few points on channel boundaries. By perturbing those points, they can update channel boundary and alter the channel structure. A reversible jump Markov Chain Monte Carlo approach with varying parameter dimension is applied to automatically update channel boundary by adding, removing or perturbing those points on the channel boundary. Nielsen et al. (2009) treated permeability field as a binary level set function and update the level set function with gradient based method. The gradient is given by using adjoint method in a reservoir simulator. Dorn and Villegas (2008) presented a level set technique for shape reconstruction in history matching for reservoirs with two or more lithofacies. They started using sequential Gaussian simulation for the initial guesses of the lithofacies, and then apply level set based shape reconstruction algorithm for history matching problem in reservoir characterization. Chang et al. (2010) used the level set function values at part of the grid nodes directly in Ensemble Kalman Filter updating. The level set function values at other nodes are obtained by numerical interpolation. By updating the level set function values, they are able to update channel reservoirs. Instead of updating the facies fields directly, Moreno et al. (2008) and Lorentzen et al. (2012) transformed the facies field into a signed distance function and updated the velocity field in level set equation by Ensemble Kalman Filter.

1.4 Dissertation Outline

The structure of this dissertation is as follows:

In chapter II, we first generalize the concept of radius of investigation to depth of

investigation to account for reservoir heterogeneity. The proposed approach is based on an asymptotic solution of the diffusion equation in heterogeneous reservoirs. Considering zero order term of the frequency in the solution, we obtain the Eikonal equation that generalizes the depth of investigation for heterogeneous reservoirs and provides a convenient and efficient way to calculate drainage volume. From drainage volume calculations, we estimate a generalized pressure solution based on a geometric approximation of the drainage volume. A major advantage of our approach is that the Eikonal equation can be solved very efficiently using a class of front tracking methods called the Fast Marching Methods (FMM). Thus, transient pressure response can be obtained in multimillion cell geologic models in seconds without resorting to reservoir simulators. To illustrate the applicability of the proposed approach, two examples are presented: a) visualization of depth of investigation and identification of flow regimes for both homogeneous and heterogeneous reservoirs with multi-stage transverse fractures; b) stimulated reservoir volume estimation for improved history matching of shale gas reservoirs. The computation is orders of magnitude faster than conventional numerical simulation and provides a foundation for future work in reservoir characterization and field development optimization.

In chapter III, we present a method for history matching and uncertainty quantification for channelized reservoir models using Level Set Method (LSM) and Markov Chain Monte Carlo (MCMC) method. Our objective is to efficiently sample realizations of the channelized permeability fields conditioned to the production data and facies

observation at the wells. In our approach, the channel field boundary is first described by a level set function, e.g., a signed distance function or any other indicator function. By solving the level set equation (motion in a prescribed direction), we are able to gradually move the channel boundaries and evolve the channelized reservoir properties by perturbing the velocity field. Our approach allows representing facies via a parameterization of the velocity field that deforms the interface. Thus facies can be parameterized in the space of smooth velocity fields. The dimension reduction can be achieved for covariance-based velocity fields by re-parameterizing with SVD techniques. After parameterization, Markov Chain Monte Carlo method is utilized to perturb the coefficients of principal components of velocity field to update channel reservoir model matching production history. One advantage of this approach is that it is easy to condition the channel model to the facies observations at well locations by constraining the random velocity field to zero at well locations. To speed up the computation and improve the acceptance rate of the MCMC algorithm, we employ two stage methods where coarse-scale simulations are used to screen out the undesired proposals. The MCMC algorithms naturally provide multiple realizations of the permeability field conditioned to well and production data and thus, allow for uncertainty assessment in the forecasting. We demonstrate the effectiveness of the level set MCMC algorithm using both 2D and 3D examples involving water-flooding history matching.

In chapter IV, we presented a different approach for history matching and uncertainty quantification for channelized reservoirs using Reversible Jump Markov Chain Monte

Carlo (RJMCMC) methods. Our objective is to efficiently sample realizations of channelized permeability fields conditioned to production data and permeability values at the wells. In our approach, the channelized permeability field is parameterized using the Discrete Cosine Transform (DCT). The parameters representing the channel structure are the coefficients in truncated frequency domain. The parameter space is searched using a RJMCMC, where the dimension of the parameter space is assumed to be unknown. For each step of the RJMCMC, the dimension of the uncertainty space can be increased or decreased according to a prescribed prior distribution. This flexibility in the parameter dimension allows an efficient search of the uncertainty space. To speed up the computation and improve the acceptance rate of the RJMCMC algorithm, we employ two-stage methods whereby coarse-scale simulations are used to screen out the undesired proposals. After simulations, multi-dimensional scaling and cluster analysis are used to select realizations from the accepted models to adequately represent the diversity of the models. We demonstrate the effectiveness of the RJMCMC algorithm using both 2D and 3D examples involving water-flooding history matching. The 2-D example shows that the RJMCMC algorithm appears to successfully match the data and identify the orientation of the channels in the reference model. The 3-D results show that the proposed algorithm may determine the large-scale features of the reference channelized permeability field based on the production data.

CHAPTER II
DEPTH OF INVESTIGATION AND DEPLETION BEHAVIOR IN UNCONVENTIONAL RESERVOIRS USING FAST MARCHING METHODS*

The concept of depth of investigation is fundamental to well test analysis. Much of the current well test analysis relies on solutions based on homogeneous or layered reservoirs. Well test analysis in spatially heterogeneous reservoirs is complicated by the fact that Green's function for heterogeneous reservoirs is difficult to obtain analytically (Deng and Horne 1993). In this chapter, we introduce a novel approach for computing the depth of investigation and pressure response in spatially heterogeneous and fractured reservoirs.

In our approach, we first present an asymptotic solution of the diffusion equation in heterogeneous reservoirs. Considering terms of highest frequencies in the solution, we obtain two equations: the Eikonal equation that governs the propagation of a pressure 'front' and the transport equation that describes the pressure amplitude as a function of space and time. The Eikonal equation generalizes the depth of investigation for heterogeneous reservoirs and provides a convenient way to calculate drainage volume. From drainage volume calculations, we estimate a generalized pressure solution based

on a geometric approximation of the drainage volume. A major advantage of our approach is that the Eikonal equation can be solved very efficiently using a class of front tracking methods called the Fast Marching Methods (FMM). Thus, transient pressure response can be obtained in multimillion cell geologic models in seconds without resorting to reservoir simulators.

We first visualize depth of investigation and pressure solution for a homogeneous reservoir with multi-stage transverse fractures and identify flow regimes from pressure diagnostic plot. And then, we apply the technique to a heterogeneous reservoir to predict depth of investigation and pressure behavior. The computation is orders of magnitude faster than conventional numerical simulation and provides a foundation for future work in reservoir characterization and field development optimization.

2.1 Introduction

Unconventional resources are playing an increasingly important role in energy supply worldwide, especially in the United States. To estimate reservoir properties and optimize hydraulic fracture design in unconventional reservoirs, well test analysis (pressure transient and rate transient analysis) is widely used. In the area of well test analysis (Gringarten 1984, 2010; Ehlig-Economides 1992), the concepts of radius of investigation (Lee 1982; Raghavan 1993) and depth of investigation (Datta-Gupta et al. 2011) are fundamental to estimate reserves, understand drainage volume and identify infill drilling location (Kang et al. 2011). These concepts can also be used in

unconventional reservoirs to help planning horizontal well, optimizing multi-stage hydraulic fractures (Sehbi et al. 2011), and understanding stimulated reservoir volume (Yin et al. 2011). Kuchuk (2009) recently summarized several definitions of radius of investigation. Most of them rely on analytical solutions based on homogeneous or layered reservoirs. However, these analytical solutions have limited applicability and are difficult to generalize to arbitrary reservoir conditions and well locations.

In addition to the depth of investigation, it is important to understand the pressure depletion behavior and flow regimes in unconventional reservoirs because of the widespread use of hydraulic fracture technology to increase production rates. In practice, by characterizing flow regimes for multistage hydraulic fracture systems, we can optimize the fracture stages. In tight gas reservoirs, Lee and Hopkins (1994) and Holditch (2006) showed flow regimes for a vertical well with hydraulic fracture. In shale gas reservoirs, Al-Kobaisi et al. (2006), Bello and Wattenbarger (2010), Clarkson et al. (2009) and Freeman et al. (2009) analyzed flow regimes for multi-stage transverse fractures. Al-Kobaisi et al. (2006) identified a pseudo-radial flow regime for a finite conductivity fracture system. Song et al. (2011) summarized flow regimes for multi-stage hydraulic fractures.

The objectives of this work are threefold: first, we propose a method to calculate the depth of investigation and drainage volume in unconventional reservoirs using fast marching methods; second, we propose geometric pressure solution based on drainage

volume calculation to predict pressure depletion behavior in unconventional reservoirs; finally, we apply the proposed approach to both homogeneous and heterogeneous reservoirs to visualize depth of investigation and identify flow regimes from pressure diagnostic plots.

2.2 Methodology

In this section, we first generalize the concept of depth of investigation to heterogeneous reservoirs and introduce the Eikonal equation to solve the diffusive time of flight by comparing to homogeneous reservoirs

2.2.1 Generalization of Depth of Investigation

Our concept of depth of investigation relies on the definition of radius of investigation given by Lee (1982). Lee defines the radius of investigation as the propagation distance of a 'peak' pressure disturbance for an impulse source or sink. For simplified flow geometries and homogeneous reservoir conditions, the radius of investigation can be calculated analytically. For example, we could write analytical solutions of radius of investigation for different flow patterns:

$$r = \sqrt{c\alpha t} \tag{2.1}$$

where, r and t are propagation distance and time of the pressure front and alpha is hydraulic diffusivity defined as $\alpha = k/\phi\mu c_t$. Moreover, c denotes different constants for different flow patterns. For example, for linear flow, c = 2, for radial flow, c = 4 and

for spherical flow, c = 6. However, such analytic solutions are severely limited for heterogeneous and fractured reservoirs, particularly for unconventional reservoirs with multistage hydraulic fractures.

To generalize the concept to heterogeneous reservoirs, we first introduce a variable called diffusive time of flight (TOF) τ. Since pressure front propagation has the scale behavior of square root of time, we define the diffusive TOF as

$$\tau = \sqrt{ct} \tag{2.2}$$

Combining **Eq. (2.1)** and **Eq. (2.2)**, we have

$$r = \sqrt{\alpha}\tau, \quad \text{and} \quad \frac{d\tau}{dr} = \frac{1}{\sqrt{\alpha}} \tag{2.3}$$

Considering one dimensional problem with reservoir heterogeneity, hydraulic diffusivity now is a function of location. We can integrate **Eq. (2.3)** along the path to calculate diffusive time of flight:

$$\tau(r) = \int_0^r \frac{1}{\sqrt{\alpha(r)}} dr$$

For two or three dimensional problems with reservoir heterogeneity, **Eq. (2.3)** can be written as

$$\sqrt{\alpha(\mathbf{x})}|\nabla\tau(\mathbf{x})| = 1 \tag{2.4}$$

This equation describes the propagation of the pressure front and is called Eikonal equation in mathematics. From a different point of view, we could also introduce the propagation equation for pressure front and concept of diffusive time of flight using asymptotic ray theory.

2.2.2 Asymptotic Solution of Diffusivity Equation

The asymptotic method has been widely used in various disciplines such as optical, medical and geophysical imaging (Virieux et al. 1994). Our approach draws upon an analogy between a propagating pressure 'front' and a propagating wave front, and many of the concepts such as rays and propagating fronts have their counterparts in petroleum engineering (Datta-Gupta and King, 2007). Specifically, a high frequency asymptotic solution of the diffusivity equation for an impulse source or sink is given by Vasco et al. (2000). Here, we revisit the asymptotic solution with an emphasis on the Eikonal equation, which governs the pressure 'front' propagation.

Our goal here is to find a solution to the diffusive pressure equation that mimics the one found in the wave propagation phenomena. The transient pressure response in a heterogeneous permeable medium is governed by the well-known diffusivity equation,

$$\phi(\mathbf{x})\mu c_t \frac{\partial P(\mathbf{x},t)}{\partial t} = \nabla\cdot\big(k(\mathbf{x})\nabla P(\mathbf{x},t)\big) \tag{2.5}$$

In **Eq. (2.5)** , $P(\mathbf{x},t)$ represents pressure; $\phi(\mathbf{x})$ denotes porosity; $k(\mathbf{x})$ denotes

permeability; μ and c_t represent fluid viscosity and total compressibility, respectively. A Fourier transform of **Eq. (2.5)** results in the following equation in the frequency domain.

$$\phi(\mathbf{x})\mu c_t(-i\omega)\tilde{P}(\mathbf{x},\omega) = k(\mathbf{x})\nabla^2\tilde{P}(\mathbf{x},\omega) + \nabla k(\mathbf{x})\cdot\nabla\tilde{P}(\mathbf{x},\omega) \tag{2.6}$$

Asymptotic approach follows if we consider a solution in terms of inverse powers of $\sqrt{-i\omega}$,

$$\tilde{P}(\mathbf{x},\omega) = e^{-\sqrt{-i\omega}\tau(\mathbf{x})}\sum_{k=0}^{\infty}\frac{A_k(\mathbf{x})}{(\sqrt{-i\omega})^k} \tag{2.7}$$

where, $\tau(\mathbf{x})$ is the propagation time of the pressure 'front' (also called 'diffusive time of flight') and $A_k(\mathbf{x})$ is pressure amplitude at k-th order.

A solution of the above form can be interpreted on physical grounds based on the scaling behavior of diffusive flow. Such asymptotic solutions have been applied to electromagnetic imaging, for example, to the 'telegraph equation' which can be considered an extension of the wave equation with an extra diffusive term (Kline and Kay 1965). Again, the high frequency solution is given by the initial terms of the asymptotic series and will correspond to the propagation of a 'pressure front'. We, therefore, consider a solution of the form:

$$\tilde{P}(\mathbf{x},\omega) = A_0(\mathbf{x})e^{-\sqrt{-i\omega}\tau(\mathbf{x})} \tag{2.8}$$

Inserting **Eq. (2.8)** into **Eq. (2.6)** and collecting terms of the highest order in $\sqrt{-i\omega}$, that is $\left(\sqrt{-i\omega}\right)^2$ results in the following equation for the propagating front,

$$\sqrt{\alpha(\mathbf{x})}|\nabla\tau(\mathbf{x})| = 1 \tag{2.9}$$

where $\alpha(\mathbf{x})$ is the diffusivity and is given by

$$\alpha(\mathbf{x}) = \frac{k(\mathbf{x})}{\phi(\mathbf{x})\mu c_t} \tag{2.10}$$

Eq. (2.9) simply tells us that the pressure 'front' propagates in the reservoir with a velocity given by the square root of diffusivity. Also, diffusive time of flight, $\tau(\mathbf{x})$ has unit of square root of time which is consistent with scaling behavior of pressure diffusion. The pressure 'front' propagation depends on reservoir and fluid properties and is independent of flow rate. Also, it has unit of square root of time which is consistent with the scaling behavior of pressure diffusion. In fact, $\tau(\mathbf{x})$ is related to physical time through a simple expression of the form $t(\mathbf{x}) = \tau^2(\mathbf{x})/c$ where the pre-factor depends on the specific flow geometry (Kim et al. 2009). For example, for linear flow, c = 2, for radial flow, c = 4 and for spherical flow, c = 6.

2.2.3 Drainage Volume Calculation Using the Fast Marching Methods

The pressure 'front' equation, **Eq. (2.9)** is a form of the Eikonal equation which can be solved very efficiently using a class of front tracking methods called the Fast Marching

Methods (Sethian 1999). We illustrate the method on rectangular orthogonal mesh, where finite difference approximation could be used to calculate the gradient. Considering **Eq. (2.9)**, we start with discretizing the Eikonal equation on 2-D rectangular grids:

$$\max\left(D_{ij}^{-x}\tau, -D_{ij}^{+x}\tau, 0\right)^2 + \max\left(D_{ij}^{-y}\tau, -D_{ij}^{+y}\tau, 0\right)^2 = 1/\alpha \qquad (2.11)$$

where, D is gradient approximated with 1st order upwind finite difference scheme. In x direction, $D_{ij}^{-x}\tau = \left(\tau_{i,j} - \tau_{i-1,j}\right)/\Delta\, x$, $D_{ij}^{+x}\tau = \left(\tau_{i+1,j} - \tau_{i,j}\right)/\Delta\, x$. The same holds in y direction, $D_{ij}^{-y}\tau = \left(\tau_{i,j} - \tau_{i,j-1}\right)/\Delta\, y$, $D_{ij}^{+y}\tau = \left(\tau_{i,j+1} - \tau_{i,j}\right)/\Delta\, y$. The discretization results in a quadratic function of $\tau(\mathbf{x})$ which can be solved very efficiently.

The calculation is illustrated as follows. Suppose the pressure front is coming from points C and D in **Figure 2.1**, the diffusive TOF at points C and D are known as τ_c and τ_d. And we want to calculate diffusive TOF at the center black point based on five point approximation. **Eq. (2.11)** can be rewritten as

$$\left(\frac{\tau - \tau_c}{\Delta\, x}\right)^2 + \left(\frac{\tau - \tau_d}{\Delta\, y}\right)^2 = \frac{1}{\alpha}$$

Hence, diffusive TOF could be expressed as a quadratic function and solved very efficiently:

$$\left(\frac{1}{\Delta x^2}+\frac{1}{\Delta y^2}\right)\tau^2-2\left(\frac{\tau_c}{\Delta x^2}+\frac{\tau_d}{\Delta y^2}\right)\tau+\left(\frac{{\tau_c}^2}{\Delta x^2}+\frac{{\tau_d}^2}{\Delta y^2}-\frac{1}{\alpha}\right)=0$$

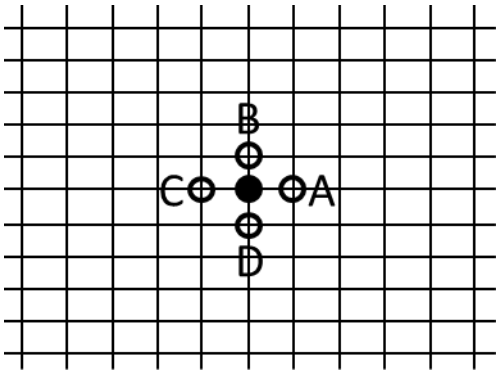

Figure 2.1 Illustration of two dimensional order upwind finite difference calculation

The key to the Fast Marching Methods lies in the observation that the upwind approximation possesses a specific causality relationship. By 'causality', we mean that the solution of **Eq. (2.11)** at each node depends only on the smaller adjacent values. Thus, we need to solve **Eq. (2.11)** concurrently in the order of increasing values of τ (Sethian and Vladimirsky 2000).

To illustrate the FMM, let us look at **Figure 2.2**. We first label well location as 'accepted' point (τ = 0) shown in **Figure 2.2a**. Its adjacent nodes are labeled as 'neighbor' points shown in **Figure 2.2b** and the rest nodes are called 'far-away' points. Now we can iterate to calculate diffusive time of flight at each point. The detailed procedure is as follows:

1. Start from 'accepted' point in black,

2. Calculate diffusive time of flight for all ‘neighbor’ points (A, B, C, D) using finite difference approximation,
3. Pick the minimum one in current ‘neighbor’ points,
    a. Label it as ‘accepted’ (point A in **Figure 2.2c**),
    b. Add its neighbors that are in ‘far-away’ as ‘neighbor’ (points E, F, G in **Figure 2.2d**),
4. Repeat step 2 and 3 until all the points in the domain are labeled as ‘accepted’.

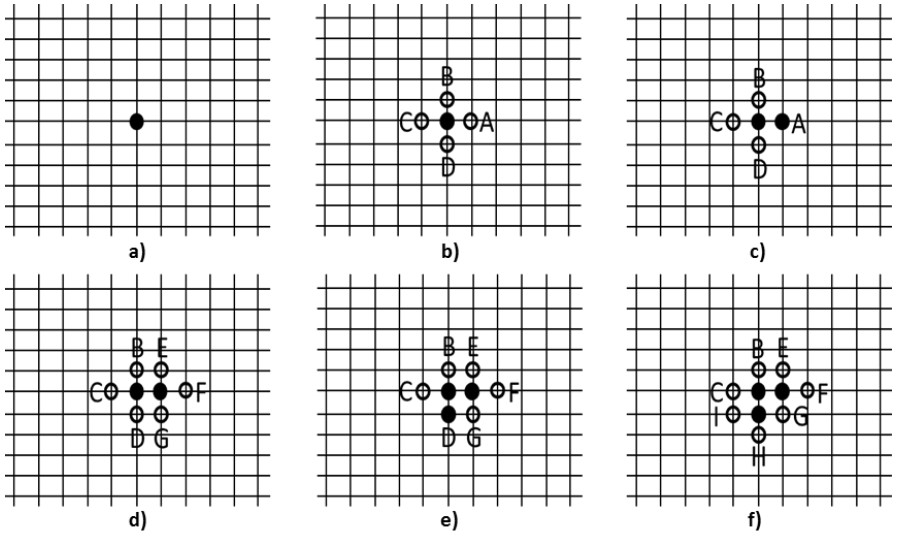

Figure 2.2 Illustration of fast marching methods

We illustrate the drainage volume calculation using fast marching methods with a heterogeneous permeability field in **Figure 2.3a.** Given the reservoir and fluid properties and the well configuration, we can solve the Eikonal equation using FMM. The result of FMM, the diffusive time of flight, is converted into physical time map which gives the

depth of investigation shown in **Figure 2.3b**. Furthermore, by contouring a specific time and summing up the pore volume inside the contour, we can obtain drainage volume at different times which leads to **Figure 2.3c**. More importantly, it takes only seconds to obtain these results.

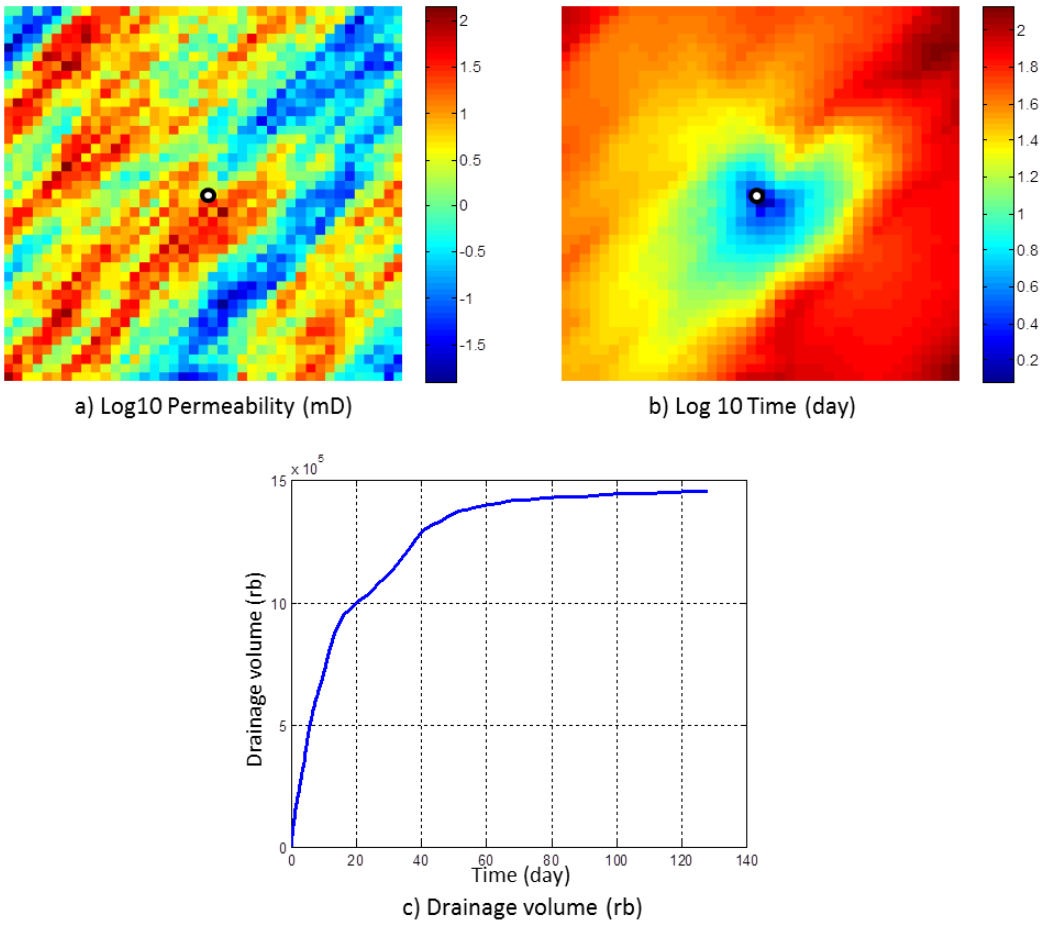

Figure 2.3 Depth of investigation and drainage volume calculation for a 2-D example: a) permeability in logarithm scale, b) time in logarithm scale, and c) drainage volume plot

Unconventional reservoirs, such as tight gas and shale gas reservoirs, involve complex interactions between pressure depletion, reservoir heterogeneity and well geometry. The

fast marching methods can be used as a fast tool to compute pressure 'front' propagation and visualize drainage volume in unconventional reservoirs. The drainage volume computed from the FMM can also be used to construct a geometric pressure solution for heterogeneous medium as discussed below.

2.2.4 Geometric Pressure Solution Based on the Drainage Volume

To introduce the geometric approximation to the pressure solution based upon the drainage volume, we must first express the diffusivity equation in a mixed form by introducing the Darcy flux, Q. Specifically, for radially symmetric flow we have:

$$\phi c_t \frac{\partial P}{\partial t} = \frac{1}{r}\frac{\partial}{\partial r}\left(\frac{k}{\mu} r \frac{\partial P}{\partial r}\right)$$

$$Q = \frac{kA(r)}{\mu}\frac{\partial P}{\partial r}$$

Thus we could write,

$$A(r)\phi c_t \frac{\partial P}{\partial t} = \frac{\partial Q}{\partial r} \tag{2.12}$$

Here, $A(r) = 2\pi \mathrm{rh}$, $r = \sqrt{x^2+y^2}$, is the surface area for cylindrical radial flow, and similarly, $A(r) = 4\pi r^2$, $r = \sqrt{x^2+y^2+z^2}$, is the surface area for spherical radial flow, and $A(r)$ is a constant, $r = |x|$, for linear flow. The sign convention we are using has $Q_w > 0$ for a producer, and Q is the inwardly directed flux. In addition, we could also

write pore volume as a function of the surface area and porosity:

$$dV_p(r) = \phi A(r) dr$$

Expressed in terms of the pore volume, **Eq. (2.12)** becomes:

$$c_t \frac{\partial P}{\partial t} = \frac{\partial Q}{\partial V_p} \tag{2.13}$$

The geometric approximation for the pressure solution is obtained from the following two approximations:

- The Darcy flux is negligible beyond the drainage volume. In other words, the drainage volume acts as a moving no flow boundary.

$$\begin{cases} Q = 0 & V_p \to V_p(r) \\ Q = Q_w & V_p \to 0 \end{cases}$$

- Within the drainage volume, the pressure is well approximated by a steady state solution.

$$\bar{P} = \frac{1}{V_p(r)} \int_0^{V_p(r)} P dV_p$$

Hence, we could simplify Eq. (9) as follows:

$$\frac{\partial P}{\partial t} \cong \frac{\partial \bar{P}}{\partial t} = \frac{1}{V_p(r)} \int_0^{V_p(r)} \frac{\partial P}{\partial t} dV_p = \frac{1}{V_p(r)} \int_0^{V_p(r)} \left(\frac{1}{c_t} \frac{\partial Q}{\partial V_p} \right) dV_p = -\frac{1}{c_t} \frac{Q_w}{V_p(r)}$$

$$\frac{\partial P}{\partial t} \cong \frac{\partial \bar{P}}{\partial t} = -\frac{1}{c_t} \frac{Q_w}{V_p(r)} \tag{2.14}$$

Here we are considering a constant rate drawdown calculation, with Q_w being the well rate. The welltest derivative can then be obtained directly from this equation, and provides an immediate interpretation in terms of the drainage volume, as a function of time.

$$\Delta \mathrm{P}' = -t \frac{\partial P}{\partial t} \cong -t \frac{\partial \bar{P}}{\partial t} = \frac{1}{c_t} \frac{Q_w t}{V_p\big(r(t)\big)} \tag{2.15}$$

The pressure drop is obtained by integrating **Eq. (2.14)** starting from a time after which the drainage volume boundary passes over the location. A similar approach has been developed by Nordbotten et al. (2004), and the relationship to drained volume has been explored by Agarwal (2010). However, no previous author has extended these results to heterogeneous reservoirs, as in the current work.

As a simple example, we can utilize the expression for the depth of investigation for infinite acting cylindrical radial flow, $r = \sqrt{4kt/\phi\mu c_t}$. We obtain the well-known expression for the well test derivative, $\Delta \mathrm{P}' = \mu Q_w / 4\pi kh$, from **Eq. (2.15)**, as an algebraic result. The approximation of the pressure drop as a natural logarithm is obtained by integrating **Eq. (2.14)**. It is not necessary to develop the full exponential

integral solution as an intermediate step to obtain these results, as is usually done. In addition, there is no requirement for a radially symmetric solution, once we apply the drainage volume concept to heterogeneous systems, as is shown in **Figure 2.4** and **Figure 2.5**.

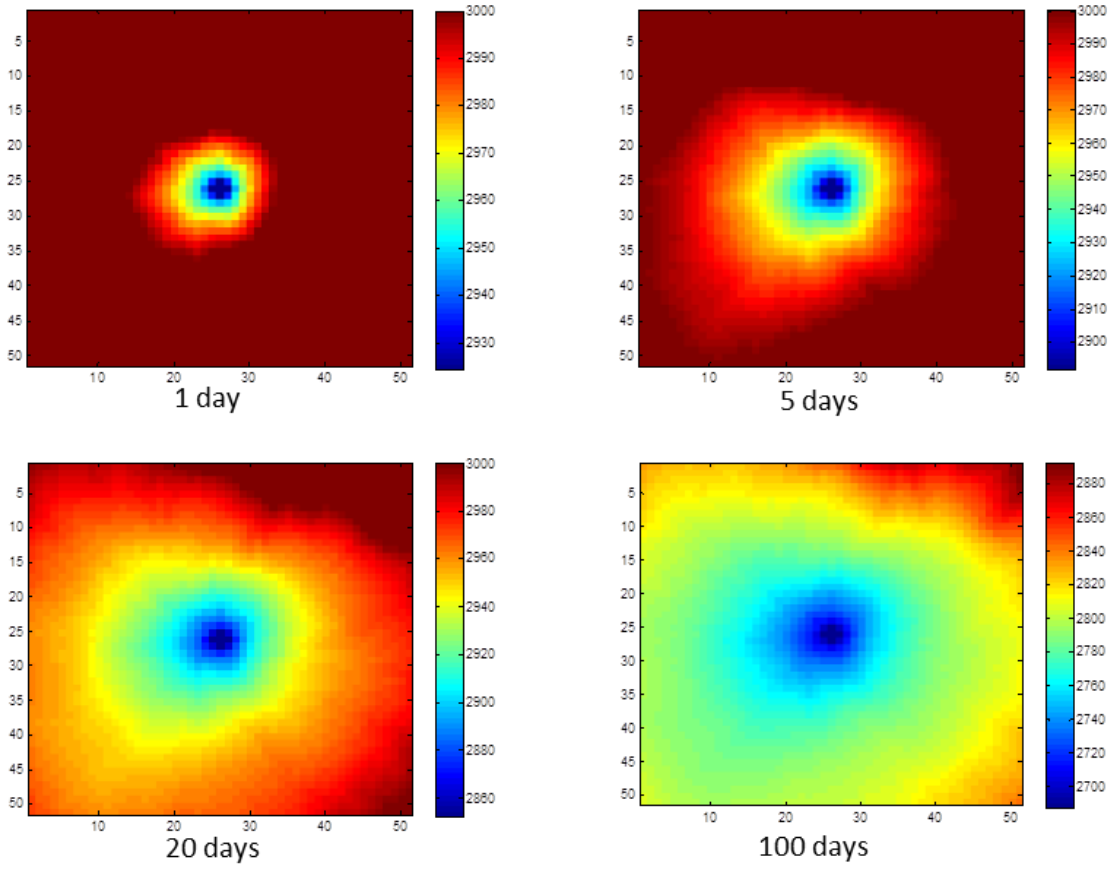

Figure 2.4 Estimated pressures based on geometric approximation solution at various times: a) 1 day, b) 5 days, c) 20 days and d) 100 days

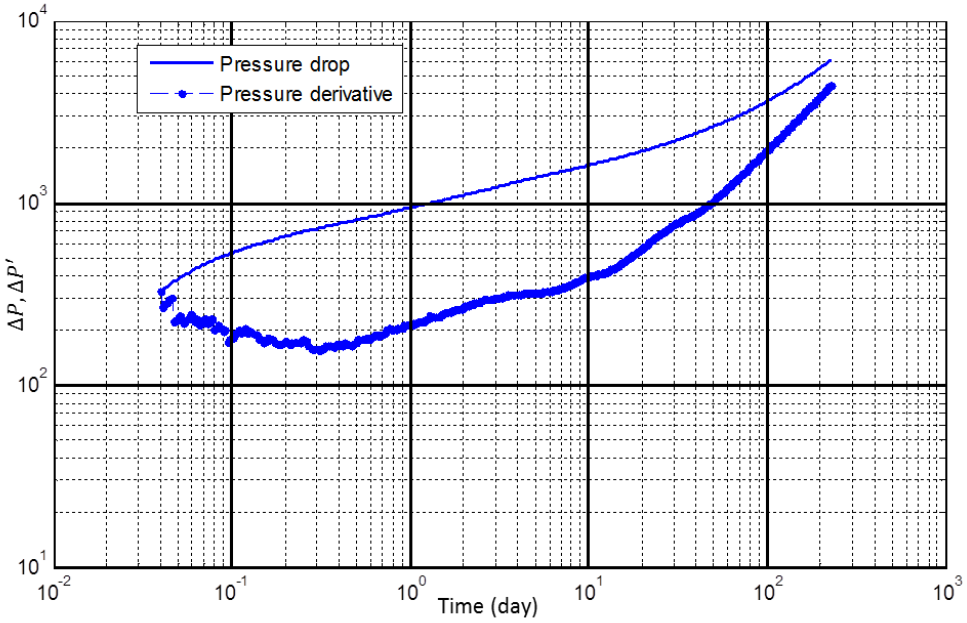

Figure 2.5 Pressure diagnostic plot for 2-D example

2.3 Flow Regime Identification and Visualization

In this section, we present two examples of application to unconventional reservoirs to illustrate the power and utility of our proposed approach. In both cases, we first visualize the depth of investigation at various times using the FMM and then present pressure diagnostic plots and identify flow regimes from these plots.

2.3.1 Multistage Hydraulic Fracture: Homogeneous Matrix Properties

For this example, the matrix permeability is assumed to be constant. We have a horizontal well with six stages of hydraulic fractures. Reservoir matrix permeability is 7.5×10^{-4} mD and effective fracture permeability is 1 mD. Thus, the hydraulic

fractures can be treated as finite conductivity fractures. Additional reservoir, fracture and fluid properties are shown in **Table 2.1**.

Table 2.1 Reservoir fracture and fluid properties for the example cases

Reservoir property	
Dimension	$440 \times 1320 \times 10$
Grid size	4 ft × 4 ft × 4 ft
Porosity	0.076
Fracture property	
Conductivity	4 mD · ft
Half length	240 ft
Fluid property	
Viscosity	0.2 cp
Total compressibility	3×10^{-5} psi^{-1}

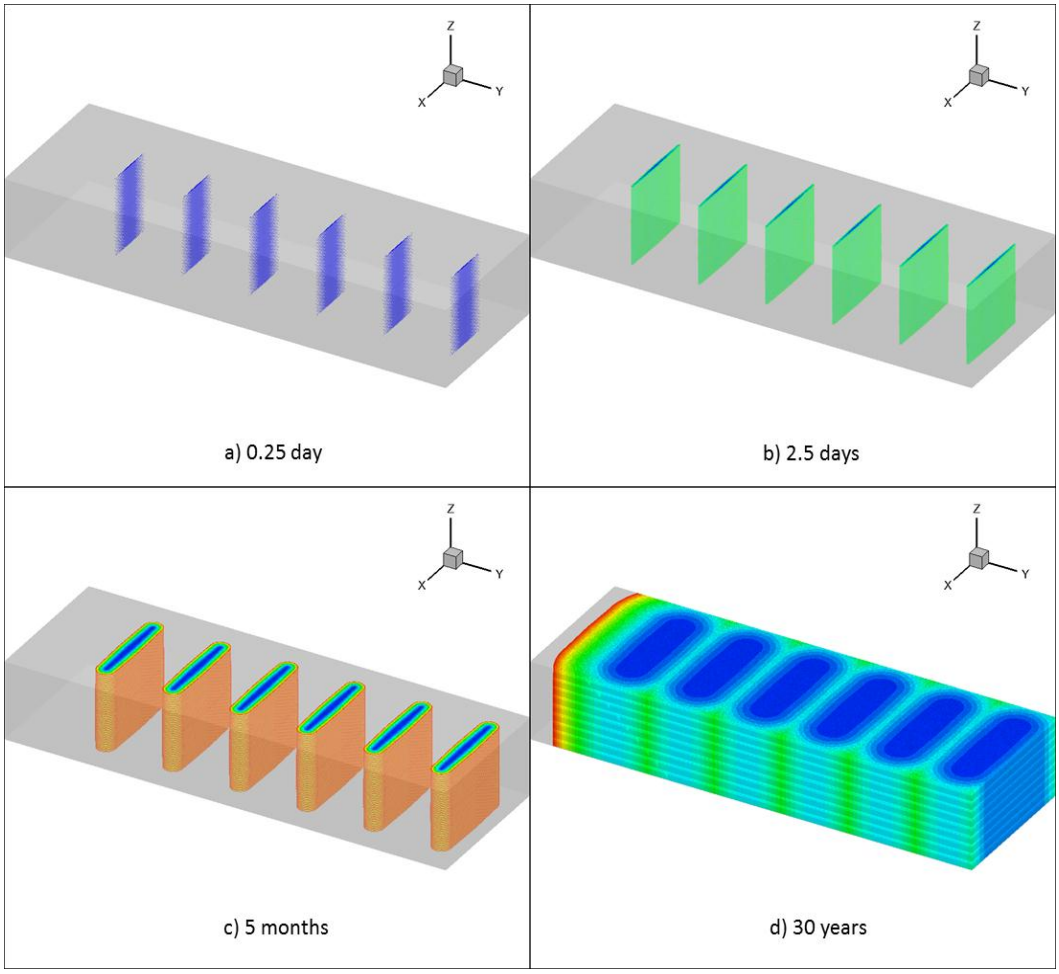

Figure 2.6 Depth of investigation for the homogeneous matrix example: a) 0.25 day, b) 2.5 days, c) 5 months and d) 30 years

Figure 2.6 displays the evolution of the depth of investigation for this example. There are four distinct flow patterns: early linear flow, pseudo-radial/elliptic flow, transition flow and pseudo steady state flow. These flow regimes can be identified from the pressure diagnostic plots as we will see later.

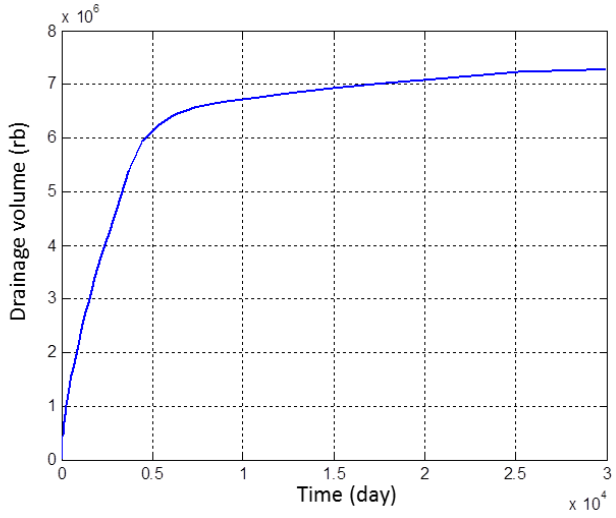

Figure 2.7 Drainage volume plot for the homogeneous matrix example

Figure 2.7 shows the drainage volumes as a function of time. Based on the computed drainage volume, we estimate transient pressure behavior using the geometric pressure solution as discussed before. **Figure 2.8** shows the pressure drop at the well location and the corresponding pressure derivatives. From the pressure derivative plot, we clearly see the four flow regimes which are highlighted in red.

- Early linear flow (half slope): Flow in hydraulic fracture towards the well.
- Pseudo-radial flow (zero slope): Pressure derivative is independent of time for a short period. This flow regime has also been identified by Al-Kobaisi et al. (2006) in the presence of multi-stage fractures.
- Transition flow: Flow pattern from pseudo-radial flow gradually changes to elliptic flow and then reaches reservoir boundaries at longer times.

- Pseudo steady state flow (unit slope): After reaching reservoir boundaries, the pressure behavior changes to volumetric depletion which yields the unit slope.

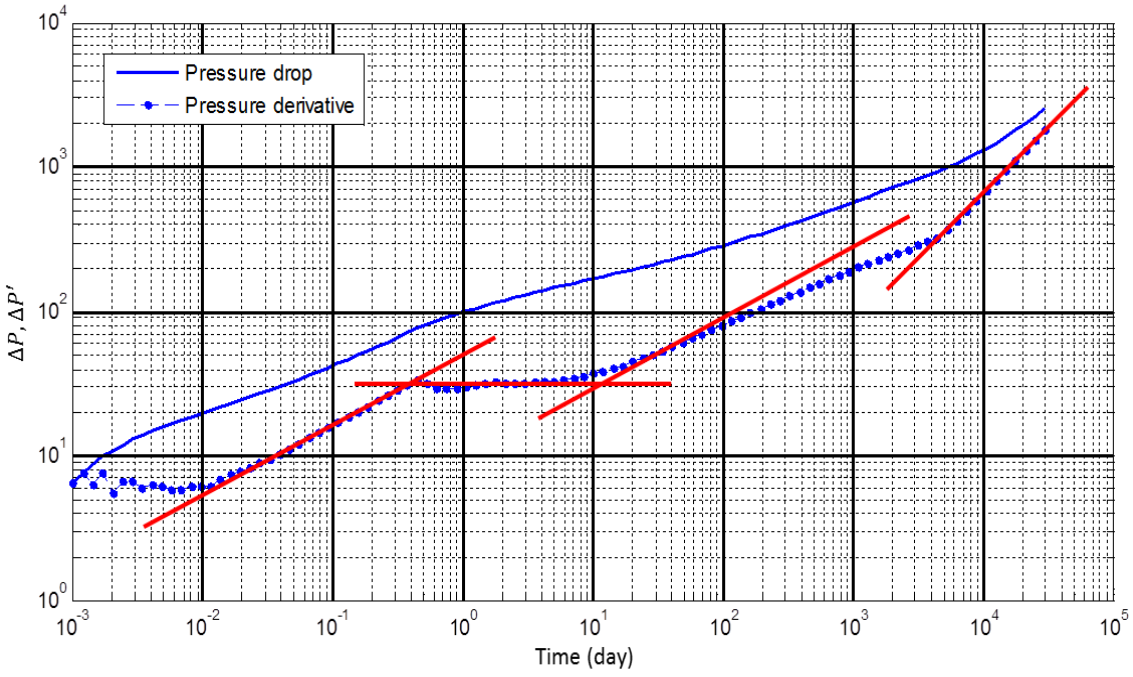

Figure 2.8 Pressure diagnostic plot for homogeneous case

2.3.2 Multistage Hydraulic Fractures: Heterogeneous Matrix Properties

In this example, we demonstrate the generality of the pressure solution by using heterogeneous matrix properties as shown in **Figure 2.9**. For this example, the reservoir matrix permeability is in the range of $[10^{-5}, 10^{-2}]$ mD. All other properties are the same as in **Table 2.1**. Following the same procedure as for the homogeneous matrix example, different flow pattern can be visualized and identified as shown in **Figure 2.10**. However, the pressure 'front' propagation is no longer smooth because of reservoir heterogeneity.

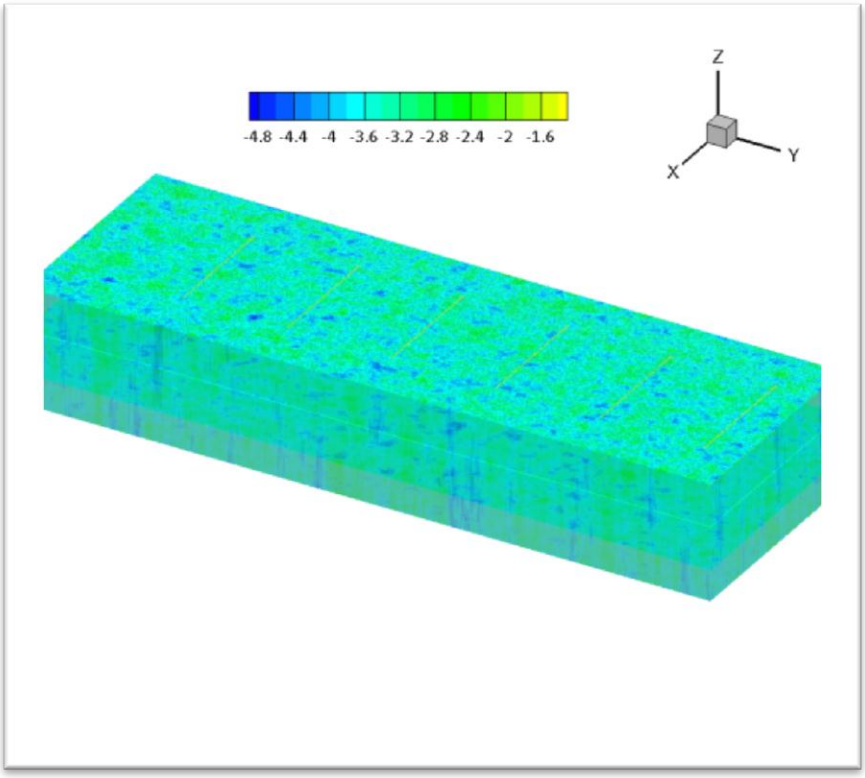

Figure 2.9 Matrix permeability field in log10 scale

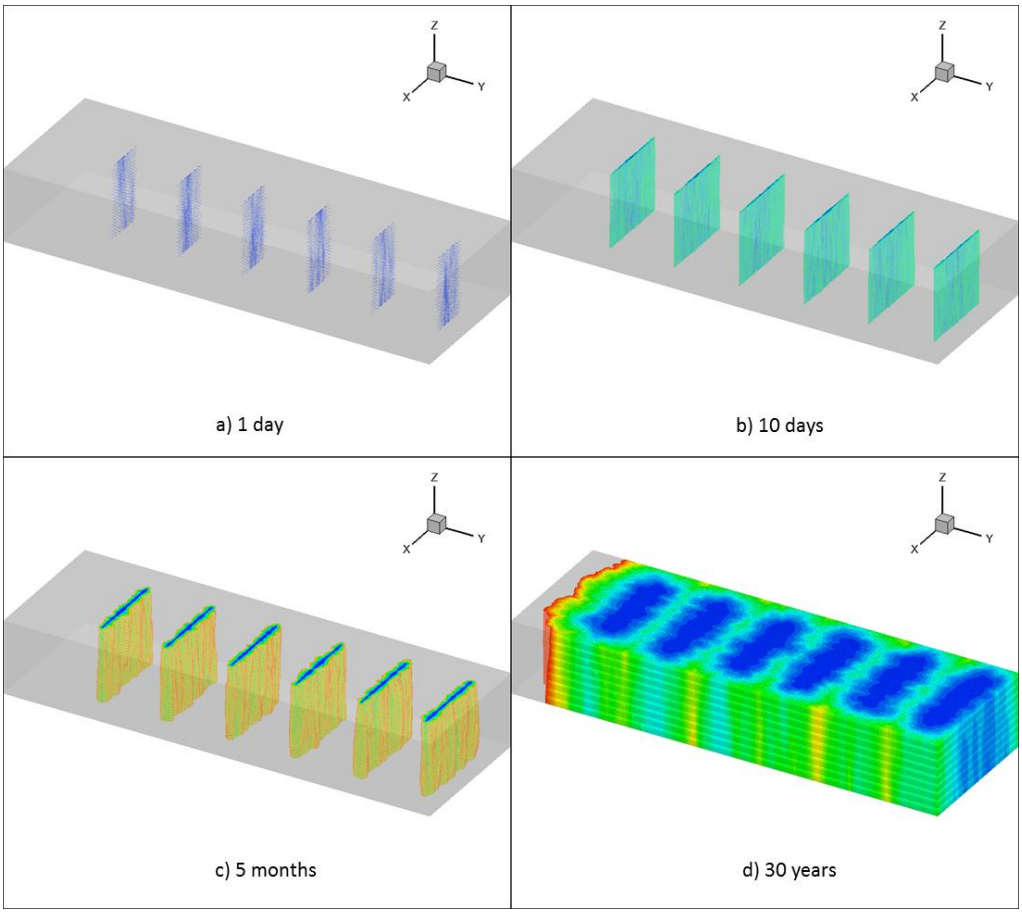

Figure 2.10 Depth of investigation for the heterogeneous matrix example with finite conductivity fracture: a) 1 day, b) 10 days, c) 5 months and d) 30 years

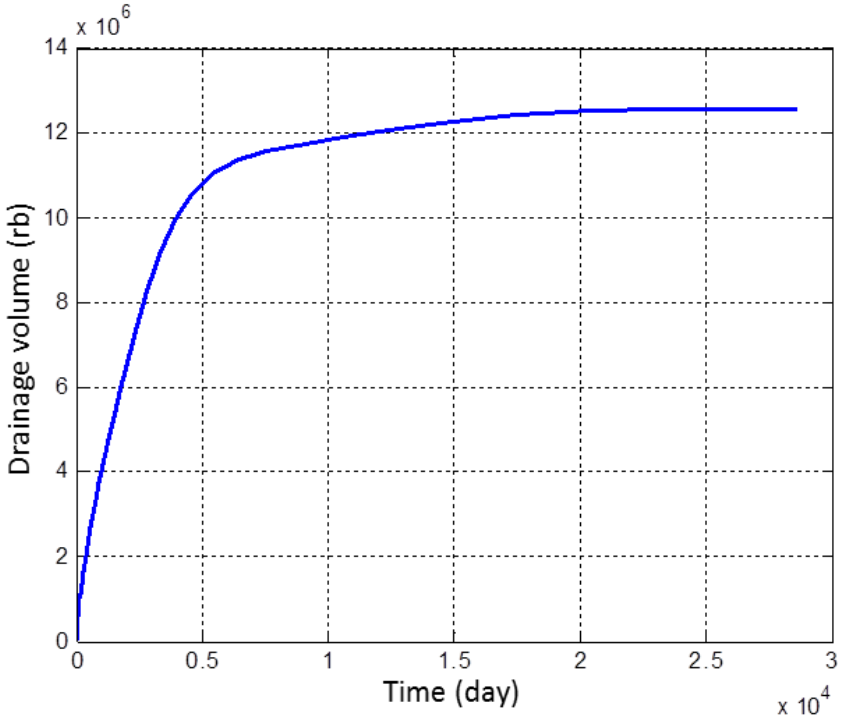

Figure 2.11 Drainage volume plot for the heterogeneous matrix example

Figure 2.11 shows the drainage volume computed as a function of time for the heterogeneous example. From the drainage volume calculations, again, we predict the transient pressure behavior and identify the flow regimes as shown in **Figure 2.12**. For the heterogeneous example, we see three distinct flow regimes: early linear flow, transition flow and pseudo steady state conditions. The pseudo-radial flow regime, however, is very short compared to the homogeneous matrix example before (**Figure 2.8)**. This can be because of the presence of reservoir heterogeneity that tends to distort the front propagation.

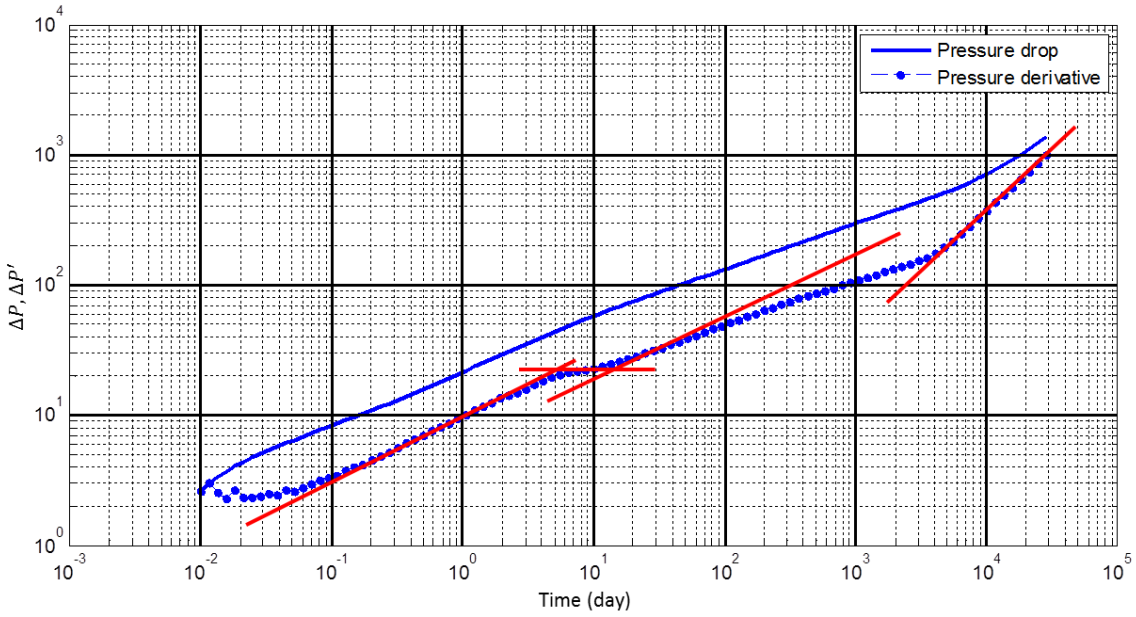

Figure 2.12 Pressure diagnostic plot for the heterogeneous matrix example with finite conductivity fractures

So far, we have limited ourselves to finite conductivity hydraulic fractures. Next, we change the fracture permeability a thousand-fold, to 1000 mD. We can now treat the hydraulic fractures as almost infinite conductivity fractures. Following the same procedure as before, we generate the depth of investigation shown in **Figure 2.13**. The pressure diagnostic plot is shown in **Figure 2.14**.

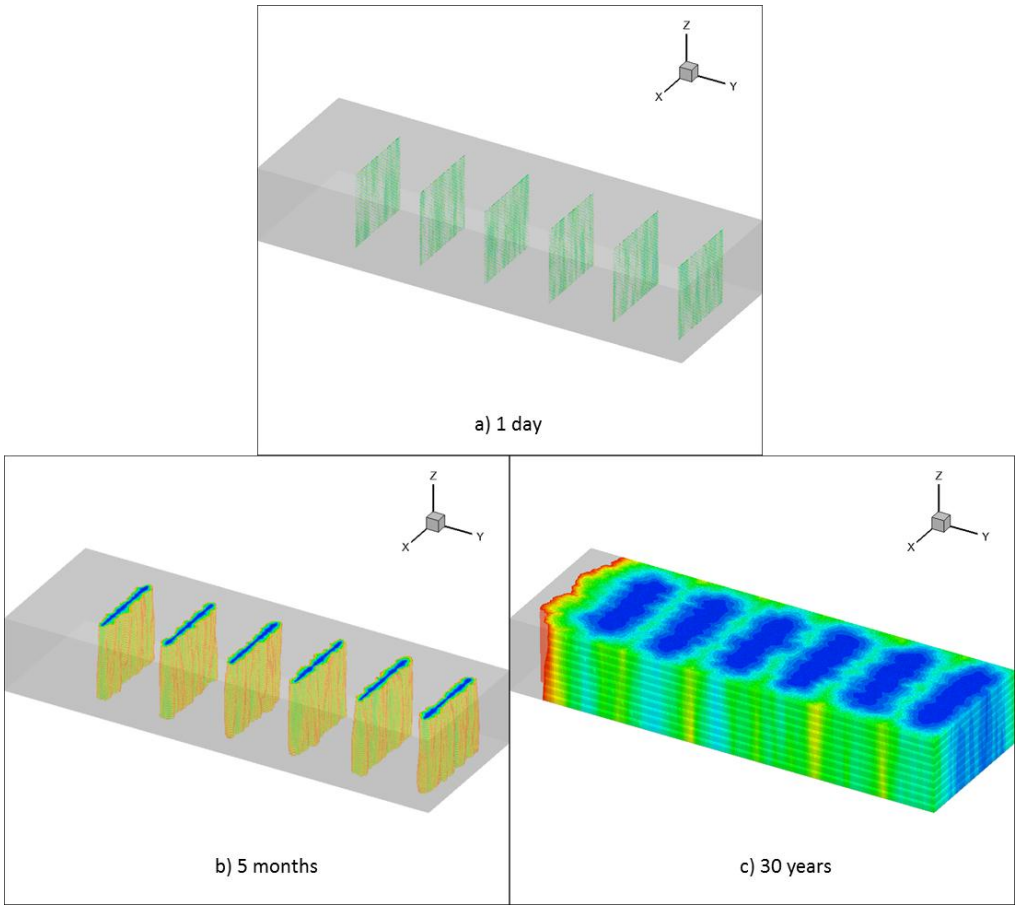

Figure 2.13 Depth of investigation for the heterogeneous matrix example with infinite conductivity fractures: a) 1 day, b) 5 months and c) 30 years

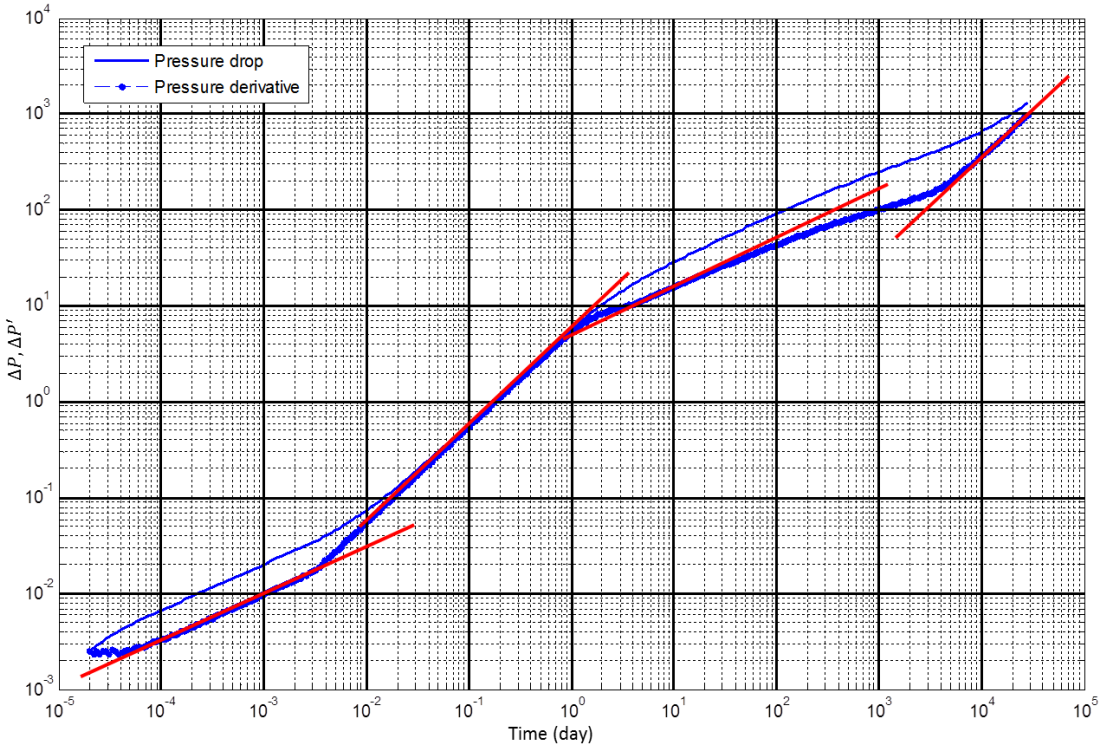

Figure 2.14 Pressure diagnostic plot for heterogeneous matrix example with infinite conductivity fracture

For this case with near infinite hydraulic fracture conductivity, we observe the following flow regimes:

- Early linear flow (half slope): Flow in hydraulic fractures towards the well at a very early time.
- Fracture storage (unit slope) accounting for the finite volume of the fractures.
- Transition flow that describes the gradual transition to pseudo-steady state flow.

- Pseudo steady state flow (unite slope) after reaching reservoir boundaries, leading to volumetric depletion and unit slope.

Thus, for both finite and infinite conductivity fractures as well as homogeneous and heterogeneous matrix properties, our proposed approach seem to yield drainage volume and pressure behavior consistent with flow patterns observed by other investigators (Freeman et al. 2009; Clarkson et al. 2009; Bello and Wattenbarger 2010 and Song et al. 2011). However, the generality of our approach makes it applicable for a much wider class of problems including complex fracture geometries, interactions with hydraulic fractures and natural fractures and non-uniform fracture conductivities.

2.4 Integration of Stimulated Reservoir Volume (SRV)[†]

For our purposes, the drainage volume is defined as the reservoir volume enclosed by the pressure 'front' at any given time. A typical evolution of a well drainage volume with time in previously mentioned illustration example is shown in **Figure 2.15**.

[†] Reproduced with permission from "Improved Characterization and Performance Assessment of Shale Gas Wells by Integrating Stimulated Reservoir Volume and Production Data" by Yin, J., Xie, J., Datta-Gupta, A. and Hill A. D. 2011. Paper SPE 148969 presented at SPE Eastern Regional Meeting, Columbus, Ohio, 17-19 August. Copyright 2011 by Society of Petroleum Engineers.

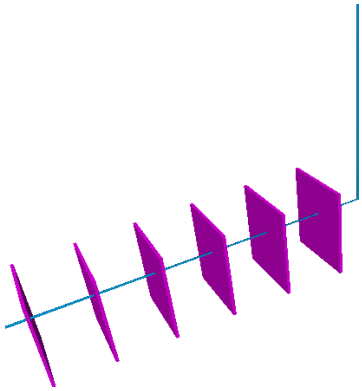

(a) well with hydraulic fractures

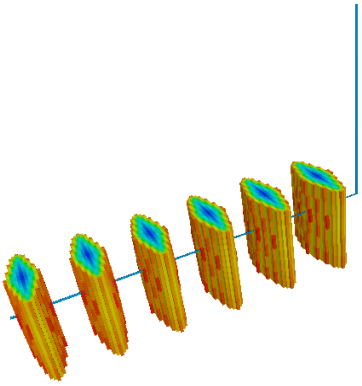

(b) depth of investigation at 3 months

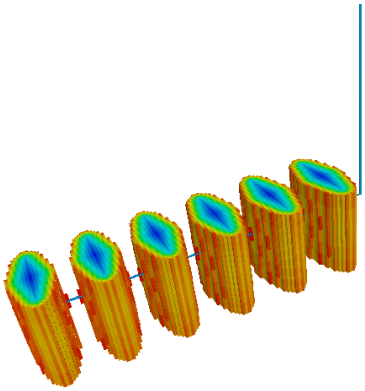

(c) depth of investigation at 6 months

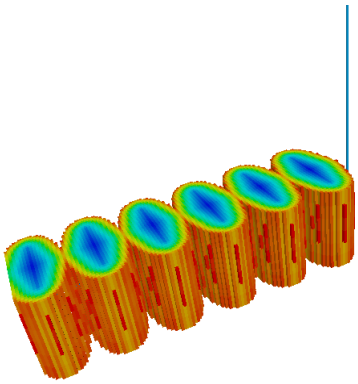

(d) depth of investigation at 1 year

Figure 2.15 Depth of investigation at various times for a horizontal well with multistage hydraulic fractures

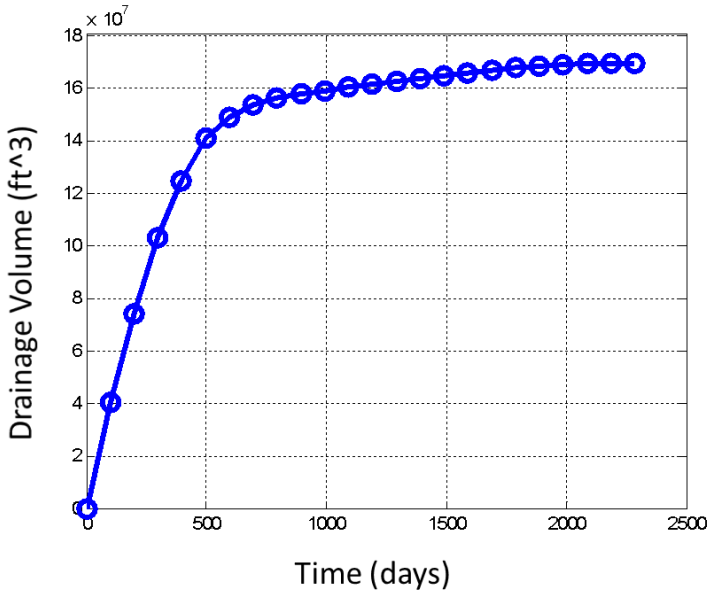

Figure 2.16 Well drainage volume versus time

We define the SRV as the volume when the drainage volume curve in **Figure 2.16** reaches an asymptote as shown. Given an estimate of SRV either from rate or pressure transient analysis or micro-seismic, we can compare the SRV with the computed well drainage volume to further screen the matrix and fracture parameters.

The steps are as follows:

- Given a set of fracture and matrix parameters, we first compute the long-time drainage volume using the method as outlined above. It must be emphasized that the computation of drainage volume is extremely fast and requires only a few seconds of computer time.
- We compare the long-term drainage volume with the estimated SRV from an

independent source.

- If the difference is substantial as determined by a threshold measure, then the given matrix fracture parameters are rejected and a new set of parameters are proposed.
- If the difference is within the threshold limit, then the parameters are accepted and the next step of calculations begins. This next step involves integration of rate/pressure response via proxy check and flow simulation.

The inclusion of SRV not only constrains the parameter space but also substantially reduces the number of flow simulations by pre-screening undesirable sets of fracture and matrix parameters in inverse modeling process.

In this section we illustrate our approach using a 3D synthetic example designed after a real field case. Two different cases are considered. First, we history match the well BHP to infer fracture and matrix parameters in a shale gas reservoir with a horizontal well with multistage fractures. Next, we assume that an estimate of the SRV is available through an independent measurement, for example micro-seismic or rate/pressure transient analysis. We then incorporate the SRV during history matching along with the well BHP response. The results clearly show the benefits of incorporating SRV in reducing the uncertainties in estimates of fracture/matrix parameters via history matching.

2.4.1 A 3-D Synthetic Example

The reference model for this case is a 3-D single-phase gas shale reservoir represented using single porosity compositional model designed after a Haynesville field case. The size of the grid is 264×64×5. The matrix permeability ranges from 80 to 150 nano-darcy. A horizontal well is completed in the center of the reservoir with 4 transverse elliptical fractures. The fracture heights fully penetrate the pay zone. Each fracture is considered surrounded by an enhanced permeability area (EPA) that represents natural fracture and/or hydraulic fracture induced permeability enhancements as shown in **Figure 2.19**. The parameters to be estimated via history matching and the associated uncertainties for this example are listed in **Table 2.2**. We assume that the fracture locations are known and are as shown in **Figure 2.18**. The horizontal well is first produced at a constant rate of 2 MMSCF/day, until bottom-hole pressure (BHP) drops to 1000 psi when the well control switches to BHP control. In this synthetic case, the first 295 days of BHP history will be integrated to predict BHP and gas production for the following 435 days. The objective function is defined as the sum of squared differences of BHP between simulation results and the reference (‘true’) case for first 295 days.

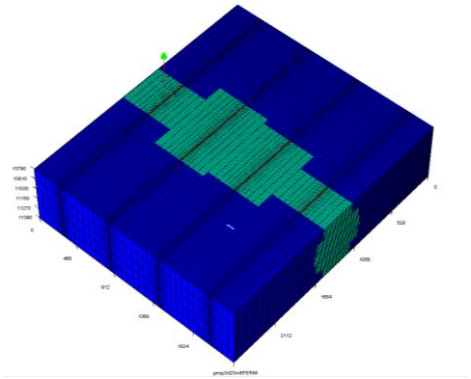

Figure 2.17 Reservoir and grid

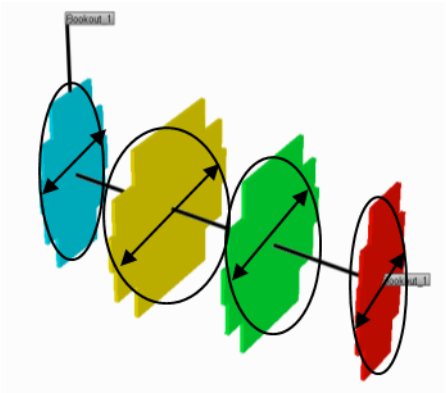

Figure 2.18 Fracture 3D elliptical structure

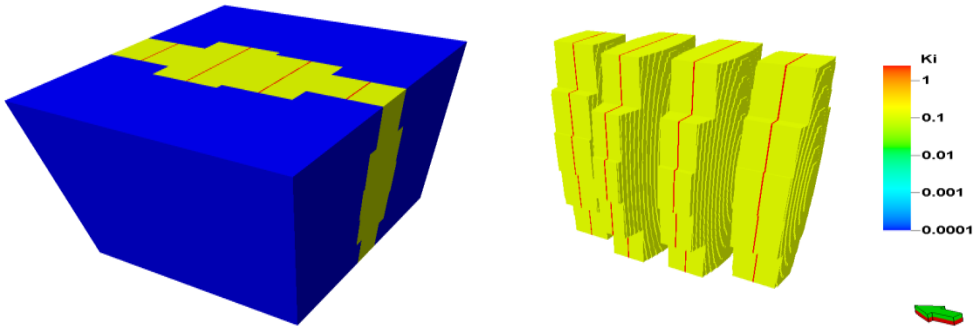

Figure 2.19 Stimulated reservoir volume defined by enhanced permeability area

Table 2.2 Parameter uncertainties for sensitivity and history matching

Uncertainty	Base	Low	High	Reference
Matrix permeability (k_M)	80.0E-6 md	70.0E-6 md	150E-6 md	100E-6 md
EPA permeability (k_E)	0.15 md	0.05 md	0.25 md	0.12 md
Fracture perm (k_F)	3.50 md	1.00 md	5.00 md	2.50 md
Matrix compaction factor (C_M)	3.00E-4 /psi	2.00E-4 /psi	5.00E-4 /psi	4.00E-4 /psi
EPA compaction factor (C_E)	5.00E-4 /psi	4.00E-4 /psi	6.50E-4 /psi	5.50E-4 /psi
Fracture compaction factor (C_F)	3.00E-4 /psi	2.00E-4 /psi	4.50E-4 /psi	3.50E-4 /psi
Fracture 1 half long axis (X_{F1})	200 ft	100 ft	300 ft	190 ft
Fracture 2 half long axis (X_{F2})	300 ft	200 ft	450 ft	350 ft
Fracture 3 half long axis (X_{F3})	300 ft	200 ft	450 ft	300 ft
Fracture 4 half long axis (X_{F4})	200 ft	100 ft	300 ft	150 ft

To evaluate the impact of various parameters on the well production performance, a sensitivity analysis was first performed on a set of preselected parameters including hydraulic fracture conductivity, fracture half length, rock compaction factors and matrix permeability. The initial distributions of the parameters are considered to be uniform. The parameter ranges and reference values are summarized in **Table 2.2**. **Figure 2.20** shows a tornado diagram of the objective function (logarithm of BHP misfit) with respect to various parameters generated by perturbing each parameter from the base model to the lower or upper bounds. From **Figure 2.20**, it can be seen that fracture permeability and EPA permeability and their compaction factors have major impacts on the BHP misfit, while matrix permeability and its compaction have relatively low impacts. This can be explained from the fact that for the time period of interest, the flow

mainly happens inside SRV (fracture and EPA). Based on the sensitivity analysis, the k_M and C_M are removed as history matching parameters.

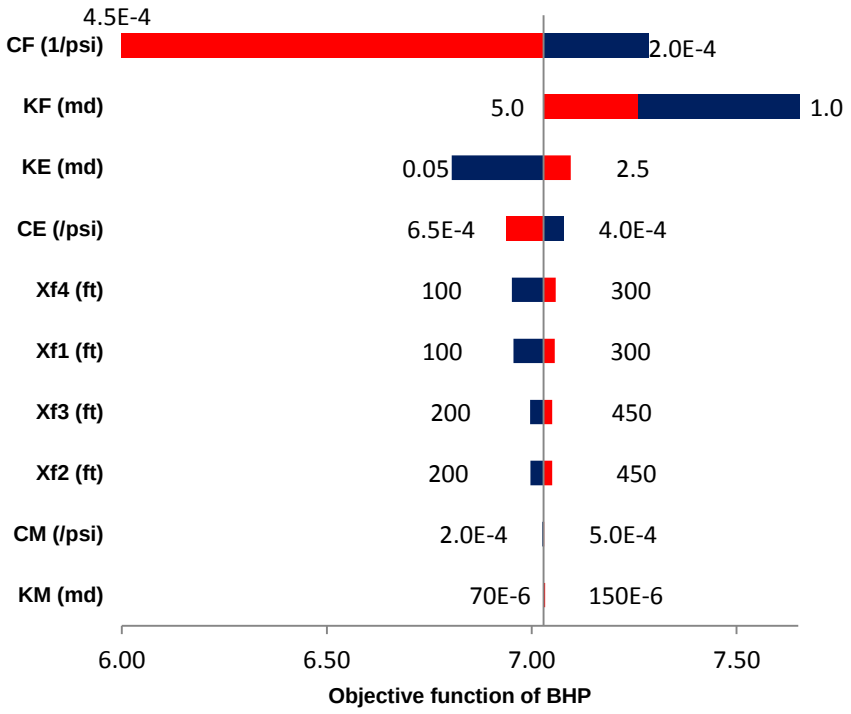

Figure 2.20 Sensitivity analysis of BHP objective

2.4.2 Integration of BHP Only

Initially, we perform a history matching of the well BHP only in order to estimate the fracture/matrix parameters as identified by the sensitivity analysis. The top eight parameters shown in **Figure 2.20** are used for the history matching. As discussed above, the history matching was done by genetic algorithm with response surface proxy (Yin et al. 2010). The history matching was followed by predictions.

Figure 2.21 compares the well responses for the initial population of GA models before and after history matching. The reference model response is shown in blue and is treated as observed data. Before history matching, a large discrepancy is observed in the production history between the reference model and the initial models reflecting the large uncertainty in the fracture/matrix parameters. After model calibration, uncertainties in parameter distributions are greatly reduced.

The effects of history matching BHP data in reducing the parameter uncertainties are shown using the box plots in **Figure 2.22**. Here, all the parameter ranges have been normalized to fall between zero and unity. The range of model parameters in the population is indicated by the blue box with the reference case indicated by the triangle. Clearly, after history matching it can be seen that the parameter ranges in the population are considerably tightened and some of them tend to converge to the reference value. However, because of the limited data and the inherent non-uniqueness, a large bias can be seen in the estimate of some of the parameters.

In **Figure 2.22** we have also shown the distribution of drainage volumes of the initial models and the final models after history matching. For comparison purposes, the drainage volume for the reference model is also shown in these figures. The bias in the parameter estimation as observed before is also evident here. All the history matched models seem to systematically over-estimate the drainage volume compared to the reference model. Part of the reason for this overestimation is the drainage volume

distribution of the initial models. A large majority of the initial models (>80%) had drainage volumes more than the reference model. Another reason can be the use of response surface as a surrogate model which can introduce bias because of lack of coverage of the complete parameter space. In the next section, we will see that such bias and non-uniqueness in the parameter estimation can be considerably reduced by incorporating additional information during history matching viz. the SRV estimate.

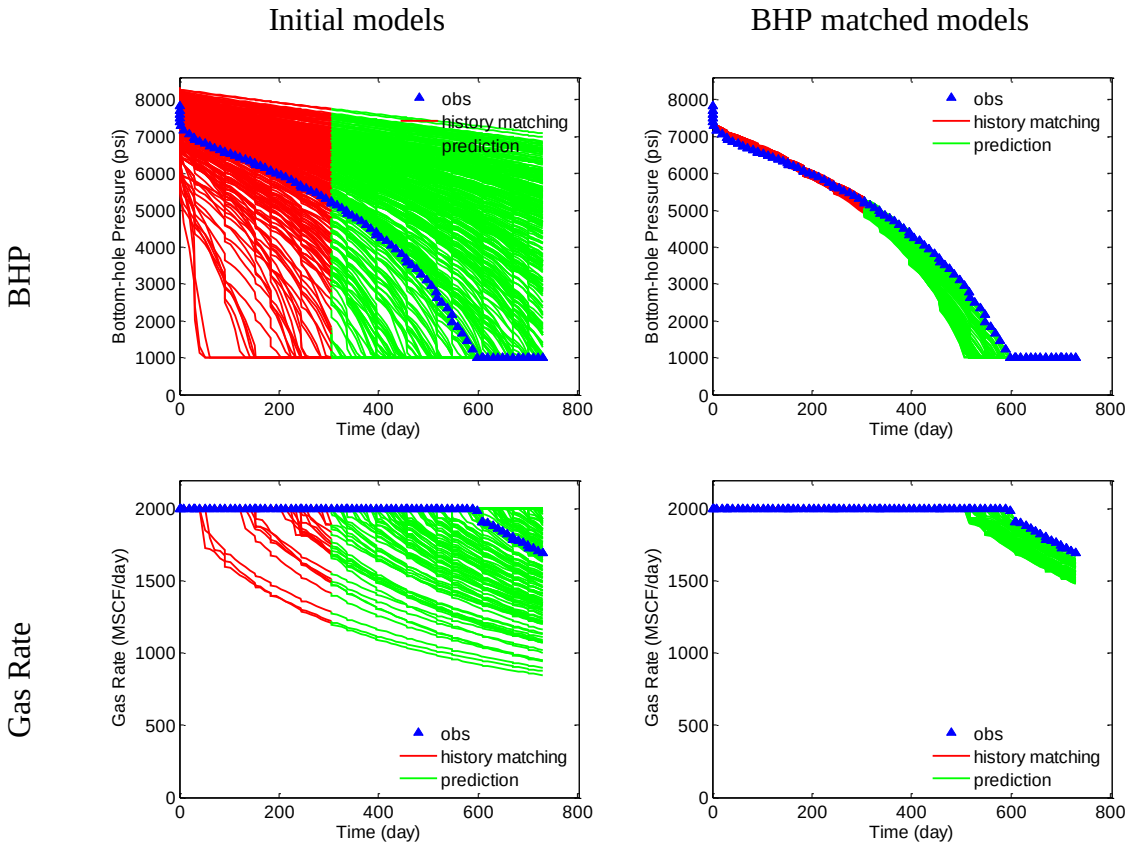

Figure 2.21 History matching and predictions by GA with response surface proxy

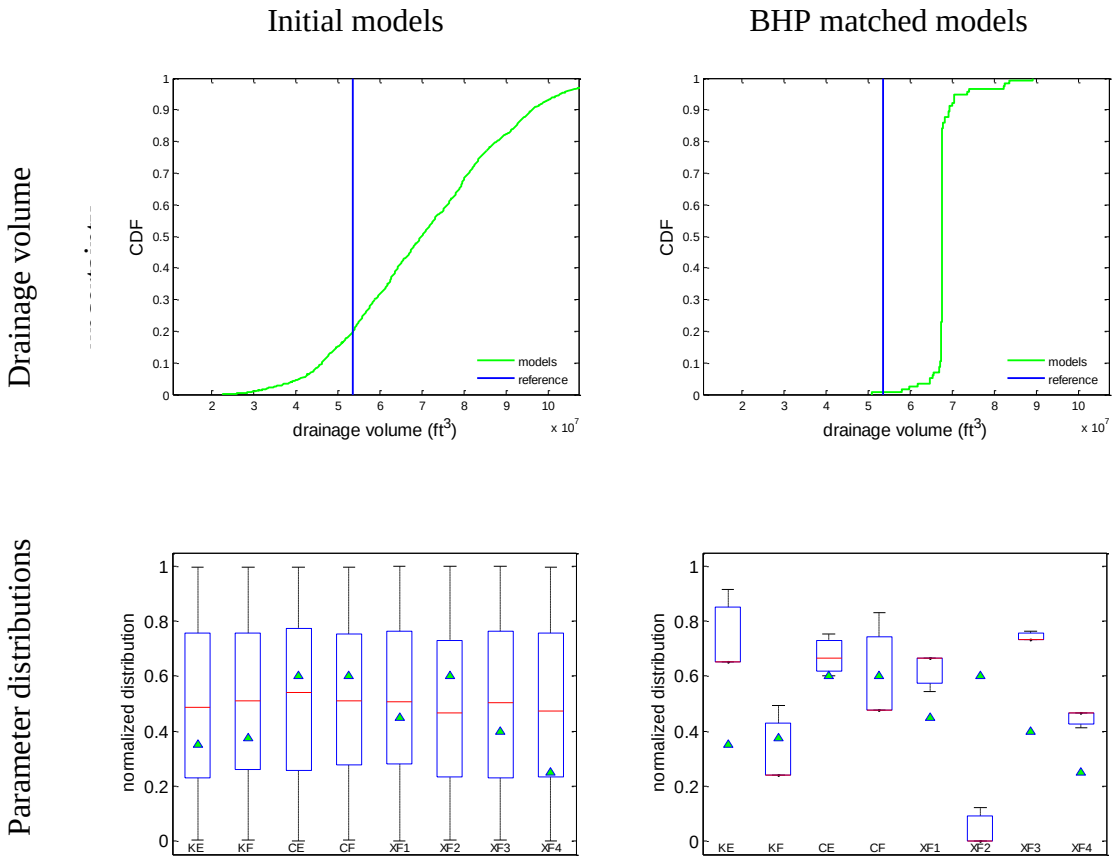

Figure 2.22 Uncertainty analysis of models by GA with response surface proxy

2.4.3 Integration of SRV and BHP

In order to improve the fracture/matrix parameter estimation, next we incorporate SRV information during history matching. Though the SRV is a static measure controlled by fracture connectivity and associated EPA, it can be approximated at a time when drainage volume defined by radius of investigation reaches pseudo-steady state, that is, the boundary effects become predominant and no dramatic increase in the well drainage

volume occurs. The situation is illustrated in **Figure 2.23** and **Figure 2.24** which show the evolution of the drainage volume as depicted by the location of the pressure 'front' at various times (color represents pressure front arrival time in log10 scale). Clearly, at early times the drainage volume increases rapidly and eventually stabilizes to SRV when pseudo steady state is reached and also fracture interference is observed.

Before history matching, we first examine the impact of various fracture/matrix parameters on the SRV. It can be seen that the drainage volume reaches plateau about 100 days-1000 days (corresponds to **Figure 2.23c** – **Figure 2.23e**). Fracture permeability (k_F) and EPA permeability (k_E) have dominant impacts in the early drainage volume development, while fracture lengths tend to influence the final values of the drainage volume. Matrix permeability has a noticeable impact only after the whole SRV has been drained (1.0E3 days-1.0E4 days, corresponds to **Figure 2.23e – Figure 2.23f**), which is typically way beyond the production schedule.

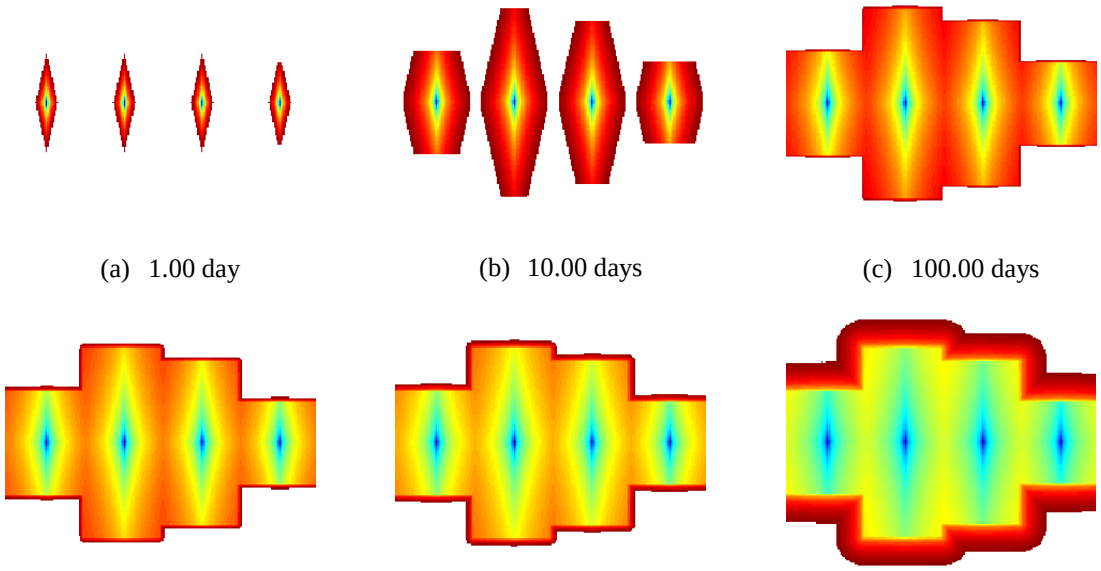

(a) 1.00 day (b) 10.00 days (c) 100.00 days

(d) 295 days (e) 730 days (f) 1.00E4 days

(end of history match) (end of prediction) (very long time)

Figure 2.23 Development of drainage volume defined by radius of investigation (center layer), colored by pressure front arrival time

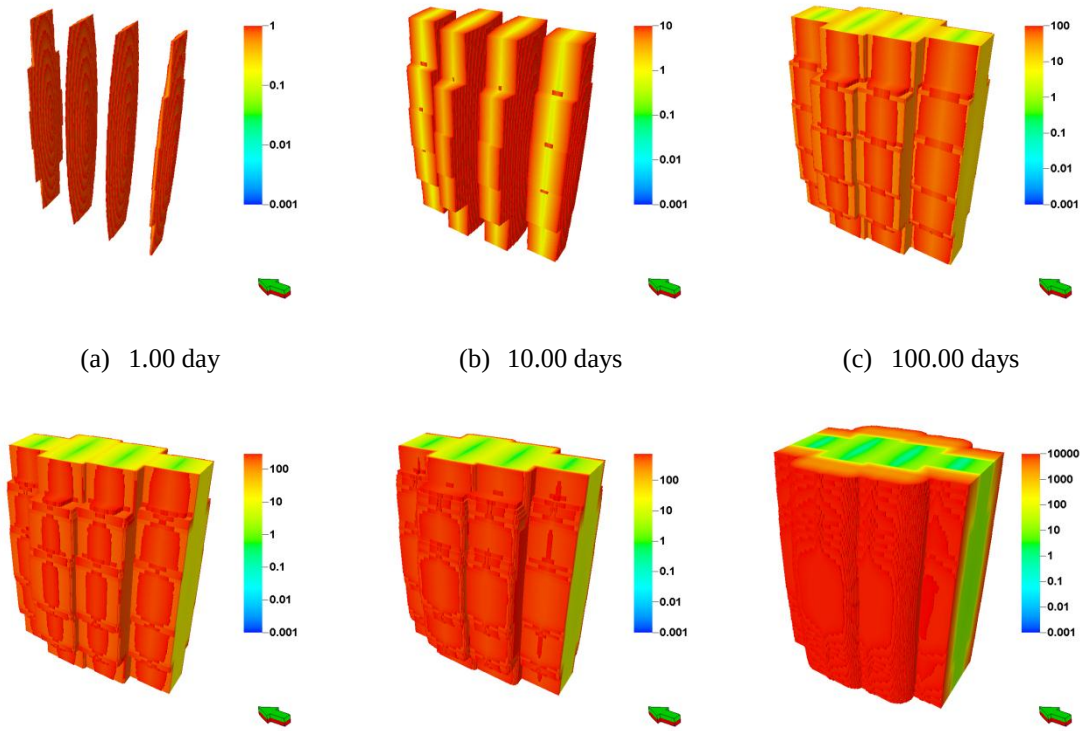

(a) 1.00 day (b) 10.00 days (c) 100.00 days

(d) 295 days (e) 730 days (f) 1.00E4 days

(end of history match) (end of prediction) (very long time)

Figure 2.24 3D drainage volume defined by radius of investigation, colored by pressure front arrival time

Next we carry out the history matching using the SRV and the BHP data. During history matching, the SRV data is incorporated as a single value that corresponds to the long-term drained volume of the well. The drainage volume is computed using the pressure 'front' propagation as discussed before. The history matching proceeds as follows:

- For each set of fracture/matrix parameters in the GA population, we first compute the drainage volume. Recall that the drainage volume computation

does not require flow simulation and can be done in seconds. The drainage volume is compared with the well SRV. If the difference is less than 10%, then the parameter set is accepted for flow simulation and BHP calculation; otherwise, the parameter set is rejected and a new set of parameters are generated by sampling the corresponding distribution.

- Once a parameter set passes the prescreening step above, the parameter combination is used to carry out a flow simulation and compute the well BHP. An objective function is constructed based on the misfit between the observed and computed BHP as well as SRV.
- The above steps are repeated for all the members of the GA population which is then resampled to create a new generation based on the selection probability. The usual GA steps of crossover and mutation then follow.
- The process is repeated until the data misfit reaches a satisfactory level or we exceed a preset number of generations.

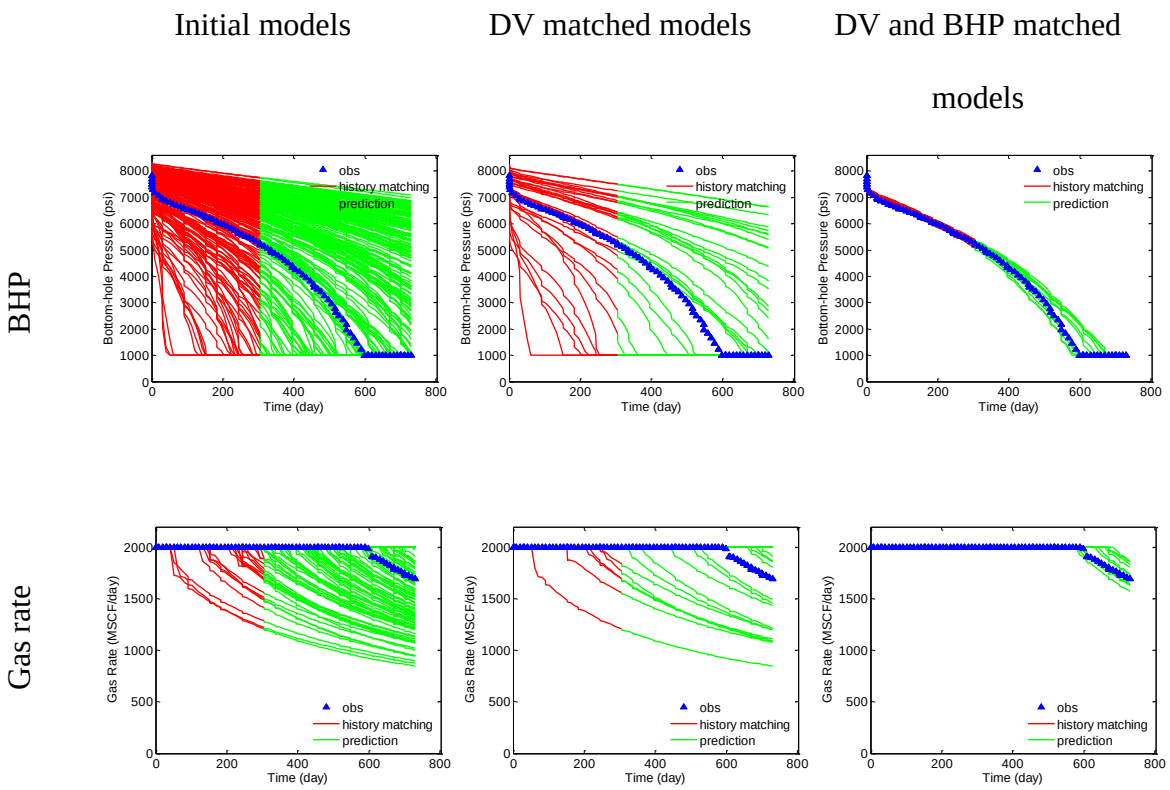

Figure 2.25 History matching and predictions by GA with SRV proxy

History matching and prediction results are shown in **Figure 2.25**. The results show that matching the SRV with the drainage volume did not improve the quality of the BHP or gas rate match and there is still a large discrepancy between the models pre-screened using SRV and the reference model response. This is expected because the SRV, as used here, is a single integrated estimate and does not provide any spatial detail. However, in **Figure 2.26** we can see the impact of SRV matching. As expected, the uncertainty in final drained volume is substantially reduced compared to the initial population. More importantly, the uncertainties in k_E, k_F, X_{F1}-X_{F4} are also greatly reduced as seen in the

box plots in **Figure 2.26**. Finally, from **Figure 2.25** after calibrating the models with BHP using GA, we can see that both BHP and gas rate matches are improved substantially. Also, the parameter ranges are also narrowed considerably as seen in **Figure 2.26**. In **Figure 2.27** we have shown the drainage volume at 295 days for a selected set of history matched models. For comparison purposes, we have also shown the SRV for the reference model. Recall that we only matched the SRV with the drainage volume, not the specific shape of the SRV. However, the results in **Figure 2.27** show a reasonable correspondence with the shape of the reference SRV within the levels of non-uniqueness to be expected for the history matching process.

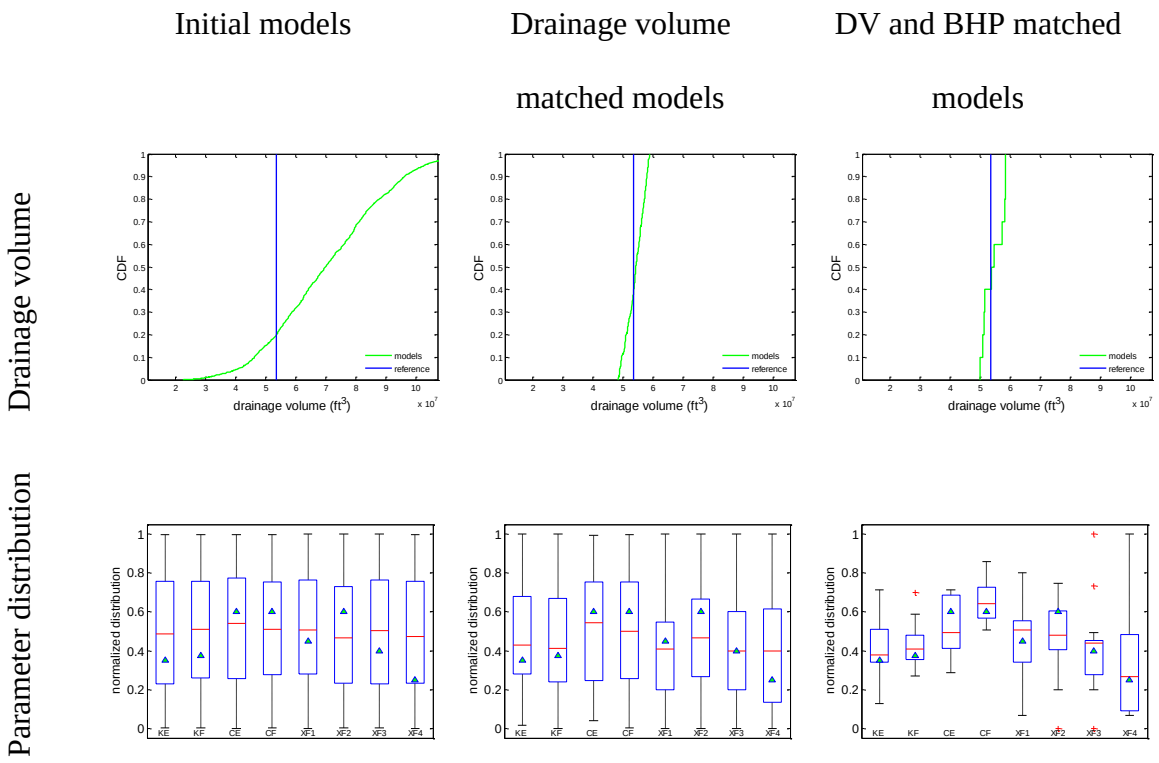

Figure 2.26 Uncertainty analysis of models by GA with SRV proxy

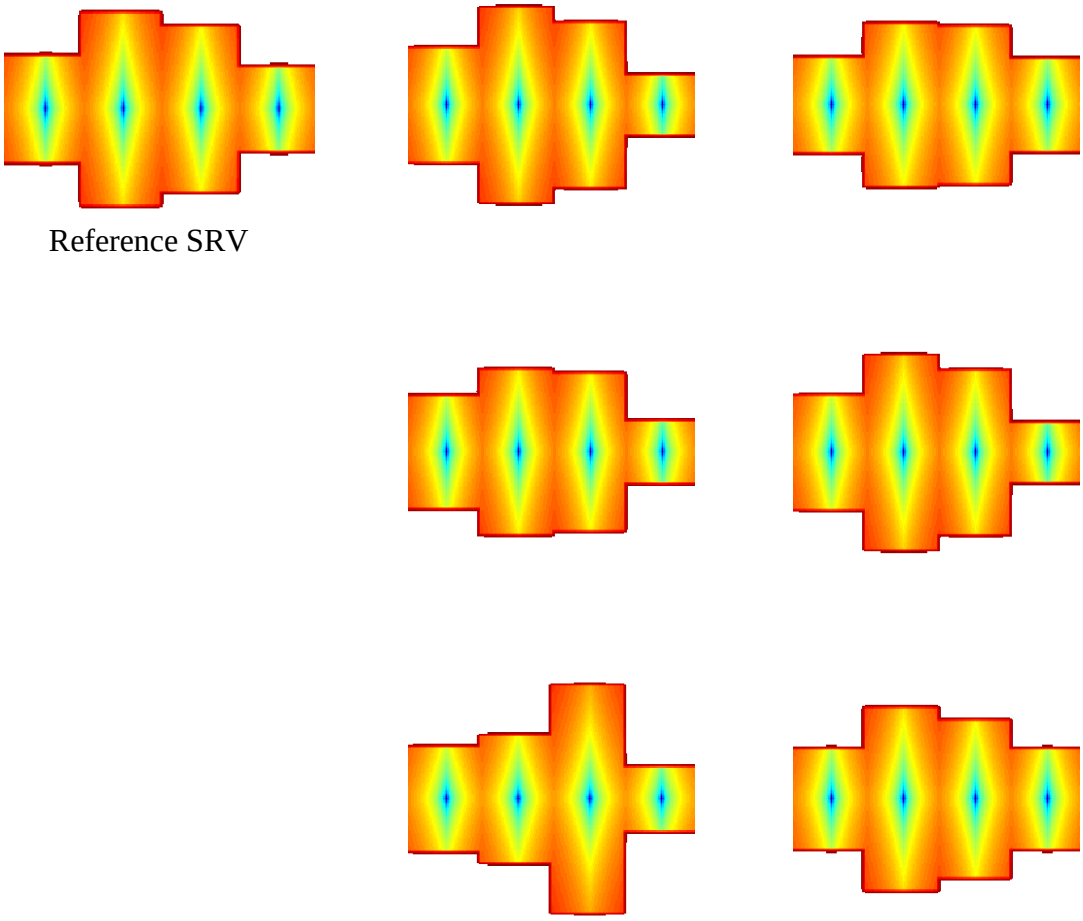

Figure 2.27 SRV of models integrated with both DV and BHP

2.5 Summary

In this chapter we presented a novel approach to compute and visualize depth of investigation in unconventional reservoirs using fast marching methods (FMM) under very general reservoir conditions and fracture geometry/properties. Based on the depth of investigation, a geometric pressure solution is proposed to estimate the transient pressure behavior in unconventional wells with multistage fractures. From the pressure

depletion behavior, well test diagnostic plot can be generated that helps us understand the reservoir drainage and identify flow regimes.

We demonstrated the applicability of our approach with two examples derived based on real field cases – one assumes homogeneous matrix properties and the other uses heterogeneous matrix properties. The homogeneous matrix example validates or approach and flow regimes consistent with analytic solutions can be identified using our proposed approach. For the heterogeneous example, we predicted the transient pressure behavior from the drainage volume calculations. The speed and versatility of our proposed method makes it ideally suited for estimating and optimizing fracture design in unconventional reservoirs through inverse modeling.

Another application of this technique is to rapidly estimate stimulated reservoir volume (SRV) using drainage volume calculation. The application is demonstrated using a 3-D synthetic example designed after a real field case. We are able to demonstrate the benefits of incorporating the SRV during the history matching process to improve history matching results. Specifically, our results show that the uncertainty in the fracture/matrix parameters are reduced significantly when SRV was incorporated in addition to Bottom-Hole Pressure (BHP) during history matching as compared to BHP matching only.

CHAPTER III
UNCERTAINTY QUANTIFICATION IN HISTORY MATCHING OF CHANNELIZED RESERVOIRS USING MARKOV CHAIN LEVEL SET APPROACHES[‡]

We present a method for history matching and uncertainty quantification for channelized reservoir models using Level Set Method and Markov Chain Monte Carlo (MCMC) method. Our objective is to efficiently sample realizations of the channelized permeability fields conditioned to the production data and facies observation at the wells. In our approach, the channel field boundary is first described by a level set function, e.g., a signed distance function or any other indicator function. By solving the level set equation (motion in a prescribed direction), we are able to gradually move the channel boundaries and evolve the channelized reservoir properties. Our approach allows representing facies via a parameterization of the velocity field that deforms the interface. Thus facies can be parameterized in the space of smooth velocity fields. The dimension reduction can be achieved for covariance-based velocity fields by re-parameterizing with SVD techniques.

After parameterization, Markov Chain Monte Carlo method is utilized to perturb the coefficients of principal components of velocity field to update channel reservoir model

[‡] Reproduced with permission from "Uncertainty Quantification in History Matching of Channelized Reservoirs using Markov Chain Level Set Approaches" by Xie, J., Efendiev, Y. and Datta-Gupta, A. 2011. Paper SPE 141811 presented at SPE Reservoir Simulation Symposium, The Woodlands, Texas, 21-23 February. Copyright 2011 by Society of Petroleum Engineers.

matching production history. One advantage of this approach is that it is easy to condition the channel model to the facies observations at well locations by constraining the random velocity field to zero at well locations. To speed up the computation and improve the acceptance rate of the MCMC algorithm, we employ two stage methods where coarse-scale simulations are used to screen out the undesired proposals. The MCMC algorithms naturally provide multiple realizations of the permeability field conditioned to well and production data and thus, allow for uncertainty assessment in the forecasting. We demonstrate the effectiveness of the level set MCMC algorithm using both 2D and 3D examples involving water-flooding history matching.

3.1 Introduction

In many geologic environments, the distribution of subsurface properties is primarily controlled by the location and distribution of distinct geologic facies with sharp contrasts in properties across facies boundaries (Weber 1982). For example in a fluvial setting, high permeability channel sands are often embedded in a nearly impermeable background causing the dominant fluid movement to be restricted within these channels. Under such conditions, the orientation of the channels and channel geometry play an important role in determining the flow behavior in the subsurface. Thus, in predicting the flow through highly heterogeneous porous formations, it is important to model facies boundaries accurately and to properly account for the uncertainties in these models.

The representation and history matching of channelized reservoirs are challenging

because of the difficulties to reproduce the large-scale continuity of the channel structure and identify the channel geometry and its orientation. The traditional two-point geostatistical techniques for reservoir characterization are unable to reproduce the channel geometry and the facies architecture (Haldorsen and Damsleth 1990; Koltermann and Gorelick 1996; Dubrule 1998). As an alternative, object-based modeling (Deutsch and Wang, 1996) and more recently, multi-point geostatistical methods (Caers and Zhang 2004; Strebelle and Journel 2001) have been used to represent the channel structure for dynamic data history matching. The object-based modeling is dependent on the parameters to specify the object size, shape, and orientation. The method is usually limited to simple channel geometry and it can be difficult to condition the generated objects to dynamic production data and well observations. The multi-point geostatistical methods use training images to generate geologic realizations conditioned to the well observations. However, the success of the multi-point geostatistical methods depends on the appropriate selection of the training image. Pixel-based approach, such as discrete cosine transform, has been applied to re-parameterize channelized reservoirs for history matching (Jafarpour and McLaughlin, 2009; Xie et al., 2010). The advantage of pixel-based approach is that it is easy to preserve the channel structure.

Level set method is a numerical technique to track object interfaces and shapes (Osher and Sethian 1988; Osher and Fedkiw 2002). One advantage of the level set method is that it is very easy to perform computations involving curves and surfaces, which is a

good fit for reservoir modeling and history matching of channelized systems. Recently, level set approaches have been applied to reservoir modeling and history matching to preserve channel structure. Mondal et al. (2010) focused on parameterizing channel structure with a few points on channel boundaries. By perturbing those points, they can update channel boundary and alter the channel structure. A reversible jump Markov Chain Monte Carlo approach with varying parameter dimension is applied to automatically update channel boundary by adding, removing or perturbing those points on the channel boundary. However, this approach is difficult to use in 3-D examples because it is hard to parameterize the channel structure with a few points on the channel boundary in 3-D cases.

Nielsen et al. (2009) treated permeability field as a binary level set function and update the level set function with gradient based method. The gradient is given by using adjoint method in a reservoir simulator. Chang et al. (2010) used the level set function values at part of the grid nodes directly in Ensemble Kalman Filter updating. The level set function values at other nodes are obtained by numerical interpolation. By updating the level set function values, they are able to update channel reservoirs. Instead of updating the facies fields directly, Moreno et al. (2008) and Lorentzen et al. (2012) transformed the facies field into a signed distance function and updated the velocity field in level set equation by Ensemble Kalman Filter.

In our level set approach, the description of the facies boundaries will be based on parameterization of the velocity fields that deform the interfaces. We will mostly focus on smooth interfaces that will require smooth velocity fields in the level set methods. The space of smooth velocity fields can be parameterized with fewer parameters. Often some a priori knowledge about spatial range of facies boundaries is known. In these cases, we will introduce region-restricted parameterization for the velocity fields. The dimension reduction can be achieved for covariance-based velocity fields by re-parameterizing with SVD techniques. After parameterization, Markov Chain Monte Carlo (MCMC) method is utilized to perturb the coefficients of principal components of velocity field to update channel reservoir model matching production history. One advantage of this approach is that it is easy to condition the channel models to the facies observations at well locations by constraining the random velocity field to zero at well locations.

A significant part of the computational expense in any dynamic data integration method is the modeling of flow and transport through high resolution geologic models. To precondition these simulations, we will adopt multi-stage MCMC approaches to minimize the number of flow simulations during the MCMC sampling. In these approaches, simplified models, e.g., coarse-scale models, are run to screen the proposals before running a detailed fine-scale simulation (Ma et al., 2008).

We demonstrate the effectiveness of our approach using both 2-D and 3-D examples.

The 2-D example shows that the level set Markov chain approach can successfully match the data and identify the connectivity of the channels in the reference model. The 3-D result shows that the proposed approach can also be applied to channelized reservoirs with strong prior information.

3.2 Methodology

In this section, we first discuss the level set method and how we describe channel facies boundary using level set function. We also present the parameterization of velocity field and a two stage Markov Chain Monte Carlo method. In order to evolve channel facies boundary, a velocity field is used to perturb the level set function and a two stage Markov Chain Monte Carlo approach is applied to update the velocity field.

3.2.1 Level Set Methods

The level set method is a numerical technique to track interfaces and shapes of objects (Osher and Sethian 1988; Osher and Fedkiw 2002). The objects are usually described as a level set function and gradually evolved into other shapes using level set equation. In our methodology, we take the same idea:

1) Representing channel facies as a level set function;
2) Evolving channel boundaries into different shapes with level set equation.

In general, our goal is to define a family of level set functions, ϕ that represent the facies boundaries and a mechanism for perturbing the level set functions. One of the challenges is evolving level set functions within iterative sampling techniques. In our approaches,

the initial level set function is given and the perturbation is proposed via adding a convective term that comes from the discretization of tracer equation

$$\frac{\partial \phi}{\partial t} + \mathrm{v}(x) \cdot \nabla \phi = 0 \tag{3.1}$$

where $\mathrm{v}(x)$ is velocity field vector that is used to evolve facies boundaries and t is a pseudo time used for evolving the interface. This equation allows us to parameterize channel facies boundaries via velocity field parameterization. Mondal et al. (2010) applied this idea to simple channel geometries and represented facies parameterization via smooth velocity parameterization. In the velocity space, various reduced parameterization techniques can be easily applied.

In our work, we first choose signed distance function as our indicator function motivated by Moreno et al. (2008) and Lorentzen et al. (2012). The signed distance function is defined as the minimum distance between any points in the space toward the facies boundary. One advantage of using signed distance function instead of using initial facies directly is that we could avoid discontinuous implicit surface. If the point is in the positive region, it is assigned as a positive distance. If it is in the negative region, it is assigned as a negative distance. Instead of calculating actual minimum distance between any points and the facies boundary, signed distance function can be achieved by evolving the re-initialization equation to steady state:

$$\frac{\partial \phi}{\partial t} + \mathrm{sign}(\phi_0)(\|\nabla \phi\| - 1) = 0 \tag{3.2}$$

$$\text{sign}(\phi) = \begin{cases} -1 & \phi \text{ in non} - \text{channel facies} \\ 1 & \phi \text{ in channel facies} \end{cases}$$

In the re-initialization equation, the input ϕ_0 denotes initial facies, in which channel is described as +1 and non-channel is described as -1. After reaching steady state, first term (time derivative) equals to zero. Thus, second term should also be zero, which leads to a very nice property of signed distance function. $\|\nabla\phi\| = 1$. The signed distance function ϕ has the same zero contour as initial facies ϕ_0, which means that signed distance function preserves facies boundaries of initial facies. **Figure 3.1** shows an example of channel facies and corresponding signed distance function.

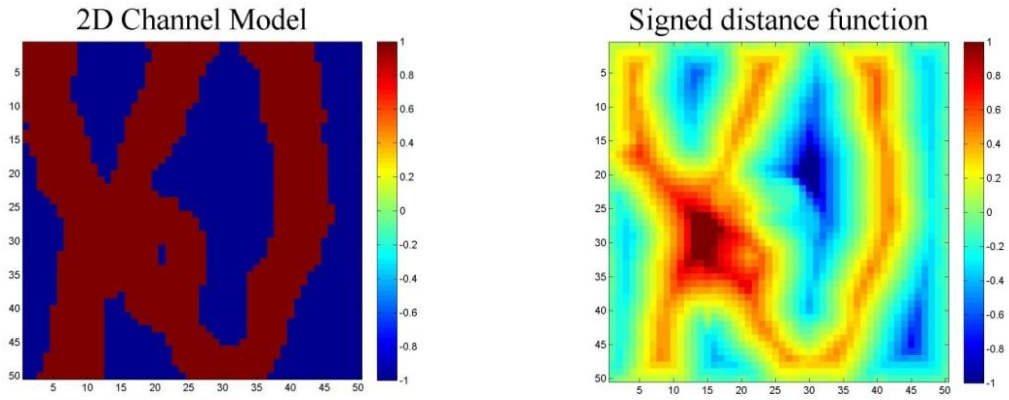

Figure 3.1 2-D channelized facies versus signed distance function

After representing channel facies as a level set function, we start evolving channel boundaries using the level set equation – motion in the normal direction:

$$\frac{\partial \phi}{\partial t} + \mathrm{v}(x)\|\nabla \phi\| = 0 \tag{3.3}$$

where ϕ denotes the signed distance function and $\mathrm{v}(x)$ (scalar field) is the velocity field in normal direction. With the property of signed distance function, $\|\nabla \phi\| = 1$, the level set equation can be rewritten as

$$\frac{\phi^{t+1} - \phi^{t}}{\Delta t} + \mathrm{v}(x) = 0 \tag{3.4}$$

We can write the equation in this way,

$$\phi^{u} = \phi - \mathrm{v}(x)\Delta t \tag{3.5}$$

In this equation, ϕ denotes the signed distance function, ϕ^{u} is updated function, $\mathrm{v}(x)$ is velocity field in normal direction and Δt denotes the step size. This equation represents the update of the channel boundaries given velocity field and a step size.

In this chapter, we assume permeability is associated with facies model and constant permeability inside each facies. One can also take variable permeability field within channels described by two-point correlation functions as it is done in Mondal et al. (2010). With updated function, we could easily generate updated facies model and then properties associated with facies as follows. **Figure 3.2** shows an example of updated function and corresponding updated facies model. Comparing to **Figure 3.1**, we can

clearly identify the channel boundary movement.

$$k = k_1 H(\phi^u) + k_2\big(1 - H(\phi^u)\big) \tag{3.6}$$

$$H(\phi^u) = \begin{cases} 0 & \phi^u < 0 \\ 1 & \phi^u > 0 \end{cases}$$

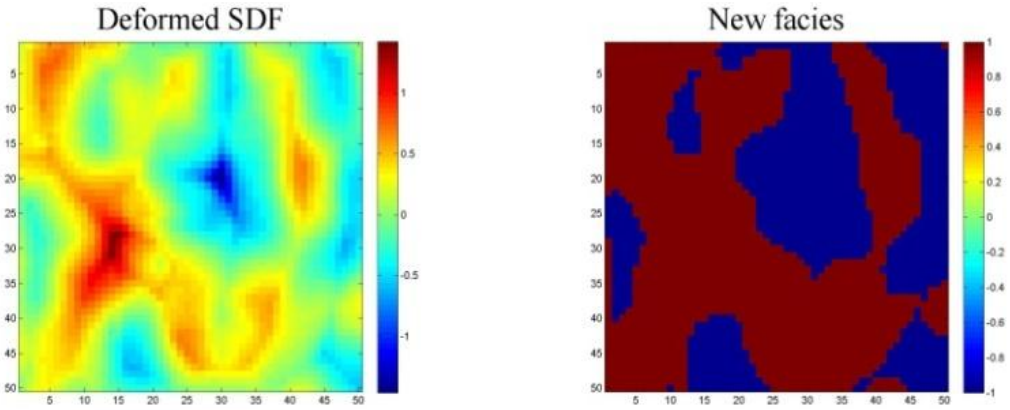

Figure 3.2 The updated function versus corresponding updated facies model

3.2.2 Velocity Parameterization

Often some a priori knowledge about spatial range of facies boundaries is known. In these cases, we introduce region-restricted parameterization for the velocity fields with the focus only on the region of interest. A dimension reduction can be achieved for covariance-based velocity fields by re-parameterizing with weighted principal component analysis.

We start with generating a velocity library of Gaussian random fields using sequential Gaussian simulation in SGeMS (Remy et al., 2009). The generated Gaussian random fields are conditioned at well locations. We will discuss why we need to condition the velocity field at well locations later. The size of velocity library depends on the resolution, velocity variations (such as variogram parameters) and size of restricted region. The purpose is to cover all the possible channel movements in the region of interest. If prior knowledge about the channel facies is known, it could help us reduce the size of the velocity library. This is a pre-process before performing history matching.

Weighted principal component analysis is applied to re-parameterize restricted regions of velocity field. The restricted regions could be the whole reservoir or a portion of reservoir based on prior knowledge and uncertainty one can allow. The covariance matrix $\boldsymbol{C}$ is computed as

$$\boldsymbol{C} = \left(\sqrt{w}\boldsymbol{X}\right)\left(\sqrt{w}\boldsymbol{X}\right)^{T} \tag{3.7}$$

where, matrix $\boldsymbol{X}$ denotes the velocity library restricted to the region of interest. Thus, the size of the covariance matrix $\boldsymbol{C}$ is usually limited to thousands by thousands, which is possible to generate. Vector w denotes the weight for each grid blocks inside restricted regions. In this part, we choose reciprocal of absolute sighed distance function $1/|\phi|$ as our weight function. More aggressively, one may choose $\exp(-|\phi|)$ as your weight function. This will put more weight at regions near channel boundaries.

$$\boldsymbol{V}^{-1}\boldsymbol{\Lambda}\boldsymbol{V} = \boldsymbol{C} \tag{3.8}$$

After singular value decomposition, velocity field v(x) is constructed with a few largest eigenvalues of $\boldsymbol{\Lambda}$ and corresponding eigenvectors that are contained in $\boldsymbol{V}$. The eigenvalues and eigenvectors are selected based on the cumulative energy cut-off. The representation of the velocity field is given by

$$\mathrm{v}(x) = \sum_{i=1}^{N} a_i \sqrt{\boldsymbol{\Lambda}_{ii}} \boldsymbol{V}_i \tag{3.9}$$

where, a_i denotes coefficients for each eigenvectors. By perturbing these coefficients, we can generate velocity field and in term, update facies boundaries. Therefore, these coefficients are our parameters for history matching. A two stage Markov Chain Monte Carlo method is utilized to perturb these coefficients to match production history.

3.2.3 Two Stage Markov Chain Monte Carlo (MCMC) Method

We will start with a brief review of the MCMC method and the Metropolis-Hastings sampling algorithm. Our objective is to sample the permeability field $\boldsymbol{k}$ from a posterior distribution that is conditioned to the dynamic observation data $\boldsymbol{d}_{obs}$ and the prior permeability $\boldsymbol{k}_{prior}$. From Bayes' theorem, the posterior distribution can be expressed as

$$\pi(\boldsymbol{k}) = P(\boldsymbol{k}|\boldsymbol{d}_{obs}) \propto P(\boldsymbol{d}_{obs}|\boldsymbol{k})P(\boldsymbol{k}) \tag{3.10}$$

where, $P(\boldsymbol{k})$ denotes prior probability distribution for permeability and $P(\boldsymbol{d}_{obs}|\boldsymbol{k})$ denotes the likelihood function that links dynamic data and the prior model. The main idea is to construct a Markov chain whose stationary distribution will be given by $\pi(\boldsymbol{k})$. If we assume a Gaussian distribution for the prior model and the data errors, the posterior distribution can be written as

$$\pi(\boldsymbol{k}) = P(\boldsymbol{k}|\boldsymbol{d}_{obs}) \propto \exp\left\{-\frac{1}{2}\begin{bmatrix}(\boldsymbol{k}-\boldsymbol{k}_{prior})^T \boldsymbol{C_k^{-1}}(\boldsymbol{k}-\boldsymbol{k}_{prior}) \\ +(g(\boldsymbol{k})-\boldsymbol{d}_{obs})^T \boldsymbol{C_D^{-1}}(g(\boldsymbol{k})-\boldsymbol{d}_{obs})\end{bmatrix}\right\} \quad (3.11)$$

where, $g(\boldsymbol{k})$ is the simulated reservoir response corresponding to the proposed permeability field $\boldsymbol{k}$. Matrices $\boldsymbol{C_k}$ and $\boldsymbol{C_D}$ are the parameter covariance and the data covariance respectively. The Metropolis-Hastings MCMC algorithm (Hastings 1970; Metropolis et al. 1953) is usually applied to sample from the posterior distribution. In this algorithm, the probability to accept a proposal for transition to state $\boldsymbol{k}$ from $\boldsymbol{k}_n$ is

$$\rho(\boldsymbol{k}_n, \boldsymbol{k}) = \min\left(1, \frac{\pi(\boldsymbol{k})q(\boldsymbol{k}_n|\boldsymbol{k})}{\pi(\boldsymbol{k}_n)q(\boldsymbol{k}|\boldsymbol{k}_n)}\right) \quad (3.12)$$

Thus, accept $\boldsymbol{k}_{n+1} = \boldsymbol{k}$ with probability $\rho(\boldsymbol{k}_n, \boldsymbol{k})$, and $\boldsymbol{k}_{n+1} = \boldsymbol{k}_n$ with probability $1 - \rho(\boldsymbol{k}_n, \boldsymbol{k})$.

The goal of the two stage method is to improve the acceptance rate of the traditional MCMC methods without sacrificing the rigor in its sampling properties or convergence rates. This is accomplished by prescreening the proposals to weed out proposals that are

likely to be rejected. This prescreening utilizes an approximate likelihood computation using a proxy model for obtaining the flow response. In our case, the proxy is a coarse-scale simulation of the flow response. The coarse-scale model is constructed via a single phase upscaling of the fine-scale model. The two stage MCMC sampling proceeds as follows (Ma et al., 2008; Mondal et al., 2010):

Suppose the chain is at the n^{th} step having permeability $\boldsymbol{k}_n$:

1. Make a model proposal $\widetilde{\boldsymbol{k}}$ conditioned to permeability observations. The proposed fine-scale permeability field is upscaled using a single phase flow-based upscaling algorithm. A coarse-scale simulation is carried out to compute the likelihood and the corresponding posterior is given by $\pi^*(\widetilde{\boldsymbol{k}})$
2. Accept the model proposal $\widetilde{\boldsymbol{k}}$ with probability

$$\alpha_p(\boldsymbol{k}_n, \widetilde{\boldsymbol{k}}) = \min\left\{1, \frac{\pi^*(\widetilde{\boldsymbol{k}})q(\boldsymbol{k}_n|\widetilde{\boldsymbol{k}})}{\pi^*(\boldsymbol{k}_n)q(\widetilde{\boldsymbol{k}}|\boldsymbol{k}_n)}\right\} \tag{3.13}$$

If we choose instrumental probability distribution $q(\cdot \mid \cdot)$ to be symmetric, we have acceptance rate:

$$\alpha_p(\boldsymbol{k}_n, \widetilde{\boldsymbol{k}}) = \min\left\{1, \frac{\pi^*(\widetilde{\boldsymbol{k}})}{\pi^*(\boldsymbol{k}_n)}\right\} \tag{3.14}$$

$$\boldsymbol{k} = \begin{cases} \widetilde{\boldsymbol{k}} & \text{with probability } \alpha_p(\boldsymbol{k_n}, \widetilde{\boldsymbol{k}}) \\ \boldsymbol{k_n} & \text{with probability } 1 - \alpha_p(\boldsymbol{k_n}, \widetilde{\boldsymbol{k}}) \end{cases}$$

If the proposal is accepted, we compute the exact likelihood and the corresponding posterior $\pi(\boldsymbol{k})$ using fine scale simulation and go to step 3; If the proposal is rejected, we go back to step 1.

3. Accept $\boldsymbol{k}$ as a sample with probability

$$\alpha_f(\boldsymbol{k_n}, \boldsymbol{k}) = \min\left\{1, \frac{\pi(\boldsymbol{k})\pi^*(\boldsymbol{k_n})}{\pi(\boldsymbol{k_n})\pi^*(\boldsymbol{k})}\right\} \tag{3.15}$$

$$\boldsymbol{k_{n+1}} = \begin{cases} \boldsymbol{k} & \text{with probability } \alpha_f(\boldsymbol{k_n}, \boldsymbol{k}) \\ \boldsymbol{k_n} & \text{with probability } 1 - \alpha_f(\boldsymbol{k_n}, \boldsymbol{k}) \end{cases}$$

The detailed argument is given in Ma et al. (2008). With two stage Markov Chain Monte Carlo method, we are able to sample the posterior distribution more efficiently.

3.2.4 Conditioning Channelized Reservoir to Observation Data

In this part, we explain how we condition our updated facies models to two types of observation data: facies types and sand shale ratio. Recall that our Gaussian random fields are conditioned to zero at well locations as mentioned before. Thus, it won't change the sign of updated function vs. signed distance function at well locations. For example, if producer 1 is in channel facies. The signed distance function at producer 1 will be a positive value and updated function at producer 1 remains positive because the velocity at this specific location is zero. Therefore, the updated facies will remain channel facies. The conditioning to facies types could be considered as a hard constraint. On the other hand, conditioning to sand shale ratio is a soft constraint. We treat the sand

shale ratio from core analysis as an observation data and insert into objective function with a fairly large weight. The calculated sand shale ratio from simulation will be close to observed one through Markov chain process.

3.3 Workflow

To summarize methodology section, the procedures for our approach are as follows. Stop criterion is either a predefined number of posterior samples or a maximum number of iterations. A flowchart of our approach is shown in **Figure 3.3**.

1. Represent initial facies model using signed distance function;
2. Generate a velocity library and perform weighted principal component analysis;
3. Construct velocity field and updated facies with perturbation of coefficients;
4. Generate Permeability field as fine scale model from updated facies;
5. Upscale to get coarse scale model using single phase flow-based upscaling;
6. Run coarse scale model and calculate objective function for coarse scale model. Check acceptance. If accepted, go to step 7; if rejected, go to step 3;
7. Run fine scale model and calculate objective function for fine scale model. Check acceptance. If accepted, go to step 8; if rejected, go to step 3;
8. Update the current facies model and objective function, and then go to step 3;
9. Collect samples until stop criterion is met.

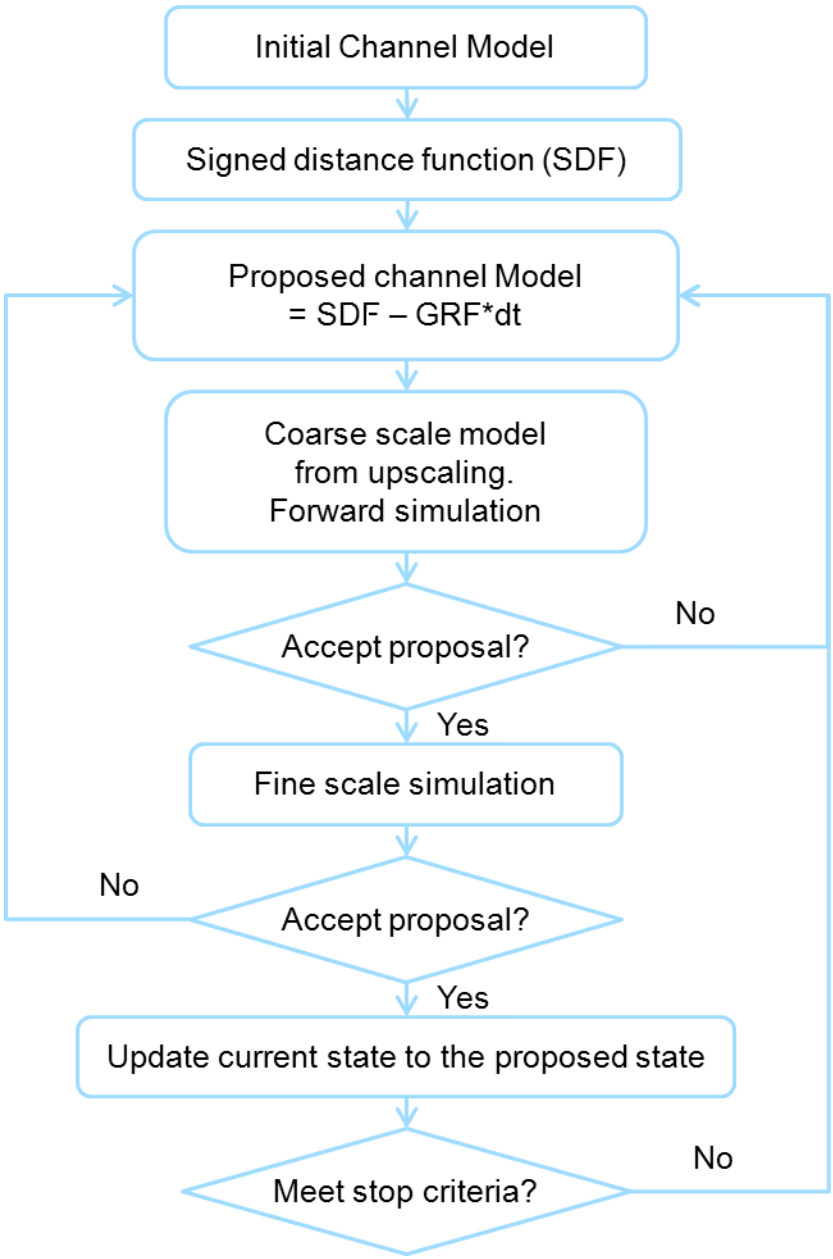

Figure 3.3 Workflow for our proposed approach

3.4 Applications

In this section, we apply our approach to both 2-D and 3-D channelized reservoir examples. In 2-D example, our objective is to reproduce the channel structure and identify large scale continuities in the reservoir during dynamic data integration. In 3-D example, we assume the initial model is not too far from true model. The purpose is to match production history while making limited facies boundary movement.

3.4.1 A 2-D Example

We consider a 2-D synthetic example that involves water-flooding in a channelized system. The model contains 50x50 grid blocks. There are 4 producers and 3 injectors: producers started with oil production rate control at 500 bbl/day and later reached bottom hole pressure limit at 1000 psi; injectors are with bottom hole pressure control all the time.

In order to get the contrast between channel and non-channel facies, permeability at channel facies is set to 300 md and permeability at non-channel facies is 1 mD. **Figure 3.4** shows the initial and true permeability field with locations of producer (black) and injector (blue). Both are generated from a training image using SNESIM (Remy et al., 2009). Comparing two permeability fields, we can see that both channel orientation and channel connectivity are quite different. For example, channel in true model is oriented in north-west and south-east direction while channel in initial model is oriented in north and south direction. The differences in channel connectivity are circled out in white

color.

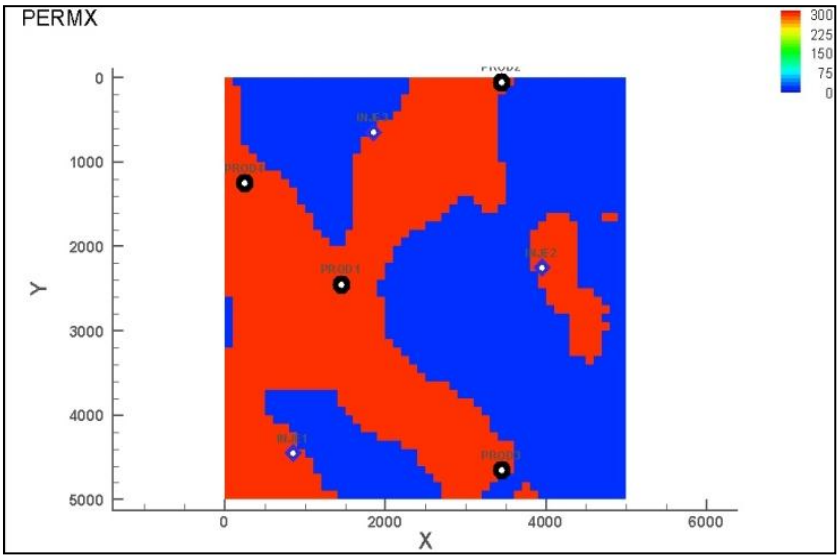

a) Reference channelized permeability field

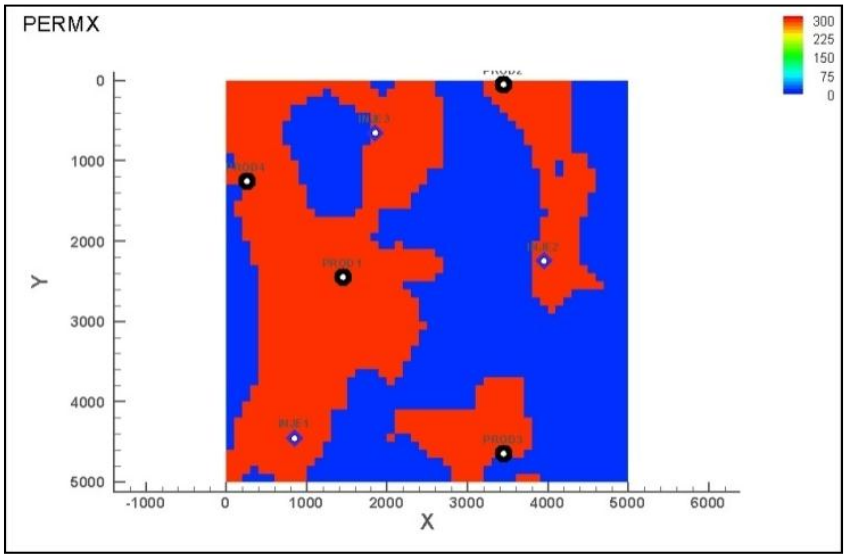

b) Initial channelized permeability field

Figure 3.4 Permeability and well locations in 2-D example: a) reference channelized permeability and b) initial channelized permeability

5,000 velocity fields are generated with conditioning to facies types at well locations, and then weighted PCA is applied to velocity fields at the whole reservoir. After singular value decomposition, largest 18 eigenvalues and eigenvectors are selected with 95% cumulative energy cut-off. We try to match the oil production rate, water-cut, producer BHP and injection rate using a two stage Markov Chain Monte Carlo method. In order to ensure the convergence, multiple Markov chains with 3,000 simulations each are carried out from same initial model. To speed up the MCMC algorithm, simulation grid is upscaled from 50x50 to a 10x10 coarse-scale model using single phase flow-based upscaling as a first stage filter to screen out the undesired proposals. The results for data misfit as a function of the number of sample are plotted in **Figure 3.5**.

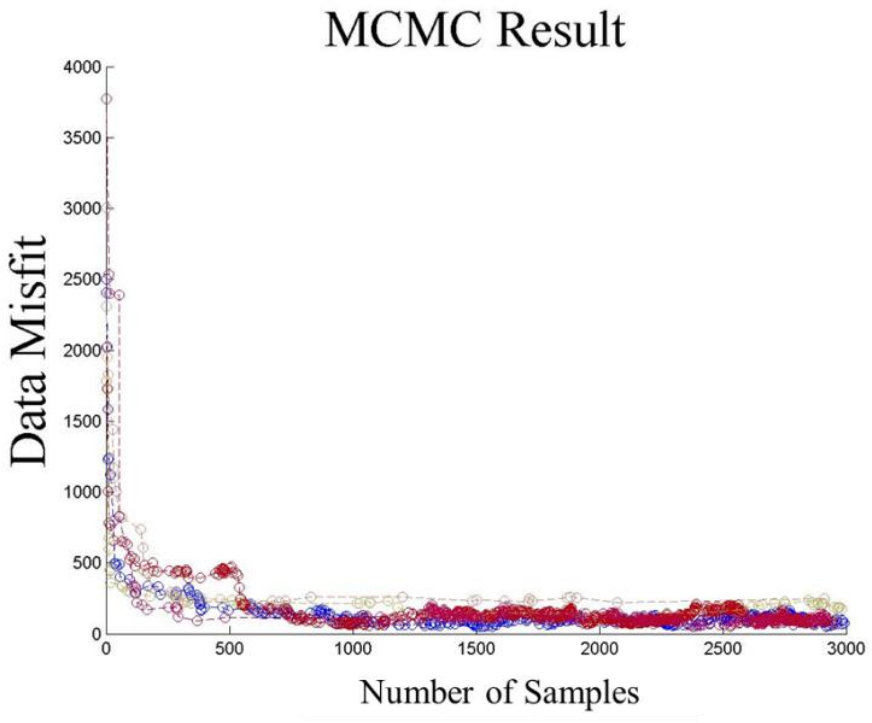

Figure 3.5 Data misfit versus number of samples (Markov chain in 2-D example)

After convergence, models are sampled from all the accepted models. Four updated models are plotted on the left compared to initial and true model shown in **Figure 3.6**. In updated models, we are able to restore the channel connectivity from true model. However channel orientation is not recovered perfectly because velocity angle specified when generating velocity library is not wide enough to cover the orientation in true model. In this case, sand shale ratio in initial model is fairly close to the ratio in true model. Sand shale ratio constraint is loosened in order to get a good history match for dynamic production data. This is the reason that sand shale ratios in updated models are not very good. But they are still fairly close to the ratio in true model.

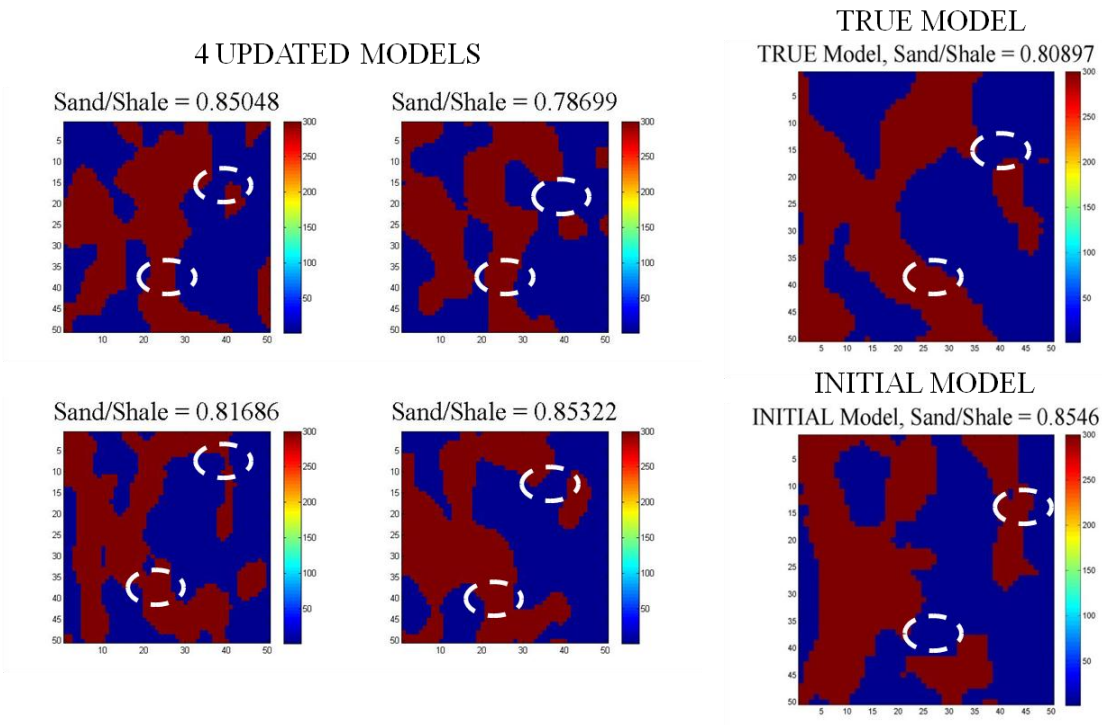

Figure 3.6 Updated permeability fields versus true and initial permeability field in 2-D example

Dynamic data history matching results are very good compared to production data of true model as shown in **Figure 3.7** (Red dot is observation data; green line is initial and blue is updated match). Next, we look at an example – injection rate of injector 2, which is the blue dot in top right. In true model, injector 2 is isolated from other producers. However, it is connected to producer 2 and gives pressure support in initial model. This is the reason that injection rate in initial model is much more than rate in the true model shown in **Figure 3.7d**. During history matching, the channel between those two (injector 2 and producer 2) are disconnected, leading to a much improved result. Also these history matching results clearly demonstrate that the two stage MCMC method could be used to efficiently sample the posterior distribution during channelized reservoir history matching.

3.4.2 A 3-D Example

The 3-D example is a two phase flow water-flooding case with 50x50x6 grid size. The channelized reservoir model is generated using FLUVSIM, a program for object-based stochastic modeling of fluvial system (Deutsch and Tran, 2002). The reference and initial model are shown in **Figure 3.8**. Permeability at channel facies is set to 300 md and permeability at non-channel facies is 1 mD. There are 3 producers and 3 injectors: producers with oil production rate control and injectors with bottom hole pressure control.

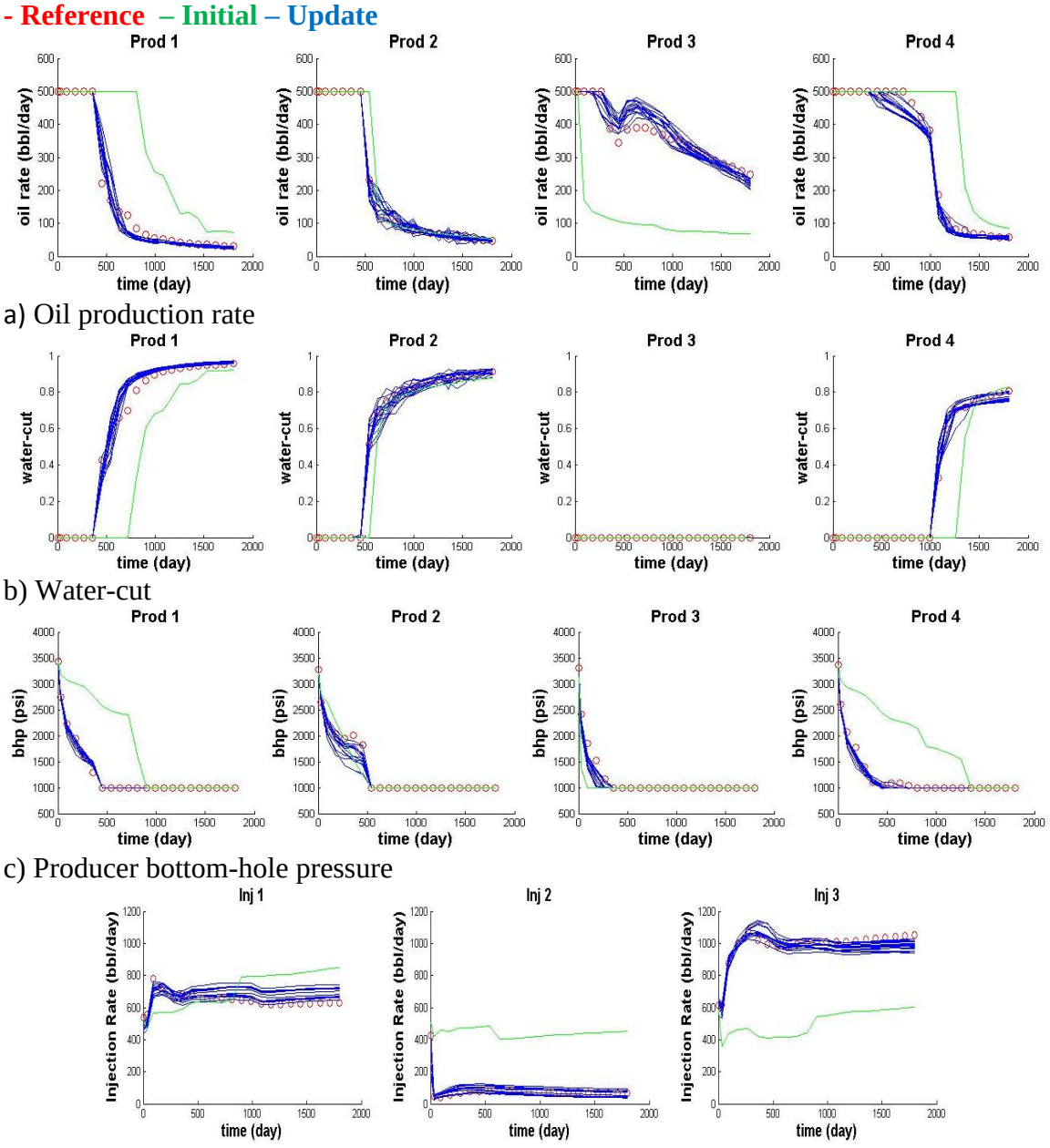

a) Oil production rate

b) Water-cut

c) Producer bottom-hole pressure

d) Injection rate

Figure 3.7 History matching results in 2-D example (reference in red dot, initial in green and updated in blue color): a) oil production rate, b) water-cut, c) producer bottom hole pressure and d) injection rate

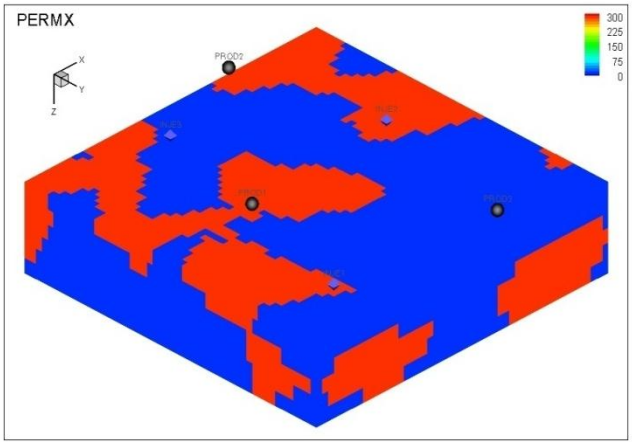

a) True permeability field

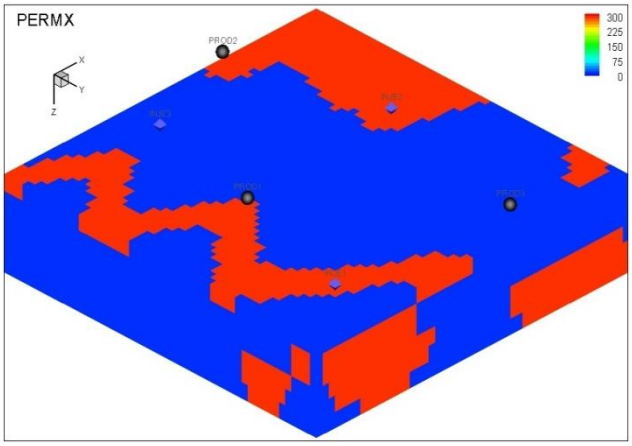

b) Initial permeability field

Figure 3.8 Permeability and well locations of 3-D example

Ten thousand velocity fields are generated with conditioning to facies types at well locations. Weighted PCA is then applied to velocity field inside a restricted region. The region is defined by a signed distance function cut-off $|\phi| \leq 1.8$. After singular value decomposition, largest 35 eigenvalues and eigenvectors are selected with 90%

cumulative energy cut-off. We try to match the oil production rate, water-cut, producer BHP and injection rate using a two stage Markov Chain Monte Carlo method. In order to ensure the convergence, multiple Markov chains with 1,000 simulations each are carried out from same initial model. To speed up the MCMC algorithm, simulation grid is upscaled from 50x50x6 to a 10x10x6 coarse-scale model using single phase flow-based upscaling as a first stage filter to screen out the undesired proposals. The results for data misfit as a function of the number of sample are plotted in **Figure 3.9**.

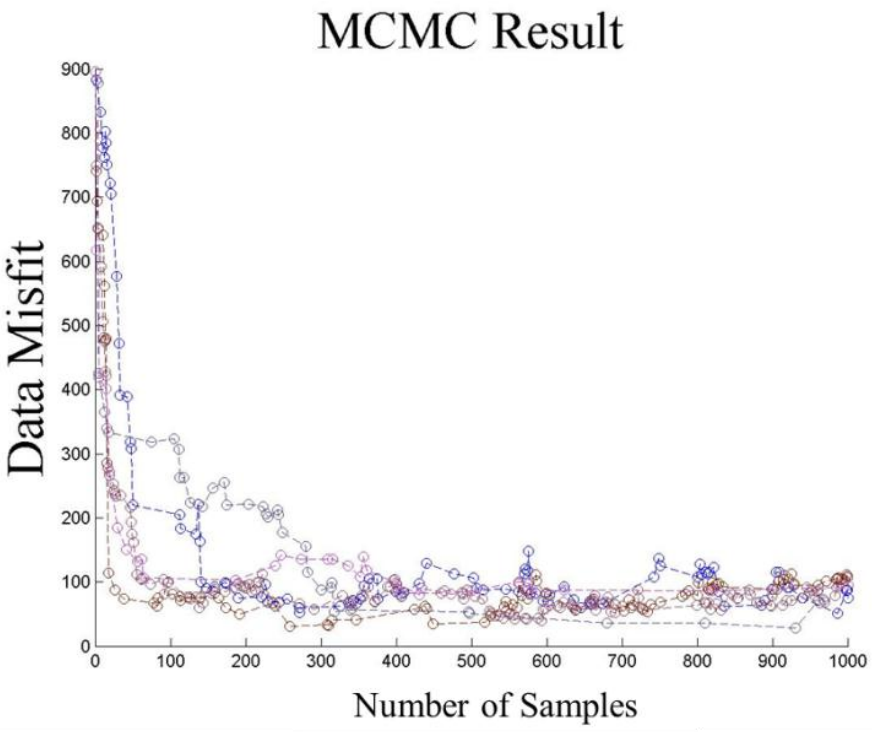

Figure 3.9 Data misfit versus samples (Markov chain in 3-D example)

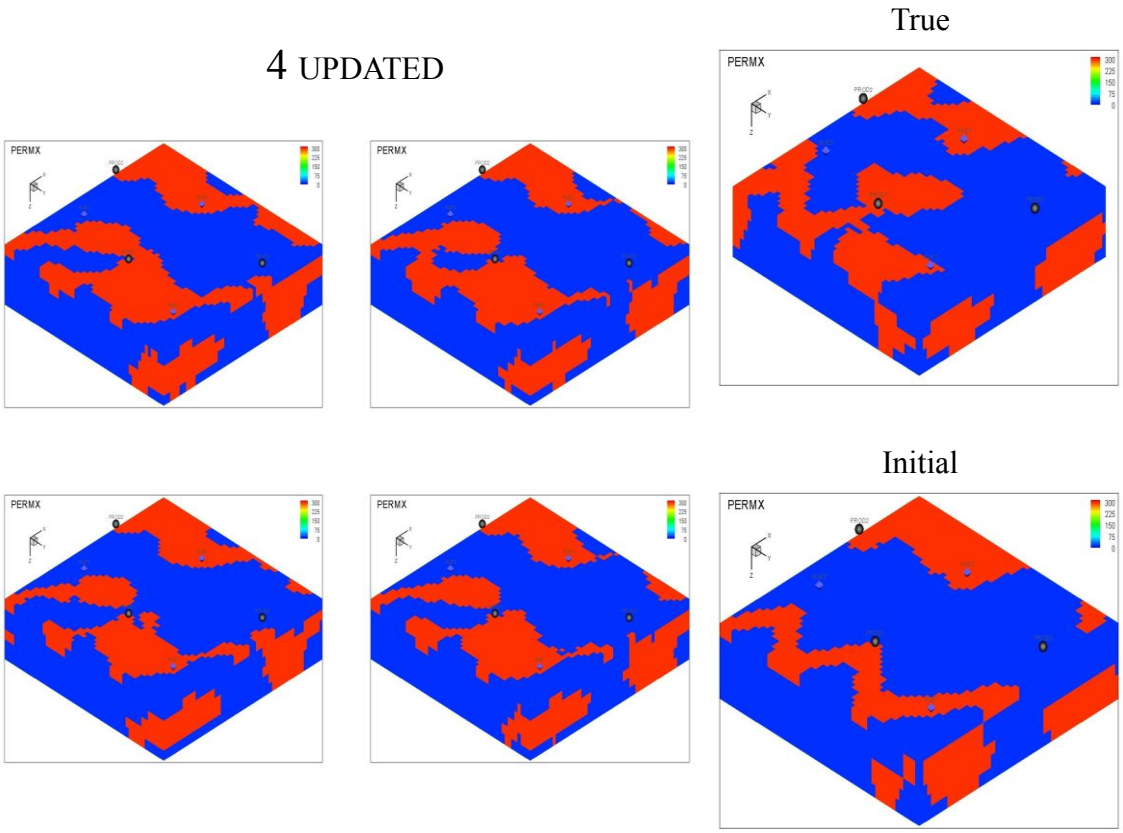

Figure 3.10 Updated permeability fields versus true and initial permeability field in 3-D example (3-D view)

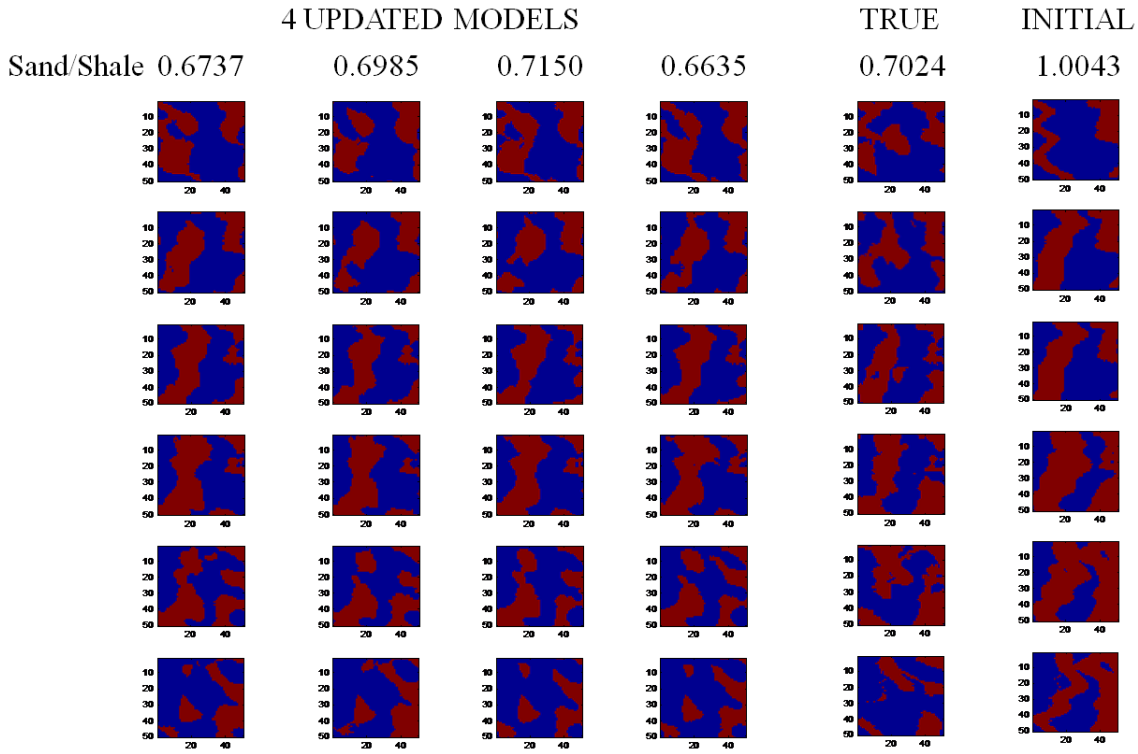

Figure 3.11 Updated permeability field versus true and initial permeability field in 3-D example (layer view)

- Reference – Initial – Update

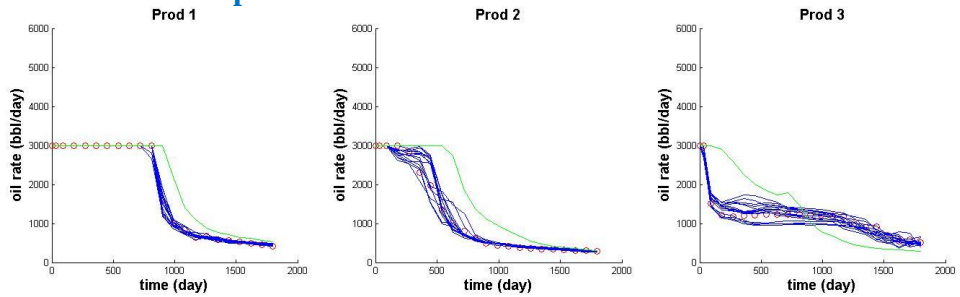

a) Oil production rate

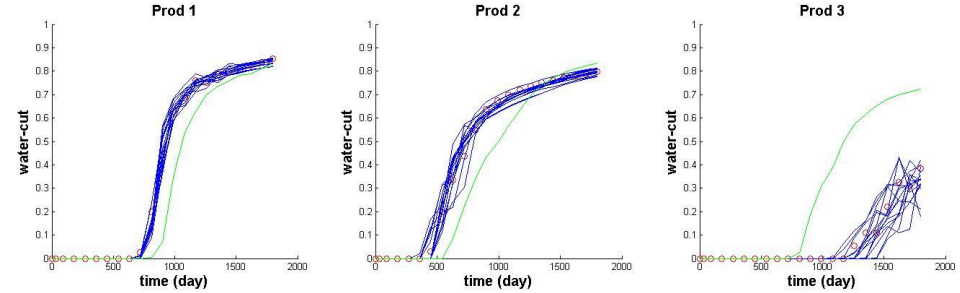

b) Water-cut

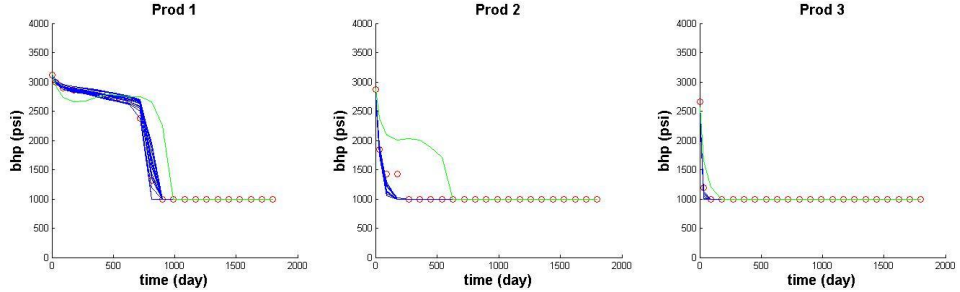

c) Producer bottom-hole pressure

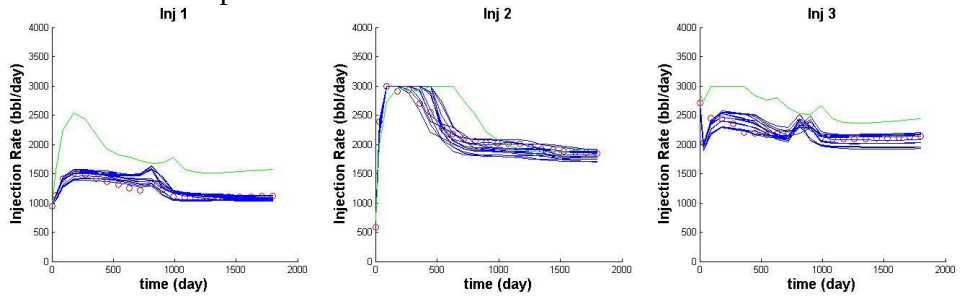

d) Injection rate

Figure 3.12 History matching results in 3-D example (reference in red dot, initial in green and updated in blue color): a) oil production rate, b) water-cut, c) producer bottom hole pressure and d) injection rate

Four collected samples are compared to the reference model and the initial model in **Figure 3.10** and **Figure 3.11**. **Figure 3.10** is the comparison in 3-D view and **Figure 3.11** is the comparison in layer view. From two figures, we observe that the difference between the initial and the true permeability field is not very big: similar channel orientation and similar channel connectivity. However, dynamic data between the initial and the true model are quite different shown in **Figure 3.12** (Red dot is observation data; green is initial data; and blue is updated data). The purpose of this example is to demonstrate that we are able to match the dynamic data history with limited channel boundaries movement inside a restricted region. After history matching, **Figure 3.12** shows updated production information compared to results from initial and true model. In this case, sand shale ratios in updated models are also improved substantially compared to the ratio in the initial and the true model. These results indicate that the application of the two stage MCMC method can be extended to a 3D channelized example.

To summarize this section, our proposed approach is successful in both 2-D and 3-D examples. In 2-D example, it helps identifying the channel connectivity while matching dynamic production history. In 3-D example, with a good prior model, it matches production data with limited channel boundary movements.

3.5 Summary

In this chapter, we presented a level set Markov chain approach for history matching and uncertainty quantification for channelized reservoirs using a two stage Markov Chain Monte Carlo method. This approach is based on level set representation of channel boundaries. Specifically, signed distance function is used to represent channelized features in the reservoir and channel structure is then updated by perturbing the signed distance function with a velocity field constrained at well locations. The velocity field can be generated with eigenvalue decomposition of large number of training velocities. The parameters representing the channel structure are the coefficients of velocity eigenvectors. A two stage sampling method is utilized to improve efficiency of Markov Chain Monte Carlo method and sample the posterior distribution rigorously.

We demonstrate the effectiveness of our approach using both 2-D and 3-D examples. The 2-D example shows that the level set Markov chain approach can successfully match the data and identify the connectivity of the channels in the reference model. The 3-D result shows that the proposed approach can also be applied to channelized reservoirs with prior information. The MCMC algorithms naturally provide multiple realizations of the permeability field conditioned to well and production data and thus, allow for uncertainty quantification in the forecasting.

CHAPTER IV
HISTORY MATCHING CHANNELIZED RESERVOIRS USING REVERSIBLE JUMP MARKOV CHAIN MONTE CARLO METHODS[§]

In this chapter, we present a different approach for history matching and uncertainty quantification for channelized reservoirs using Reversible Jump Markov Chain Monte Carlo (RJMCMC) methods. Our objective is to efficiently sample realizations of channelized permeability fields conditioned to production data and permeability values at the wells.

In our approach, the channelized permeability field is parameterized using the Discrete Cosine Transform (DCT). The parameters representing the channel structure are the coefficients in truncated frequency domain. The parameter space is searched using a RJMCMC, where the dimension of the parameter space is assumed to be unknown. For each step of the RJMCMC, the dimension of the uncertainty space can be increased or decreased according to a prescribed prior distribution. This flexibility in the parameter dimension allows an efficient search of the uncertainty space. To speed up the computation and improve the acceptance rate of the RJMCMC algorithm, we employ two-stage methods whereby coarse-scale simulations are used to screen out the

undesired proposals. After simulations, multi-dimensional scaling and cluster analysis are used to select realizations from the accepted models to adequately represent the diversity of the models.

We demonstrate the effectiveness of the RJMCMC algorithm using both 2D and 3D examples involving water-flooding history matching. The 2-D example shows that the RJMCMC algorithm appears to successfully match the data and identify the orientation of the channels in the reference model. The 3-D results show that the proposed algorithm may determine the large-scale features of the reference channelized permeability field based on the production data. The MCMC algorithms naturally provide multiple realizations of the permeability field conditioned to well and production data and thus, allow for uncertainty quantification in the forecasting.

4.1 Introduction

Subsurface is complex geological formation encompassing a wide range of physical and chemical heterogeneities. The goal of stochastic models is to characterize its different attributes such as permeability, porosity, fluid saturation etc. Flow in the subsurface is primarily controlled by the connectivity of the extreme permeability (high and low) which is generally associated with geological patterns that create preferential flow paths/barriers.

In many geologic environments, the distribution of subsurface properties is closely

associated with the location and distribution of distinct geologic facies with sharp contrasts in properties across facies boundaries (Weber 1982). For example in a fluvial setting, high permeability channel sands are often embedded in a nearly impermeable background causing the dominant fluid movement to be restricted within these channels. Under such conditions, the orientation of the channels and channel geometry determine the flow behavior in the subsurface rather than the detailed variations in properties within the channels. Traditional geostatistical techniques for subsurface characterization have typically relied on variograms that are unable to reproduce the channel geometry and the facies architecture (Haldorsen and Damsleth 1990; Koltermann and Gorelick 1996; Dubrule 1998). Discrete Boolean or object-based models can reproduce geologically realistic shapes and have been successfully used to model fluid flow and transport in many fluvial type environments (Egeland et al. 1993). The success of these object-based models, however, is heavily dependent on the parameters to specify the object size, shapes, proportion and orientation. Typically, these parameters are highly uncertain, particularly in the early stages of subsurface characterization (Dubrule 1998; Caumon et al. 2004). For example, in a channel type environment, the channel sands may be observed at only a few well locations. There are many plausible channel geometries that will satisfy the channel sand and well intersections. Thus, the stochastic models for channels will require specification of random variables that govern the channel principal direction, its horizontal and vertical sinuosity, channel width to thickness ratio etc. All these parameters have considerable uncertainty associated with them and will profoundly impact fluid flow in the subsurface.

A considerable amount of prior information is typically available for building the facies models for fluid flow simulation (Weber 1982). These include well logs and cores, seismic data and geologic conceptualization based on outcrops and analogues. Although the prior information play a vital role in reducing uncertainty and preserving geologic realism, it is imperative that the geologic models reproduce the dynamic response based on the flow and transport data. These include pressure measurements at the wells, tracer concentration histories and in the case of multiphase flow, the production of individual phases at the wells. The reproduction of dynamic data is a necessary step to have credibility in our geologic and flow modeling and confidence in any performance forecasting.

The representation and history matching of channelized reservoirs are challenging because of the difficulties to reproduce the large-scale continuity of the channel structure and identify the channel geometry and its orientation. The traditional two-point geostatistical techniques for reservoir characterization are unable to reproduce the channel geometry and the facies architecture (Haldorsen and Damsleth 1990; Koltermann and Gorelick 1996; Dubrule 1998). As an alternative, object-based modeling (Deutsch and Wang 1996) and more recently, multi-point geostatistical methods (Caers and Zhang 2004; Strebelle and Journel 2001) have been used to represent the channel structure for dynamic data history matching. The object-based modeling is dependent on the parameters to specify the object size, shape, and orientation. The method is usually limited to simple channel geometry and it can be

difficult to condition the generated objects to dynamic production data and well observations. The multi-point geostatistical methods use training images to generate geologic realizations conditioned to the well observations. However, the success of the multi-point geostatistical methods depends on the appropriate selection of the training image.

Conventional history matching methods very often fail to preserve the large-scale channel continuity during dynamic data integration. To circumvent the problem, in this chapter we reparameterize the permeability distribution with a few global parameters. Specifically, we adopt the idea of discrete cosine transform (DCT) parameterization and consider truncated DCT frequency domain as the parameter space for representing channelized reservoirs (Jafarpour and McLaughlin 2009). We then use Reversible Jump Markov Chain Monte Carlo methods to explore the parameter space to condition the channelized reservoir models to dynamic production data and well permeability observations. Use of RJMCMC allows us to dynamically select the important DCT coefficients to represent the channel structure as the chain proceeds. In conventional MCMC methods, the dimension of parameter space is kept fixed. The number of parameters needs to be selected a priori, often resulting in a higher dimensional parameter space, longer computational time and slower convergence.

The Reversible Jump Markov Chain Monte Carlo (RJMCMC) method was originally proposed in statistics (Green 1995). The method has been applied to history matching

channelized reservoirs by explicitly sampling and moving the channel boundaries (Mondal et al. 2010). In RJMCMC methods, the dimension of parameter space is flexible, which allows an efficient sampling of the uncertainty space with fewer DCT coefficients. The dimension transition is performed by a birth or a death step at each of iteration of the RJMCMC method. In the birth step, we add one DCT coefficient and thus increase the dimension by one whereas in the death step, we delete one DCT coefficient from current DCT subset and reduce the dimension by one. We also have a jump step that allows us to make a random walk as in conventional MCMC methods. Thus, in RJMCMC method, we are able to dynamically identify the important DCT coefficients by adding or dropping the coefficients.

To speed up the RJMCMC algorithm, we employ a two-stage method to improve model proposals (Ma et al. 2008). In two-stage methods, a coarse-scale simulation is first used as a filter to screen out the undesired proposals during MCMC simulation. The coarse-scale model is obtained via upscaling the fine-scale permeability model using single phase flow-based upscaling. It has been shown that the two-stage MCMC methods can improve the acceptance rate of Markov chain (Ma et al. 2008). We also propose a conditioning step to honor the well permeability observations after each model proposal during MCMC.

4.2 Approach

In this section, we first discuss the channelized reservoir parameterization using the

discrete cosine transform (DCT). We then introduce the two-stage RJMCMC methods to sample the truncated DCT domain for conditioning channel models to well and production data. The RJMCMC approach will result in multiple realizations of the geologic model. We summarize this section with an outline of the workflow of our approach.

4.2.1 Parameterization Using the Discrete Cosine Transform

The use of the discrete cosine transform (DCT) for parameterization of reservoir permeability distribution was recently introduced (Jafarpour and McLaughlin 2008, 2009). The advantage of applying discrete cosine transform to channelized reservoirs is that the geological property image can be transformed and truncated to a few DCT coefficients while preserving the large-scale continuity of the property. By suitably identifying the lower frequency DCT coefficients subset, we are able to maintain the channel orientation and the channel structure. The discrete cosine transform is particularly well-suited for channelized reservoir systems with limited prior information because it does not require prior covariance information unlike the Karhunen-Loeve transform (Jafarpour and McLaughlin 2009).

The 1-D DCT of a function $u(n)$ has the following form (Jain 1989):

$$v(k) = \alpha(k) \sum_{n=0}^{N-1} u(n) \cdot \cos\left[\frac{\pi(2n+1)k}{2N}\right] \quad 0 \le k \le N-1 \tag{4.1}$$

where, $\alpha(k)$ are given by

$$\alpha(0) = \sqrt{\frac{1}{N}}, \qquad \alpha(k > 0) = \sqrt{\frac{2}{N}} \tag{4.2}$$

The inverse DCT is:

$$u(n) = \sum_{k=0}^{N-1} \alpha(k) v(k) \cdot \cos\left[\frac{\pi(2n+1)k}{2N}\right] \quad 0 \le n \le N-1 \tag{4.3}$$

For parameterizing the permeability field, we can write the DCT in the matrix-vector form as follows

$$\boldsymbol{\alpha} = \boldsymbol{\Phi} \cdot \boldsymbol{k} \tag{4.4}$$

where, $\boldsymbol{k}$ is the reservoir permeability vector, $\boldsymbol{\alpha}$ is the vector of DCT coefficients and $\boldsymbol{\Phi}$ is a matrix containing the DCT basis. In our implementation, we use $\log(\boldsymbol{k})$ instead of $\boldsymbol{k}$. Note that $\boldsymbol{\Phi}$ is an orthogonal matrix, so the inverse DCT is described as

$$\boldsymbol{k} = \boldsymbol{\Phi}^T \cdot \boldsymbol{\alpha} \tag{4.5}$$

The DCT is a computationally efficient parameterization technique because the higher dimensional transform can be performed by applying the 1-D transform in each direction (Jafarpour and McLaughlin 2009).

When compressing an image, the low frequency DCT coefficients preserve the large-

scale continuity of the image while the higher frequency coefficients give the detailed image information (Jafarpour and McLaughlin 2009). This is illustrated in **Figure 4.1** where we have truncated the higher frequency DCT coefficients and use a few low frequency coefficients to reconstruct the large-scale continuity of the permeability field. **Figure 4.1a** shows the permeability field and **Figure 4.1b** shows the corresponding DCT coefficients reduced from the original 50x50 to a truncated 6x6 domain and further reduced to just 20 coefficients. With less than 1% of the DCT coefficients, we can preserve the large-scale continuity although the detailed information is smeared away. From the example, we can see that the permeability field can be parameterized with a few DCT coefficients inside the truncated DCT domain. The RJMCMC method described below allows us to sample the parameter space using Markov Chain Monte Carlo methods and at the same time dynamically select the important DCT coefficients from the truncated subset.

4.2.2 Two Stage Markov Chain Monte Carlo Method

As mentioned before, for conditioning the permeability field to production data, we will use a two-stage RJMCMC method. In this section, we will briefly introduce the RJMCMC while pointing out some of its advantages. We will start with a brief review of the MCMC method and the Metropolis-Hastings sampling algorithm. Then we introduce the RJMCMC methods and the two-stage MCMC methods coupled with reversible jump.

a) log-permeability

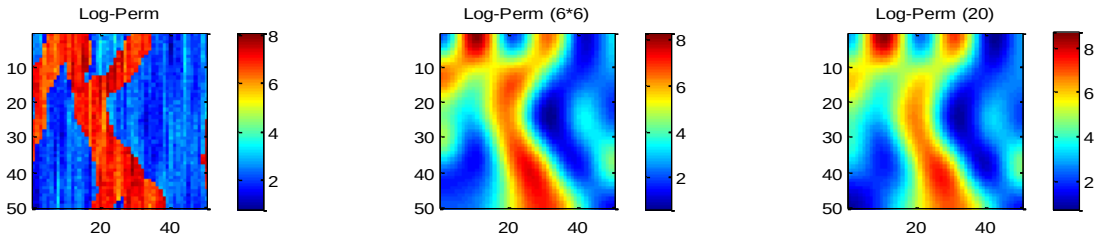

b) log|DCT|

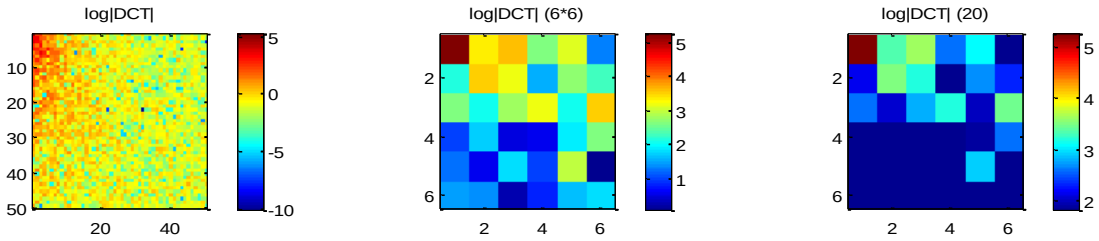

Figure 4.1 Permeability and DCT coefficients corresponding to the low frequency coefficient truncation: a) log-perm with 2500, 36, 20 coefficients and b) log|DCT| with 2500, 36, 20 coefficients

Our objective is to sample the permeability field $\boldsymbol{k}$ from a posterior distribution that is conditioned to the dynamic observation data $\boldsymbol{d}_{obs}$ and the prior permeability $\boldsymbol{k}_{prior}$. From Bayes' theorem, the posterior distribution can be expressed as

$$\pi(\boldsymbol{k}) = P(\boldsymbol{k}|\boldsymbol{d}_{obs}) \propto P(\boldsymbol{d}_{obs}|\boldsymbol{k})P(\boldsymbol{k}) \tag{4.6}$$

where, $P(\boldsymbol{k})$ denotes prior probability distribution for permeability and $P(\boldsymbol{d}_{obs}|\boldsymbol{k})$ denotes the likelihood function that links dynamic data and the prior model. The main idea is to construct a Markov chain whose stationary distribution will be given by $\pi(\boldsymbol{k})$. If we assume a Gaussian distribution for the prior model and the data errors, the posterior distribution can be written as

$$\pi(\boldsymbol{k}) = P(\boldsymbol{k}|\boldsymbol{d}_{obs}) \propto \exp\left\{-\frac{1}{2}\begin{bmatrix}(\boldsymbol{k}-\boldsymbol{k}_{prior})^T \boldsymbol{C_k^{-1}}(\boldsymbol{k}-\boldsymbol{k}_{prior}) \\ +(g(\boldsymbol{k})-\boldsymbol{d}_{obs})^T \boldsymbol{C_D^{-1}}(g(\boldsymbol{k})-\boldsymbol{d}_{obs})\end{bmatrix}\right\} \quad (4.7)$$

where, $g(\boldsymbol{k})$ is the simulated reservoir response corresponding to the proposed permeability field $\boldsymbol{k}$. $\boldsymbol{C_k}$ and $\boldsymbol{C_D}$ are the parameter covariance and the data covariance respectively. The Metropolis-Hastings MCMC algorithm (Metropolis et al. 1953; Hastings 1970) is usually applied to sample from the posterior distribution. In this algorithm, the probability to accept a proposal for transition to state $\boldsymbol{k}$ from $\boldsymbol{k}_n$ is

$$\rho(\boldsymbol{k}_n, \boldsymbol{k}) = \min\left(1, \frac{\pi(\boldsymbol{k})q(\boldsymbol{k}_n|\boldsymbol{k})}{\pi(\boldsymbol{k}_n)q(\boldsymbol{k}|\boldsymbol{k}_n)}\right) \quad (4.8)$$

Thus, accept $\boldsymbol{k}_{n+1} = \boldsymbol{k}$ with probability$\rho(\boldsymbol{k}_n, \boldsymbol{k})$, and $\boldsymbol{k}_{n+1} = \boldsymbol{k}_n$ with probability$1 - \rho(\boldsymbol{k}_n, \boldsymbol{k})$.

4.2.2.1 Reversible Jump Markov Chain Monte Carlo

The Reversible Jump Markov Chain Monte Carlo method is an extension of the Markov Chain Monte Carlo method. It allows sampling of the posterior distribution using a

parameter space with varying dimensions (Green 1995). Before we explain the reversible jump MCMC, let us first take a look at a constructive representation in terms of random numbers.

Suppose initially that we have a simpler state space, $\chi \subset \mathcal{R}^n$. As usual with the Metropolis–Hastings algorithm, we can satisfy the detailed balance condition by applying a protocol that proposes a new state for the chain and then accepts this proposed state with an appropriately derived probability. This probability is obtained by considering a transition and its reverse simultaneously. Let the density of the invariant distribution π also be denoted by π. At the current state x, we generate, say, r random numbers u from a known joint density g. The proposed new state of the chain x' is then constructed by some suitable deterministic function h such that $(x', u') = h(x, u)$. Here, u' are the r-dimensional random numbers, generated from a known joint density g' that would be required for the reverse move from x' to x, using the inverse function h' of h. If the move from x to x' is accepted with probability $\alpha(x, x')$ and likewise, the reverse move is accepted with probability $\alpha(x', x)$, the detailed balance requirement can be written as

$$\int_{(x,x')\in A\times B} \pi(x)g(u)\alpha(x,x')dxdu = \int_{(x,x')\in A\times B} \pi(x')g'(u')\alpha(x',x)dx'du' \tag{4.9}$$

If the transformation h from (x, u) to (x', u') and its inverse h' are differentiable, then we can apply the standard change-of-variable formula to the right hand side of **Eq. (4.9)**. We then see that the $(n + r)$-dimensional integral equality holds if

$$\pi(x)g(u)\alpha(x, x') = \pi(x')g'(u')\alpha(x', x)\left|\frac{\partial(x', u')}{\partial(x, u)}\right|$$

where the last factor is the Jacobian of the transformation from (x, u) to (x', u'). Thus, a valid choice for α is

$$\alpha(x, x') = \min\left\{1, \frac{\pi(x')g'(u')}{\pi(x)g(u)}\left|\frac{\partial(x', u')}{\partial(x, u)}\right|\right\},$$

involving only ordinary joint densities (Green 1995).

Here we are giving a brief discussion to the reversible jump MCMC. The detailed explanation can be found in Green's publication. Suppose we need to make a reversible jump between models i and j, this can be accomplished by an invertible function g_{ij} that transforms the parameters:

$$g_{ij}\left(\theta^{(i)}, u^{(i)}\right) = \left(\theta^{(j)}, u^{(j)}\right)$$

and retains the dimensions

$$d\left(\theta^{(i)}\right) + d\left(u^{(i)}\right) = d\left(\theta^{(j)}\right) + d\left(u^{(j)}\right)$$

where, $\theta^{(i)}$ and $\theta^{(j)}$ denote parameters of model i and j, $u^{(i)}$ and $u^{(j)}$ are parameters needed to make a reversible jump. The inverse transform g_{ij}^{-1} gives the move to the other direction. $d()$ represents the dimension of parameter space.

If $q_{ij}\left(\theta^{(i)}, u^{(i)}\right)$ is the probability density for the proposed move and $p(i,j)$ is the probability for the move $i \rightarrow j$, the acceptance probability can be written as

$$\alpha_{ij}\left(\theta^{(i)}, \theta^{(j)}\right) = \min\left\{1, \underbrace{\frac{\pi_j\left(\theta^{(j)}\right)}{\pi_i\left(\theta^{(i)}\right)}}_{\text{posterior ratio}} \times \underbrace{\frac{p(j,i)}{p(i,j)} \times \frac{q_{ji}\left(\theta^{(j)}, u^{(j)}\right)}{q_{ij}\left(\theta^{(i)}, u^{(i)}\right)}}_{\text{proposal ratio}} \times \underbrace{\left|\frac{\partial\left(\theta^{(j)}, u^{(j)}\right)}{\partial\left(\theta^{(i)}, u^{(i)}\right)}\right|}_{\text{Jacobian}}\right\} \tag{4.10}$$

In our approach, the permeability field $\boldsymbol{k}$ is represented by m DCT coefficients, $\boldsymbol{\alpha}$ and their locations $\boldsymbol{x}$. The unknown number of DCT coefficients m is a model parameter in the range $[n, N]$, hence we have an unknown dimension problem. The posterior distribution can be written as

$$\begin{aligned}\pi(\boldsymbol{k}) = P(\boldsymbol{k}|\boldsymbol{d}_{obs}) &\propto P(\boldsymbol{d}_{obs}|\boldsymbol{k})P(\boldsymbol{k}) \\ &= P(\boldsymbol{d}_{obs}|\boldsymbol{k})P(\boldsymbol{k}|\boldsymbol{\alpha}, \boldsymbol{x}, m)P(\boldsymbol{\alpha}|\boldsymbol{x}, m)P(\boldsymbol{x}|m)P(m)\end{aligned} \tag{4.11}$$

where, $P(\boldsymbol{d}_{obs}|\boldsymbol{k})$ denotes the likelihood distribution. Note that $P(\boldsymbol{k}|\boldsymbol{\alpha}, \boldsymbol{x}, m) = 1$ as permeability field $\boldsymbol{k}$ is determined by m number of DCT coefficients $\boldsymbol{\alpha}$ and their locations $\boldsymbol{x}$. Also, $P(\boldsymbol{\alpha}|\boldsymbol{x}, m)$ is the prior probability distribution of m number of DCT coefficient value given its location $\boldsymbol{x}$. This probability could be calculated from the DCT

coefficients of an ensemble of prior models. In our examples, only one initial model is used and thus, $P(\boldsymbol{\alpha}|\boldsymbol{x}, m) = 1$. $P(\boldsymbol{x}|m)$ is the probability to select m DCT locations from total N locations given by $P(\boldsymbol{x}|m) = 1/P_N^m = (N-m)!/N!$. We are now left with $P(m)$ which is uniform distribution given by $P(m) = 1/N - n + 1$. Thus, the posterior distribution is:

$$\pi(\boldsymbol{k}) = P(\boldsymbol{k}|\boldsymbol{d}_{obs}) \propto P(\boldsymbol{d}_{obs}|\boldsymbol{k})P(\boldsymbol{x}) \tag{4.12}$$

When we make a new model proposal using Reversible Jump Markov Chain Monte Carlo method, there are three options:

1. Birth step: adding one DCT coefficient
2. Death step: dropping one DCT coefficient
3. Jump step: keeping the same dimension and making a perturbation of DCT coefficients.

We assume that the three options have the probability as follows:

$$P_m^{add} = P_m^{del} = P_m^{jump} = \frac{1}{3}, \text{when } n < m < N$$

$$P_m^{add} = 0, P_m^{del} = \frac{2}{3}, P_m^{jump} = \frac{1}{3}, \text{at upper bound } m = N$$

$$P_m^{add} = \frac{2}{3}, P_m^{del} = 0, P_m^{jump} = \frac{1}{3}, \text{at lower bound } m = n$$

where, the dimension of the DCT coefficients is in the range $[n, N]$. The density

probability q_{ij} ratio is calculated as follows: $q_{ij} = 1/(N-m)$ and $q_{ji} = 1$ for a birth step, so the density probability ratio $q_{ji}/q_{ij} = N - m$; $q_{ij} = 1$ and $q_{ji} = 1/(N-m+1)$ for a death step, so the ratio is $q_{ji}/q_{ij} = 1/(N-m+1)$.

Now suppose we are at state i with $\left(\boldsymbol{\alpha}^{(i)}, \boldsymbol{x}^{(i)}\right)$ with m coefficients and want to make a proposal to state j with $\left(\boldsymbol{\alpha}^{(j)}, \boldsymbol{x}^{(j)}\right)$ by a birth, death or jump step:

1. **Birth Step**: one DCT coefficient is added. The proposed DCT coefficient set is given by $\boldsymbol{\alpha}^{(j)} = \boldsymbol{\alpha}^{(i)} + u^{(i)}$ with dimension $m+1$.

   The posterior ratio is:

$$\frac{\pi_j\left(\boldsymbol{k}^{(j)}\right)}{\pi_i(\boldsymbol{k}^{(i)})} = \frac{P\left(\boldsymbol{d}_{obs}\middle|\boldsymbol{k}^{(j)}\right)}{P(\boldsymbol{d}_{obs}|\boldsymbol{k}^{(i)})} \times \frac{P\left(\boldsymbol{x}^{(j)}\right)}{P(\boldsymbol{x}^{(i)})} = \frac{P\left(\boldsymbol{d}_{obs}\middle|\boldsymbol{k}^{(j)}\right)}{P(\boldsymbol{d}_{obs}|\boldsymbol{k}^{(i)})} \times \frac{1}{N-m}$$

   The proposal ratio is:

$$\frac{p(j,i)}{p(i,j)} \times \frac{q_{ji}\left(\boldsymbol{\alpha}^{(j)}\right)}{q_{ij}(\boldsymbol{\alpha}^{(i)}, u^{(i)})} = \frac{P_m^{del}}{P_m^{add}} \times \frac{1}{1/(N-m)}$$

   The Jacobian is:

$$J = \left|\frac{\partial\left(\boldsymbol{\alpha}^{(j)}\right)}{\partial(\boldsymbol{\alpha}^{(i)}, u^{(i)})}\right| = |I| = 1$$

Thus, the acceptance probability is given by

$$\alpha_p(i,j) = \min\left\{1, \frac{P\left(\boldsymbol{d}_{obs}\middle|\boldsymbol{k}^{(j)}\right)}{P(\boldsymbol{d}_{obs}|\boldsymbol{k}^{(i)})} \times \frac{P_m^{del}}{P_m^{add}}\right\} \tag{4.13}$$

2. **Death Step**: one DCT coefficient is dropped from current set. The proposed DCT coefficient set is given by $\boldsymbol{\alpha}^{(j)} + u^{(j)} = \boldsymbol{\alpha}^{(i)}$ with dimension $m-1$.

   The posterior ratio is:

$$\frac{\pi_j\left(\boldsymbol{k}^{(j)}\right)}{\pi_i(\boldsymbol{k}^{(i)})} = \frac{P\left(\boldsymbol{d}_{obs}\middle|\boldsymbol{k}^{(j)}\right)}{P(\boldsymbol{d}_{obs}|\boldsymbol{k}^{(i)})} \times \frac{P\left(\boldsymbol{x}^{(j)}\right)}{P(\boldsymbol{x}^{(i)})} = \frac{P\left(\boldsymbol{d}_{obs}\middle|\boldsymbol{k}^{(j)}\right)}{P(\boldsymbol{d}_{obs}|\boldsymbol{k}^{(i)})} \times (N-m+1)$$

   The proposal ratio is:

$$\frac{p(j,i)}{p(i,j)} \times \frac{q_{ji}\left(\boldsymbol{\alpha}^{(j)}, u^{(j)}\right)}{q_{ij}(\boldsymbol{\alpha}^{(i)})} = \frac{P_m^{del}}{P_m^{add}} \times \frac{1/(N-m+1)}{1}$$

   Jacobian is:

$$J = \left|\frac{\partial\left(\boldsymbol{\alpha}^{(j)}, u^{(j)}\right)}{\partial(\boldsymbol{\alpha}^{(i)})}\right| = |I| = 1$$

   Thus, the acceptance probability is given by

$$\alpha_p(i,j) = \min\left\{1, \frac{P\left(\boldsymbol{d}_{obs}\middle|\boldsymbol{k}^{(j)}\right)}{P(\boldsymbol{d}_{obs}|\boldsymbol{k}^{(i)})} \times \frac{P_m^{del}}{P_m^{add}}\right\} \tag{4.14}$$

3. **Jump Step**: The DCT coefficients are perturbed without changing any dimension. It's a conventional Markov Chain Monte Carlo with standard Metropolis-Hastings step. The acceptance probability is given by

$$\alpha_p(i,j) = \min\left\{1, \frac{\pi\left(\boldsymbol{k}^{(j)}\right)}{\pi(\boldsymbol{k}^{(i)})}\right\} = \min\left\{1, \frac{P\left(\boldsymbol{d}_{obs}\middle|\boldsymbol{k}^{(j)}\right)}{P(\boldsymbol{d}_{obs}|\boldsymbol{k}^{(i)})}\right\} \tag{4.15}$$

The steps of the RJMCMC algorithm are as follows:

From model state $\boldsymbol{k}_n$ at n^{th} step with parameters$\left(\boldsymbol{\alpha}^{(n)}, \boldsymbol{x}^{(n)}\right)$:

1. We choose instrumental probability distribution $q(\cdot \mid \cdot)$ to be symmetric and choose a new model $\widetilde{\boldsymbol{k}}$ by make a birth, death or jump move.
2. Accept the proposal as

$$\boldsymbol{k}_{n+1} = \begin{cases} \widetilde{\boldsymbol{k}} & \text{with probability } \alpha_p \\ \boldsymbol{k}_n & \text{with probability 1-}\alpha_p \end{cases}$$

4.2.2.2 Two-stage Reversible Jump Markov Chain Monte Carlo Algorithm

The goal of the two-stage method is to improve the acceptance rate of the traditional MCMC methods without sacrificing the rigor in its sampling properties or convergence rates. This is accomplished by prescreening the proposals to weed out proposals that are likely to be rejected. This prescreening utilizes an approximate likelihood computation using a proxy model for obtaining the flow response. In our case, the proxy is a coarse-

scale simulation of the flow response. The coarse-scale model is constructed via a single phase upscaling of the fine-scale model. The two-stage MCMC sampling proceeds as follows (Ma et al. 2008; Mondal et al. 2010):

Suppose the chain is at the n^{th} step having permeability $\boldsymbol{k}_n$ with parameters $\left(\boldsymbol{\alpha}^{(n)}, \boldsymbol{x}^{(n)}\right)$:

1. Make a model proposal $\widetilde{\boldsymbol{k}}$ conditioned to permeability observations. The proposed fine-scale permeability field is upscaled using a single phase flow-based upscaling algorithm. A coarse-scale simulation is carried out to compute the likelihood and the corresponding posterior is given by $\pi^*\left(\widetilde{\boldsymbol{k}}\right)$.
2. Accept the model proposal $\widetilde{\boldsymbol{k}}$ with probability $\alpha_p\left(\boldsymbol{k}_n, \widetilde{\boldsymbol{k}}\right) = \min\left\{1, \pi^*\left(\widetilde{\boldsymbol{k}}\right)/\pi^*(\boldsymbol{k}_n)\right\}$ as shown in **Eq. (18), (22)** and **(23)**. We choose the instrumental probability distribution $q(\cdot \mid \cdot)$ to be symmetric.

$$\boldsymbol{k} = \begin{cases} \widetilde{\boldsymbol{k}} & \text{with probability } \alpha_p\left(\boldsymbol{k}_n, \widetilde{\boldsymbol{k}}\right) \\ \boldsymbol{k}_n & \text{with probability 1-}\alpha_p\left(\boldsymbol{k}_n, \widetilde{\boldsymbol{k}}\right) \end{cases}$$

   If the proposal is accepted, we compute the exact likelihood and the corresponding posterior $\pi(\boldsymbol{k})$ using fine scale simulation and go to step 3; If the proposal is rejected, we go back to step 1.

3. Accept $\boldsymbol{k}$ as a sample with probability

$$\alpha_f(\boldsymbol{k}_n, \boldsymbol{k}) = \min\left\{1, \frac{\pi(\boldsymbol{k})\pi^*(\boldsymbol{k}_n)}{\pi(\boldsymbol{k}_n)\pi^*(\boldsymbol{k})}\right\} \tag{4.16}$$

$$\boldsymbol{k}_{n+1} = \begin{cases} \boldsymbol{k} & \text{with probability } \alpha_f(\boldsymbol{k}_n, \boldsymbol{k}) \\ \boldsymbol{k}_n & \text{with probability 1-}\alpha_f(\boldsymbol{k}_n, \boldsymbol{k}) \end{cases}$$

The detailed argument is given in (Ma et al. 2008). With two-stage Markov Chain Monte Carlo method, we are able to sample the posterior distribution efficiently.

4.2.3 Conditioning Model to Permeability Observations

When perturbing the DCT coefficients using the RJMCMC, the proposed permeability field is not automatically conditioned to the permeability at well locations. We need to ensure that the proposed model honors the permeability observations at well locations.

Given the permeability observations $\boldsymbol{k}_{obs}$ at well locations and the truncated DCT coefficient locations, we can construct a reduced DCT basis $\boldsymbol{M}$ from the DCT basis $\boldsymbol{\Phi}^T$ so that

$$\boldsymbol{M} \cdot \boldsymbol{\alpha} = \boldsymbol{k}_{obs} \tag{4.17}$$

Using this equation, we are able to solve the truncated DCT coefficients directly and the generated permeability is conditioned to permeability observations. However, these DCT coefficients often result in permeability fields that lack geologic continuity due to the higher frequency coefficients used. To avoid the problem, we minimize the following equation to condition the model to permeability observations instead of solving the

matrix problem directly.

$$\tilde{\boldsymbol{\alpha}} = \text{argmin}(\boldsymbol{M} \cdot \boldsymbol{\alpha} - \boldsymbol{k}_{obs})^T (\boldsymbol{M} \cdot \boldsymbol{\alpha} - \boldsymbol{k}_{obs})$$

We expand and reorganize the equation:

$$\tilde{\boldsymbol{\alpha}} = \text{argmin}\left(-\frac{1}{2}\boldsymbol{\alpha}^T \boldsymbol{M}^T \boldsymbol{M}\boldsymbol{\alpha} - \boldsymbol{k}_{obs}{}^T \boldsymbol{M}\boldsymbol{\alpha}\right) \tag{4.18}$$

This is a quadratic minimization problem. The following constraints are added to preserve the large scale continuity of the proposed model and avoid none physical updates:

$$\boldsymbol{\Phi} \cdot \boldsymbol{\alpha} \leq \boldsymbol{k}_{max}$$

$$\boldsymbol{\alpha}_{low} \leq \boldsymbol{\alpha} \leq \boldsymbol{\alpha}_{up}$$

$$\boldsymbol{\alpha}_{init} = \boldsymbol{\alpha}_0$$

The minimization problem starts with the proposed DCT coefficients, $\boldsymbol{\alpha}_0$. The inequality constraint limits the permeability to the max permeability, $\boldsymbol{k}_{max}$. The other constraint sets the upper boundary, $\boldsymbol{\alpha}_{up}$ and lower boundary, $\boldsymbol{\alpha}_{low}$ of the DCT coefficients.

An example of conditioning the permeability at well locations is shown in **Figure 4.2**. We can see that the updated permeability field preserves the features of the proposal permeability. **Table 4.1 and Table 4.2** show that in the original proposal, the

permeabilities at well locations are far from the observed permeability. The updated permeabilities at well locations are very close to the permeability observations after conditioning.

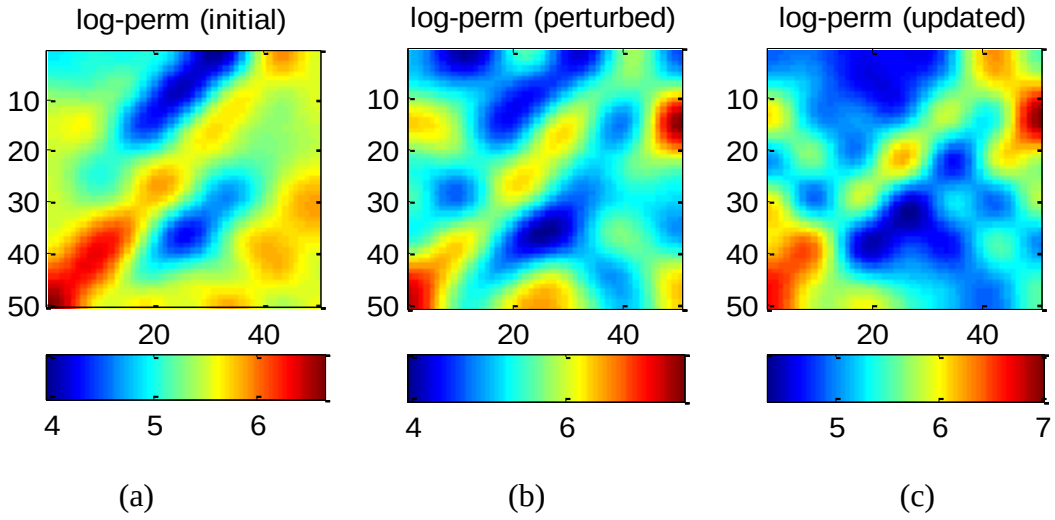

Figure 4.2 Conditioning the proposed model to the permeability observations at wells: a) the initial permeability field, b) the proposed permeability field using perturbation and c) the updated permeability field after conditioning

Table 4.1 Permeability differences (perturbation – observation) at well locations in a nine-spot pattern

-18.6501	-87.5461	150.5276
11.4676	-73.2840	82.7810
-727.3377	-396.1496	299.5839

Table 4.2 Permeability differences (updated – observation) at well locations in a nine-spot pattern

1.0e-12*

-0.1137	-0.0853	-0.2274
-0.6253	-0.2274	0.2274
0	-0.4263	-0.4547

4.2.4 Model Selection Using Multi-Dimensional Scaling & Cluster Analysis

Uncertainty analysis and model selection are conducted using the multi-dimensional scaling (MDS) and cluster analysis to visualize and select channelized reservoir models. The MDS is proposed to parameterize the spatial uncertainty of geostatistical realizations (Scheidt and Caers 2009). In the chapter, they used the distance function of dynamic responses to account for uncertainty in multiple geostatistical realizations and

then distinct members using kernel principal component analysis (KPCA) or kernel clustering methods. The idea has been applied to visualize the spread of ensemble members in Ensemble Kalman Filter (Watanabe et al. 2009).

We adopt the same approach here except that the dissimilarities are based on the evolution of the reservoir swept volume change with time computed using various threshold of streamline time-of-flight. The streamline trajectories and swept volume are generated using the fluid-flux information from a finite-difference simulator. No additional reservoir simulation is needed. The swept volume changes as a function of time-of-flight is considered as the dissimilarity measure as shown below

$$\Delta SPV(t) = SPV(t = \tau_1) - SPV(t = \tau_2) \tag{4.19}$$

The dissimilarity measure between the swept volume changes of two individual realizations i and j is defined as

$$\delta_{ij} = \sum_{t=1}^{N} \left[\Delta SPV_i(t) - \Delta SPV_j(t)\right]^2 \tag{4.20}$$

The distance matrix can be written as $D_{ij} = -\frac{1}{2}\delta_{ij}^2$. After centering the distance matrix and conducting a principal component analysis, we apply k-mean cluster analysis based on the first two or three principal components and select the model near the center of

each cluster to reduce the model replicates.

4.3 Workflow

An outline of the procedure for our approach is given in **Figure 4.3.** The stop criterion is that either a predefined number of posterior samples or a maximum number of iterations. The major steps of our approach are as follows:

1. Parameterize the permeability field by taking its discrete cosine transform, define the truncated DCT domain and select a set of DCT coefficients as the subspace;
2. Run forward simulation for the initial model and calculate the dynamic response misfit;
3. Perturb the DCT coefficients to generate a new channelized model using RJMCMC. We have three options here:
    - Birth: randomly add a DCT coefficient to the DCT subspace;
    - Death: randomly drop a DCT coefficient from the DCT subspace;
    - Jump: Perturb the value of DCT coefficients;
4. Condition the proposed model to the permeability at well locations;
5. Upscale the proposed model and perform first stage coarse-scale simulation;
6. Check the acceptance of the proposed model using the Metropolis-Hastings algorithm. If the proposed model is accepted, go to step 7, else go to step 3 and make a new proposal;

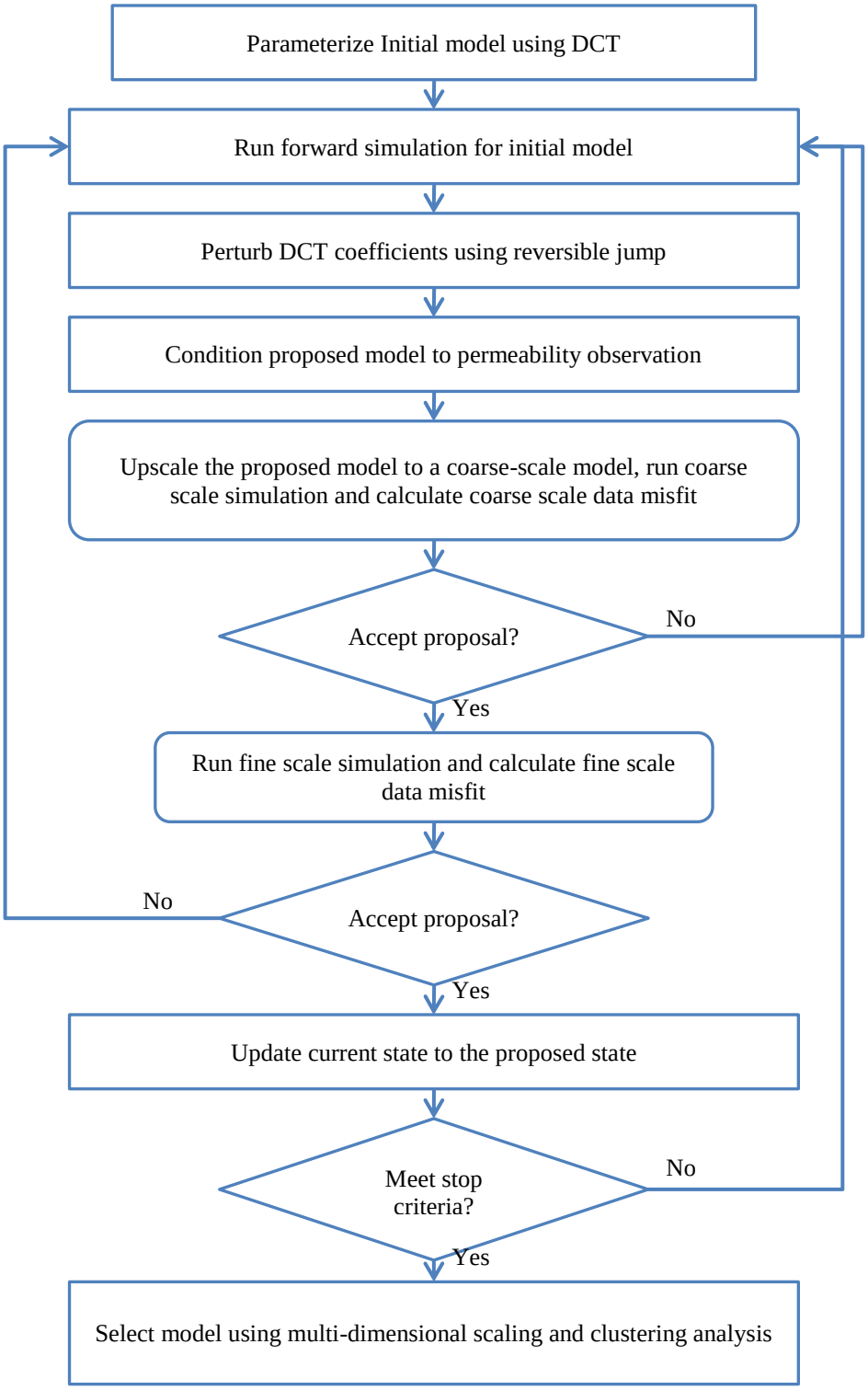

Figure 4.3 Flow chart of our approach for channelized reservoir history matching

7. Run fine-scale simulation and calculate dynamic response misfit;
8. Check the acceptance using updated acceptance probability. If the proposed model is accepted, update current model, else go to step 3;
9. Collect samples when the stop criterion is met.

4.4 Applications

In this section, we apply our approach to both 2-D and 3-D synthetic channelized reservoir examples. Our objective is to reproduce the channel structure and identify the large scale continuity in the reservoir with dynamic data integration.

4.4.1 A 2-D Synthetic Example

We consider a 2-D synthetic example that involves water-flooding in a nine-spot pattern as shown in **Figure 4.4**. The 2-D channelized reservoir model is generated from a training image using multi-point geostatistics (Remy et al. 2009). For comparison purposes, the reference permeability field is selected to be the original channel model with reduced DCT coefficients. The initial permeability field is generated by conditioning the permeability at well locations as discussed earlier. From **Figure 4.5**, we can see that the channel connectivity and orientation of the initial model is completely different from the reference model.

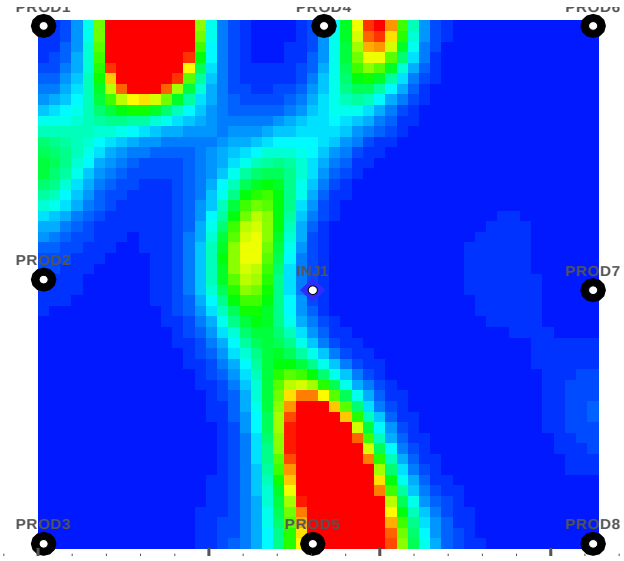

Figure 4.4 A 2-D 50x50 channelized reservoir example with a nine-spot pattern

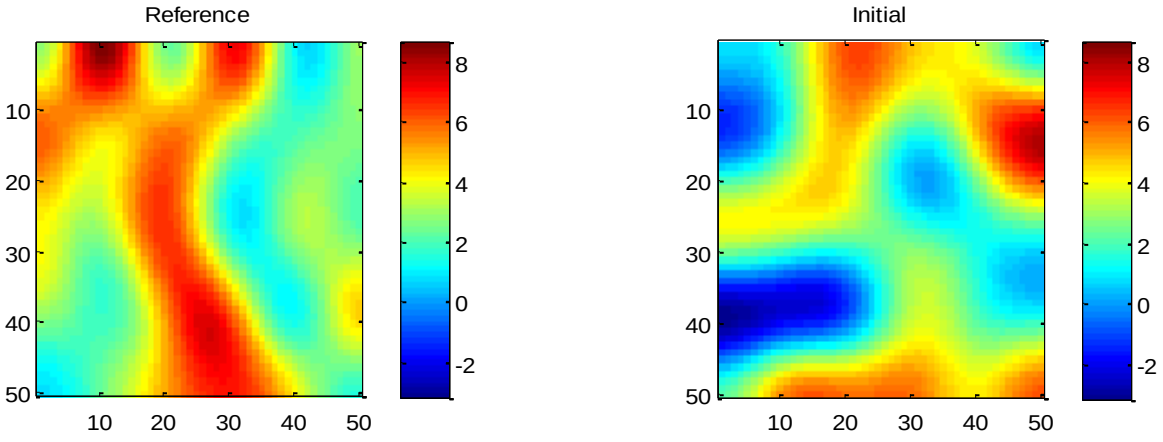

Figure 4.5 Reference and initial permeability field in 2-D example

The two-stage RJMCMC is carried out to condition the channel model to dynamic production data. In this example, we are history matching the oil production rate, water-

cut and bottom-hole pressure at producers. We start with 15 DCT coefficients out of the 6x6 subspace. The RJMCMC allows us to search the parameter space flexibly between 15 and 35 DCT coefficients in the 6x6 subspace. To speed up the RJMCMC algorithm, the simulation grid is upscaled from 50x50 to a 10x10 coarse-scale model using single phase flow-based upscaling as a first stage filter to screen out the undesired proposals. The residual sum of square (RMS) reduction of two-stage RJMCMC is plotted in **Figure 4.6**. After the Markov chain is converged, multi-dimensional scaling and cluster analysis are used to select samples from all the accepted models (Scheidt and Caers 2009). **Figure 4.7** shows the model separations compared to the true model using the first two and three principal components. The multi-dimensional scaling was a dissimilarity measure to select a subset of models from an ensemble. For our approach, the dissimilarity measure is given by changes in swept volume as illustrated in **Figure 4.8**. The multi-dimensional scaling and cluster analysis are briefly discussed before. **Figure 4.9** shows the result of cluster analysis and selected samples.

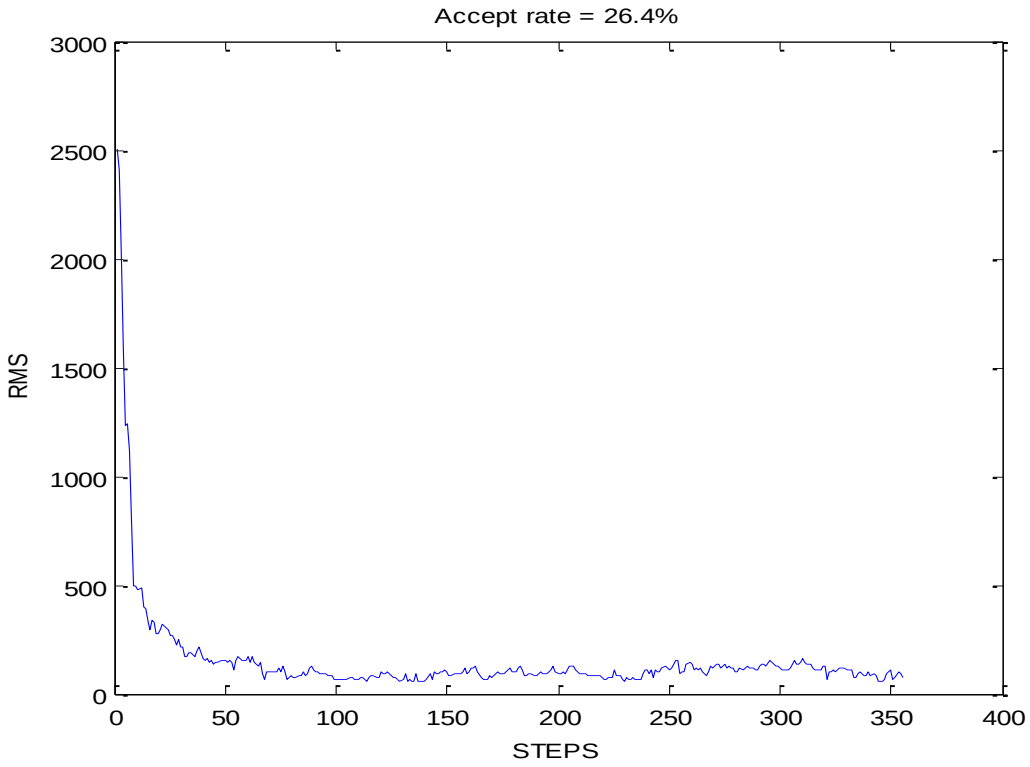

Figure 4.6 Reductions in RMS per simulation run for two stage RJMCMC in 2-D example

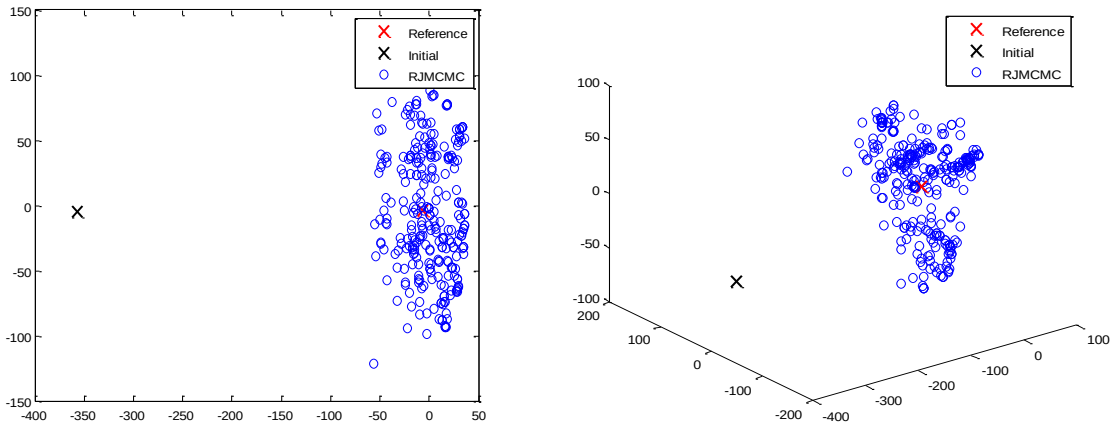

a) 2-D b) 3-D

Figure 4.7 Collected samples from two stage RJMCMC compared to reference and initial model using multi-dimensional scaling in 2-D example: a) 2-D visualization and b) 3-D visualization

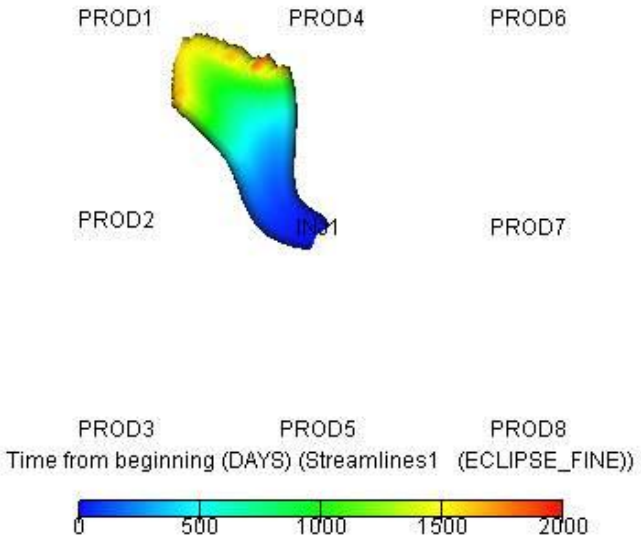

Figure 4.8 The swept volume from injector to producer 1 at TOF = 2000

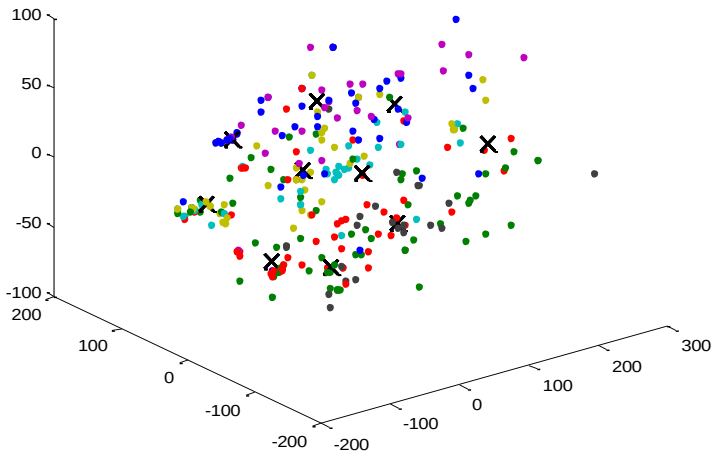

Figure 4.9 Ten samples selected from all collected samples using multi-dimensional scaling and cluster analysis in 2-D example

The reference model and the initial model are shown in **Figure 4.10a** and two selected samples with sample mean are shown in **Figure 4.10b**. **Figure 4.10** indicates that we successfully reconstruct the channel structure and identify the channel orientation based on the dynamic production history and permeability observations. The dynamic data history matching results are shown in **Figure 4.11**, **Figure 4.12** and **Figure 4.13** (Red dot is observation data; green is initial data; and blue is updated data). These results clearly demonstrate that the two-stage RJMCMC can be used to sample the posterior distribution during channelized reservoir history matching.

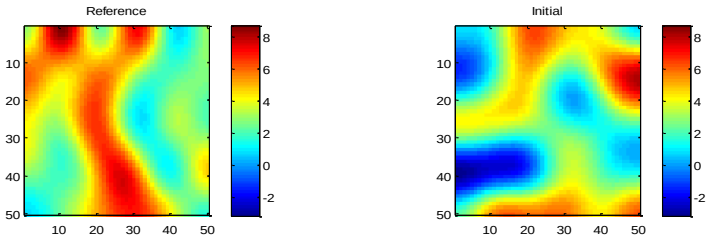

a) Reference and initial model

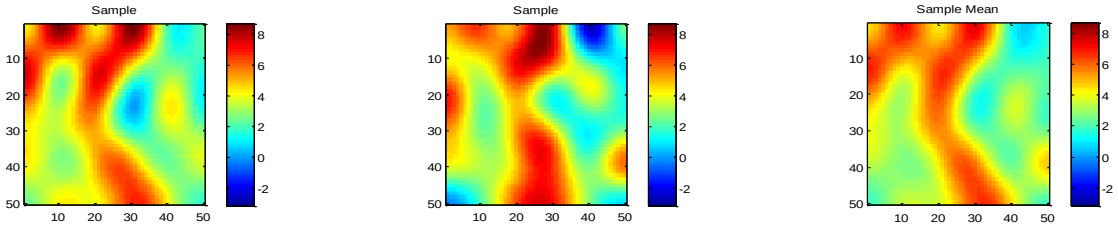

b) Two collected samples and sample mean

Figure 4.10 Collected samples from two stage RJMCMC and sample mean compared to reference and initial model

- Reference – Initial – Update

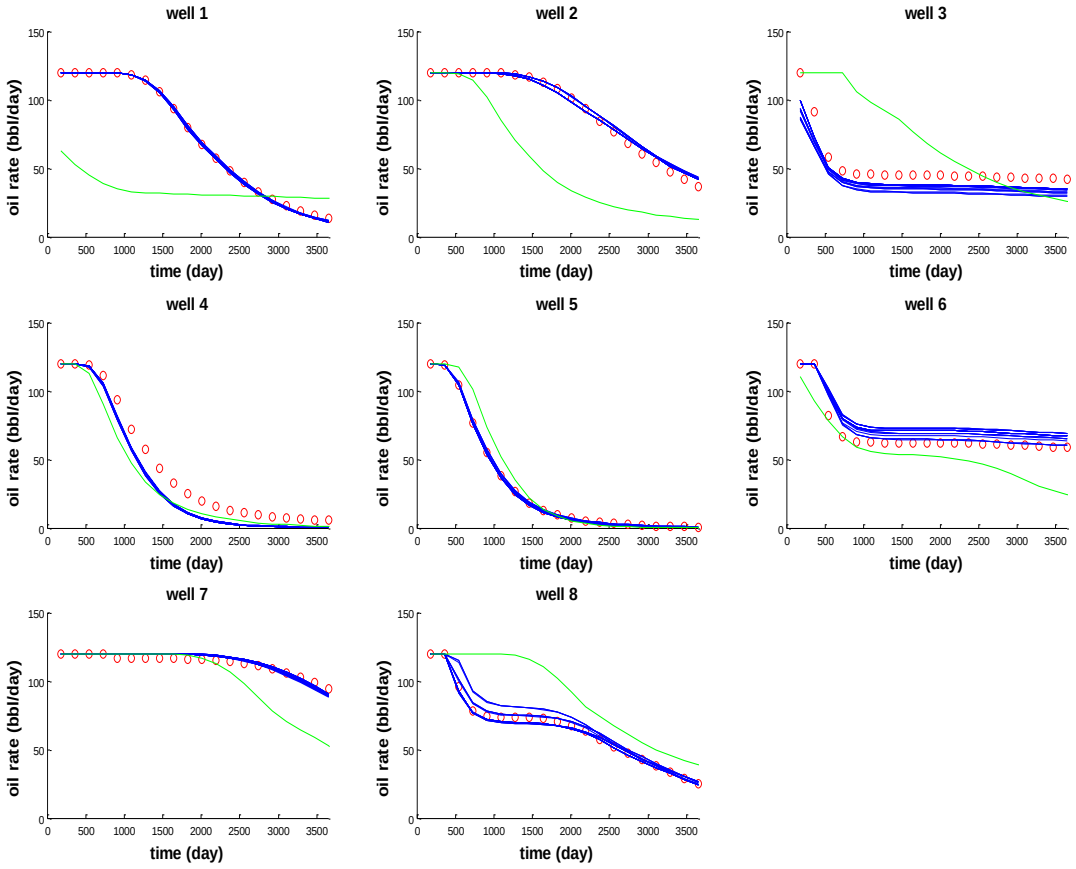

Figure 4.11 Oil production rate history matching in 2-D example

Reference – Initial – Update

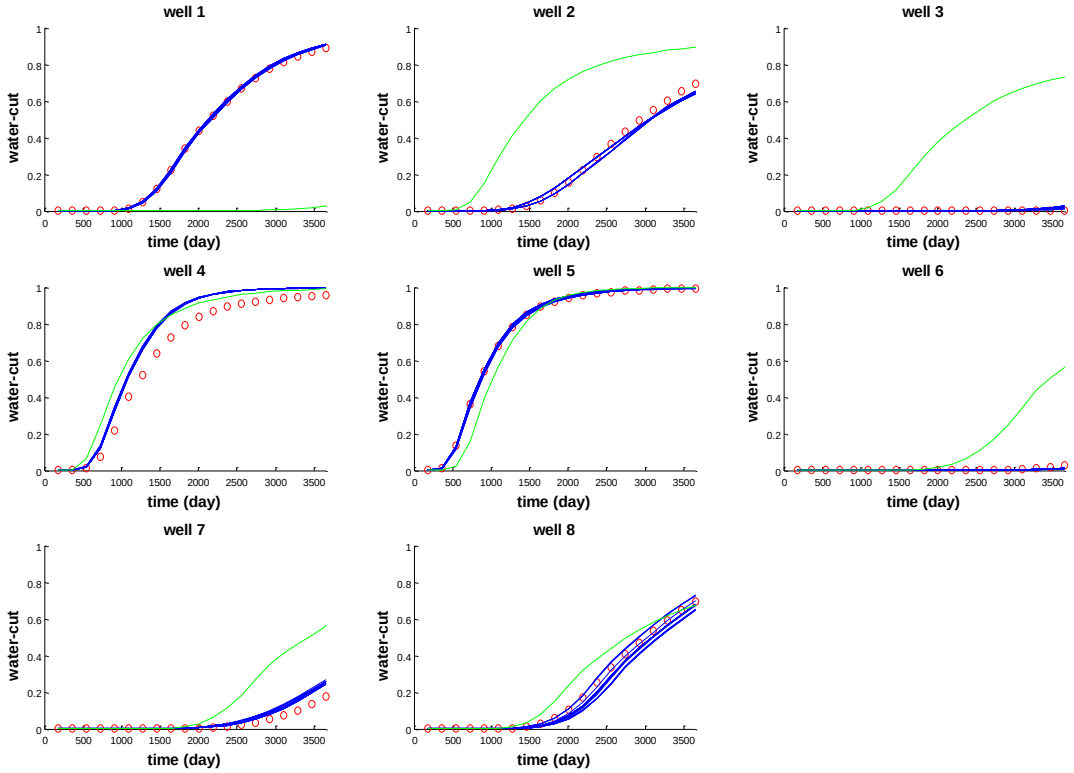

Figure 4.12 Water-cut history matching in 2-D example

- Reference – Initial – Update

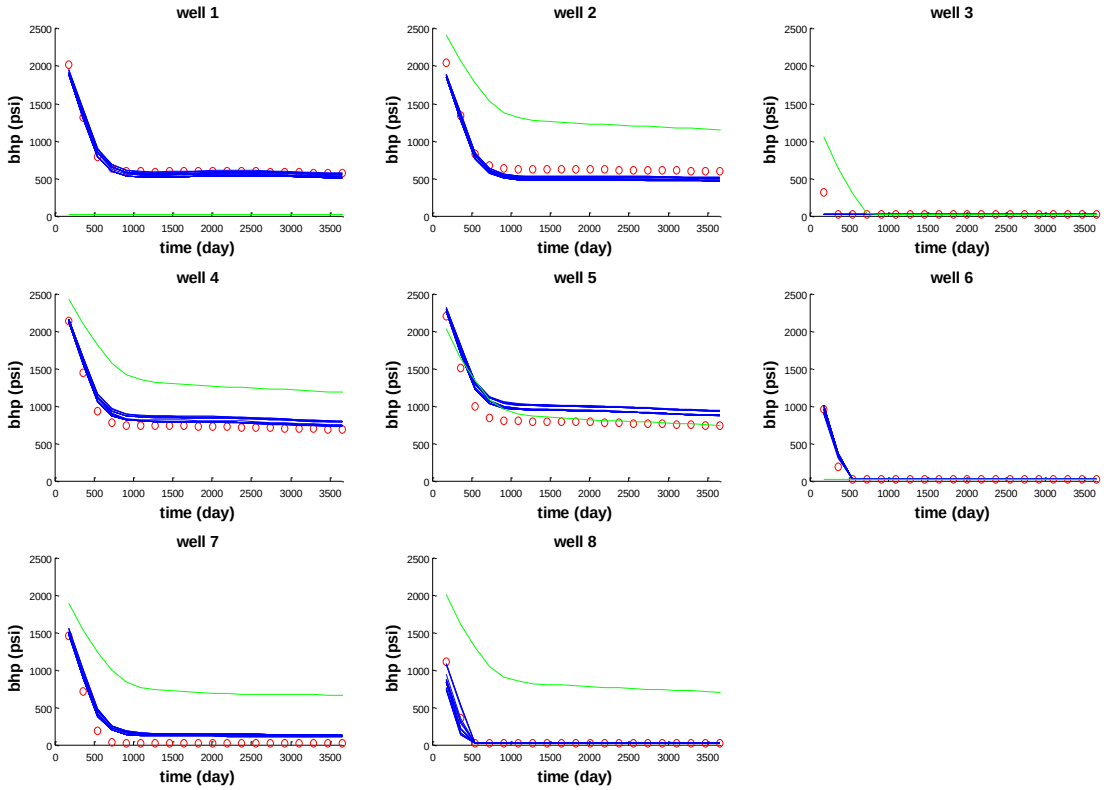

Figure 4.13 Well bottom hole pressure (BHP) history matching in 2-D example

4.4.2 A 3-D Synthetic Example

The 3-D synthetic example is a two phase flow water-flooding case with 50x50x6 grid size as in **Figure 4.14**. The channelized reservoir model is generated using FLUVSIM, a program for object-based stochastic modeling of fluvial system (Deutsch and Tran 2002). The reference and initial model are shown in **Figure 4.15**. The initial reservoir model is conditioned to the permeability observations at well locations.

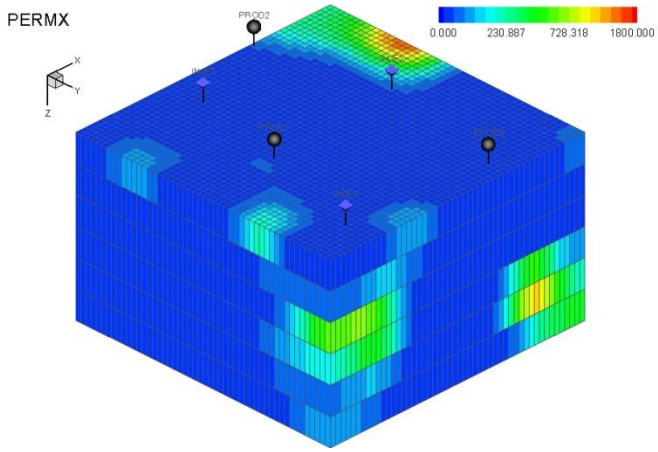

Figure 4.14 A 3-D 50x50x6 channelized reservoir example

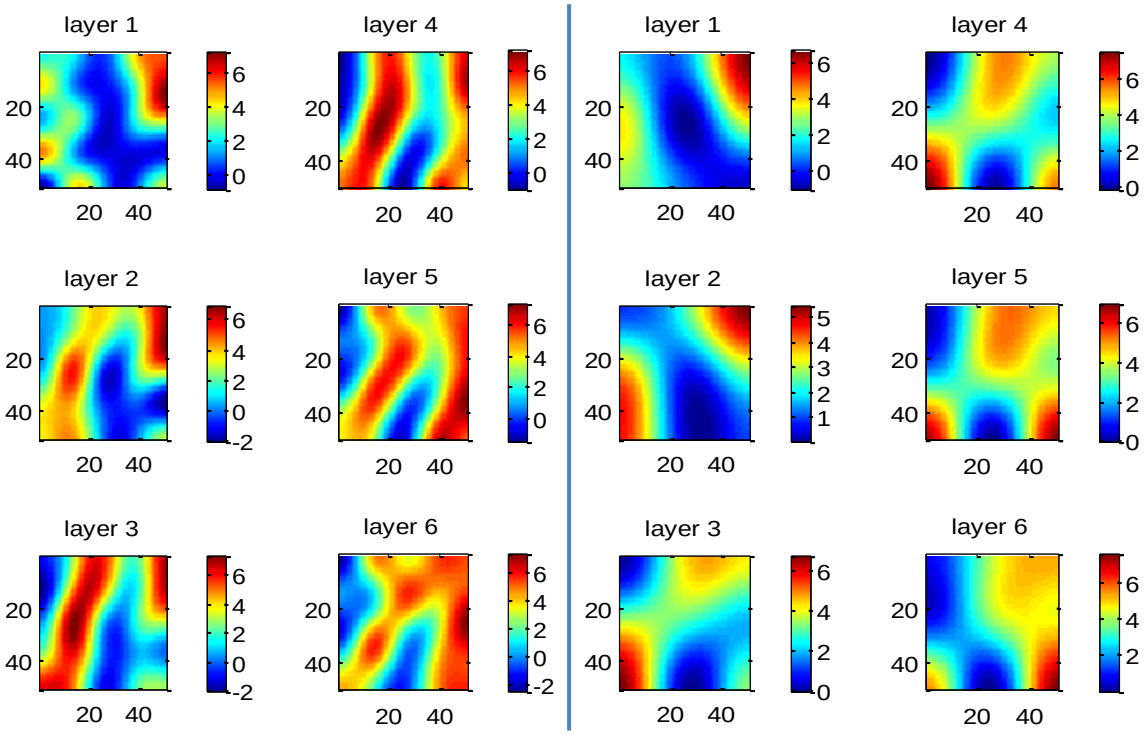

a) Reference field b) Initial field

Figure 4.15 Layer view of reference and initial permeability field in 3-D example: a) reference permeability field and b) initial permeability field

Two-stage RJMCMC is carried out to condition the channel model to the dynamic production data. In this example, we are history matching the oil production rate, water-cut and bottom-hole pressure at producers and water injection rate at injectors. In this case, we start with 18 (=3x3x2) DCT coefficients out of the 5x5x4 DCT subspace. The RJMCMC allows us to search the parameter space flexibly between 18 and 50 DCT coefficients in the DCT subspace. The coarse scale simulation is also used as a screening step. The reservoir model is upscaled from 50x50x6 to a 10x10x6 coarse-scale model

using single phase flow-based upscaling. The residual sum of square reduction of the two-stage RJMCMC is plotted in **Figure 4.16**. After simulations, multi-dimensional scaling and cluster analysis are used to select samples from all the collected models. **Figure 4.17** shows the model separations compared to the true model using the first two and three principal components. **Figure 4.18** shows the result of cluster analysis and the selected models.

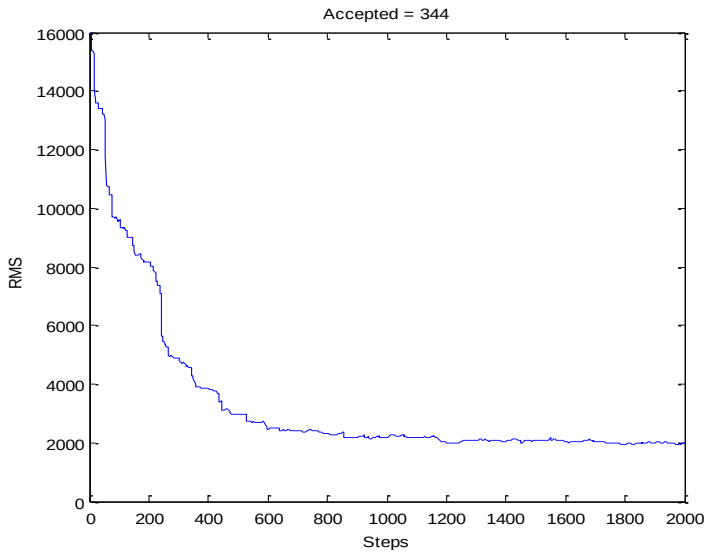

Figure 4.16 Reductions in RMS per simulation run for two stage RJMCMC in 3-D example

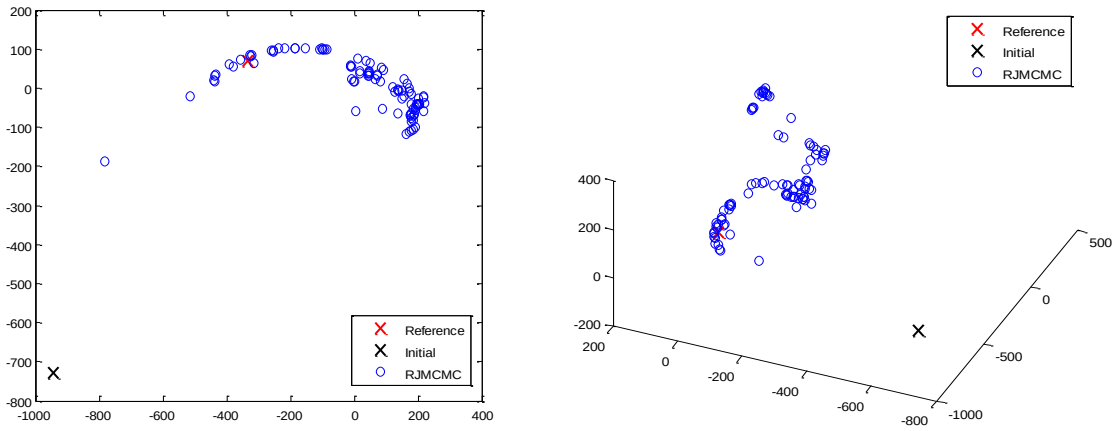

a) 2-D b) 3-D

Figure 4.17 Collected samples from two stage RJMCMC compared to reference and initial model using multi-dimensional scaling in 3-D example: a) 2-D visualization and b) 3-D visualization

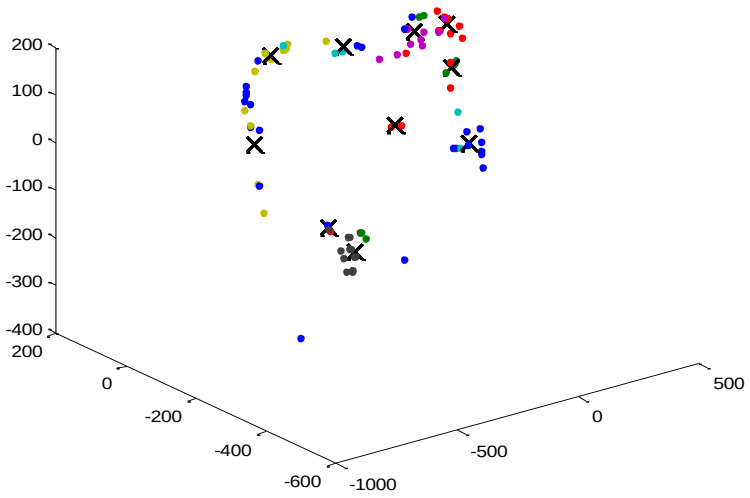

Figure 4.18 Ten samples selected from all collected samples using multi-dimensional scaling and cluster analysis in 3-D example

Four collected samples are compared to the reference model and the initial model in **Figure 4.19**. From the figure, we can see that the channel structure and orientation are identified given the dynamic production data and permeability observations. The dynamic data history matching results are shown in **Figure 4.20** (Red dot is observation data; green is initial data; and blue is updated data). These results show that the application of two-stage RJMCMC can be extended to a 3D example.

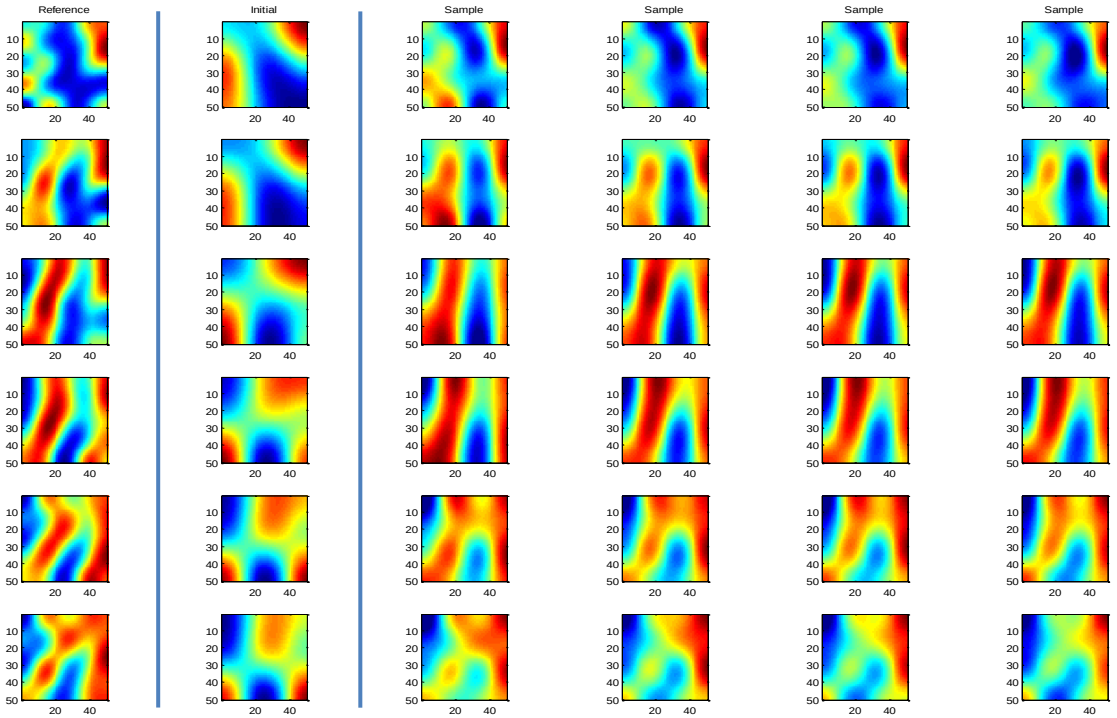

Figure 4.19 Four selected models compared with reference and initial model in 3-D example: a) reference model, c) initial model and c) 4 selected sample models

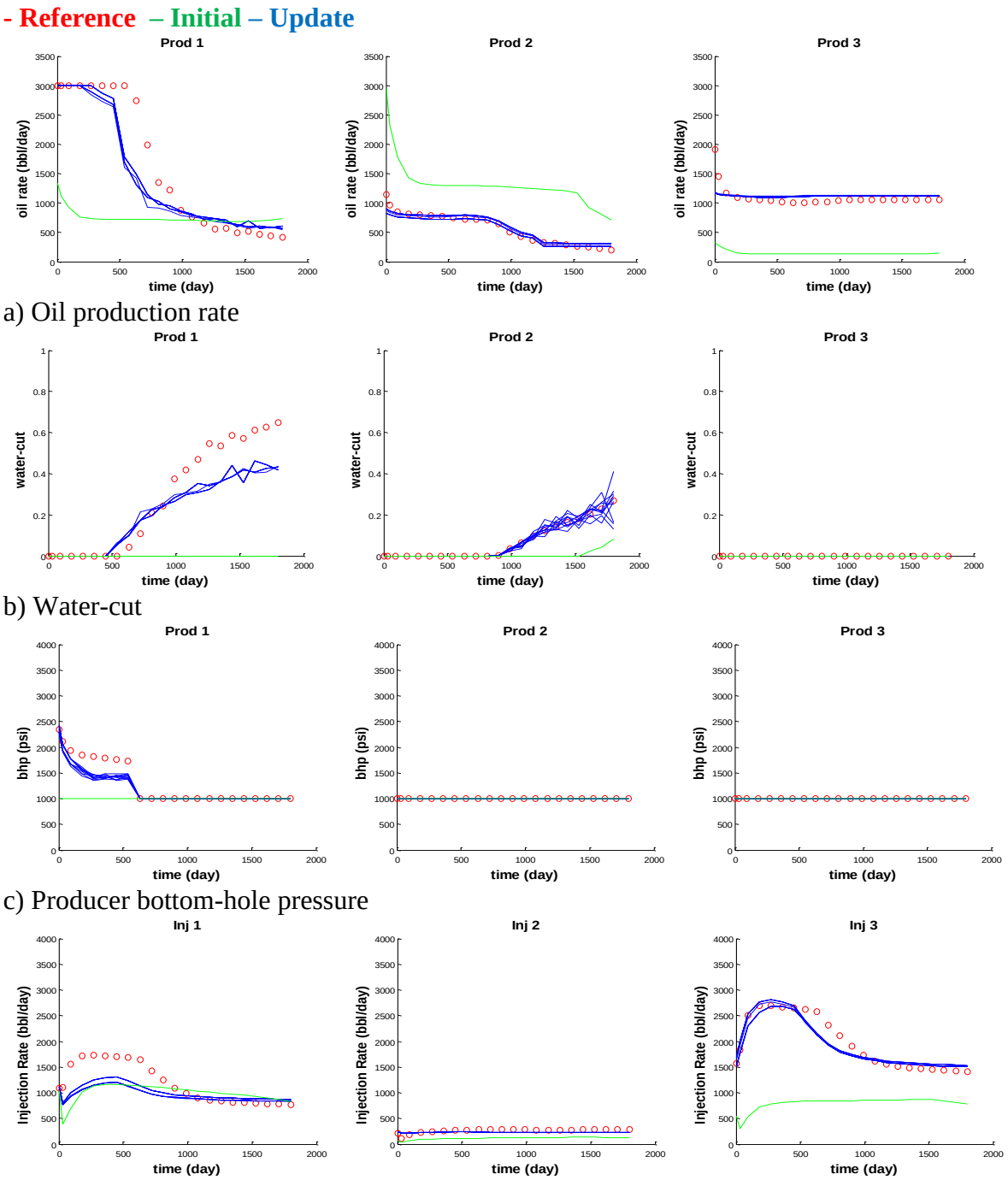

Figure 4.20 Dynamic production data history matching in 3-D example: a) oil production rate history matching, b) water cut history matching, c) producer bottom hole pressure history matching and d) injection rate history matching

4.5 Summary

In this chapter, we presented a novel method for history matching and uncertainty quantification for channelized reservoirs using Reversible Jump Markov Chain Monte Carlo (RJMCMC) methods.

In order to preserve large-scale continuity, the channelized permeability field is parameterized using the discrete cosine transform (DCT). The parameters representing the channel structure are the coefficients in the truncated frequency domain. The parameter space is searched using the RJMCMC method, whereby the dimension of the parameter space is flexible. For each step of the RJMCMC, the dimension of the uncertainty space can be increased or decreased according to a prescribed prior distribution. This flexibility in the parameter dimension allows an efficient search of the uncertainty space. Two-stage MCMC method was used to screen out the undesired proposals. After simulations, multi-dimensional scaling and cluster analysis were used to select realizations from the accepted models.

We demonstrate the effectiveness of the RJMCMC algorithm using both 2D and 3D examples involving water-flooding history matching. The 2-D example shows that the RJMCMC algorithm can successfully match the data and identify the orientation of the channels in the reference model. The 3-D result shows that the proposed algorithm can determine the large-scale features of the reference channelized permeability field based on the production data. The MCMC algorithms naturally provide multiple realizations of

the permeability field conditioned to well and production data and thus, allow for uncertainty quantification in the forecasting.

CHAPTER V
CONCLUSIONS AND RECOMMENDATIONS

In this work, we presented two applications of Level Set Methods (LSM) and Fast Marching Methods (FMM) in the field of reservoir characterization: drainage volume and pressure depletion calculation in unconventional wells, and history matching and uncertainty quantification of channelized reservoirs.

First, Fast Marching Methods are successfully used to compute and visualize depth of investigation in unconventional reservoirs under very general reservoir conditions and fracture geometry/properties. The FMM essentially solve the Eikonal equation which describes the propagation of a pressure front. It provides an efficient way to calculate drainage volume, which leads to estimation of pressure depletion behavior based on a pressure geometric approximation of the drainage volume. The applicability of the proposed approach is demonstrated with two examples derived based on real field cases – one assumes homogeneous matrix properties and the other uses heterogeneous matrix properties. In both examples, we identify and visualize the drainage volume and transient pressure behavior. The speed and versatility of our proposed method makes it ideally suited for estimating matrix/fracture properties and optimizing fracture design in unconventional reservoirs through inverse modeling. We can also estimate Stimulated Reservoir Volume (SRV) based on drainage volume calculation. The application is demonstrated using a 3-D synthetic example designed after a real field case. We are able

to demonstrate the benefits of incorporating the SRV during the history matching process to improve history matching results. Specifically, our results show that the uncertainty in the fracture/matrix parameters are reduced significantly when SRV was incorporated in addition to Bottom-Hole Pressure (BHP) during history matching as compared to BHP matching only.

Second, we propose a level set Markov chain approach for history matching and uncertainty quantification for channelized reservoirs using a two stage Markov Chain Monte Carlo method. This approach is based on level set representation of channel boundaries. Specifically, signed distance function is used to represent channelized features in the reservoir and channel structure is then updated by perturbing the signed distance function with a velocity field constrained at well locations. The velocity field can be generated with eigenvalue decomposition of large number of training velocities. The parameters representing the channel structure are the coefficients of eigenvectors which from the velocity basis. A two stage sampling method is utilized to improve efficiency of Markov Chain Monte Carlo method and sample the posterior distribution rigorously. We demonstrate the effectiveness of our approach using both 2-D and 3-D examples. Two examples show that the level set Markov chain approach can successfully match the production data and identify the connectivity of the channels in the reference model. The MCMC algorithms naturally provide multiple realizations of the permeability field conditioned to well and production data and thus, allow for uncertainty quantification in the forecasting.

In addition, we also exploit a different approach for history matching channelized reservoirs using Reversible Jump Markov Chain Monte Carlo (RJMCMC). In order to preserve large-scale continuity, the channelized permeability field is parameterized using the discrete cosine transform (DCT). The parameters representing the channel structure are the coefficients in the truncated frequency domain. The parameter space is searched using the RJMCMC method, whereby the dimension of the parameter space is flexible. For each step of the RJMCMC, the dimension of the uncertainty space can be increased or decreased according to a prescribed prior distribution. This flexibility in the parameter dimension allows an efficient search of the uncertainty space. Two-stage MCMC method was used to screen out the undesired proposals. After simulations, multi-dimensional scaling and cluster analysis were used to select realizations from the accepted models. The effectiveness of the RJMCMC algorithm is demonstrated using two examples involving water-flooding history matching. Both examples show that the proposed algorithm can update the large-scale features of the reference channelized permeability field conditioned to dynamic production information.

REFERENCES

Agarwal, R. G. 2010. Direct Method of Estimating Average Reservoir Pressure for Flowing Oil and Gas Wells. Paper SPE 135804 presented at SPE Annual Technical Conference and Exhibition, Florence, Italy, 19-22 September.

Al-Kobaisi, M., Ozkan, E., Kasogi, H., et al. 2006. Pressure Transient Analysis of Horizontal Wells with Transverse Finite-conductivity Fractures. PETSOC 2006-126 presented at Canadian International Petroleum Conference, Calgary, Alberta, 13-15 June.

Bello, R. O., Wattenbarger, R. A. 2010. Multi-stage Hydraulically Fractured Shale Gas Rate Transient Analysis. Paper SPE 126754 presented at SPE North Africa Technical Conference and Exhibition, Cairo, Egypt, 14-17 February.

Caers, J. K. and Zhang, T. 2004. Multiple-point Geostatistics: A Quantitative Vehicle for Integrating Geologic Analogs into Multiple Reservoir Models. *AAPG Memoir* **80**: 383-394.

Cameron, M., Sethian J. A. and Fomel, S. 2006. Seismic Velocity Estimation and Time to Depth Conversion of Time-migrated Images. Paper presented at SEG Annual Meeting, New Orleans, Louisiana, 1-6 October.

Caumon, G., Strebelle S., Caers J. K., et al. 2004. Assessment of Global Uncertainty for Early Appraisal of Hydrocarbon Fields. Paper SPE 89943 presented at SPE Annual Technical Conference and Exhibition, Houston, Texas, 26-29 September.

Chang, H., Zhang, D., and Lu, Z. 2010. History Matching of Facies Distribution with the

EnKF and Level Set Parameterization. *J. Comput. Phys.* **229** (20): 8011-8030.

Clarkson, C. R., Jordan, C. L., Ilk, D., et al. 2009. Production Data Analysis of Fractured and Horizontal CBM Wells. Paper SPE 125929 presented at SPE Eastern Regional Meeting, Charleston, West Virginia, 23-25 September.

Datta-Gupta, A. and King, M. J. 2007. *Streamline Simulation: Theory and Practice*. Richardson, Texas: Textbook Series, SPE.

Datta-Gupta, A., Xie, J., Gupta, N., et al. 2011. Radius of Investigation and Its Generalization to Unconventional Reservoirs. *Journal of Petroleum Technology*, **63** (7): 52-55.

Deng, X., and Horne, R. N. 1993. Well Test Analysis of Heterogeneous Reservoirs. Paper SPE 26458 presented at SPE Annual Technical Conference and Exhibition, Houston, Texas, 3-6 October.

Deutsch, C. V. and Tran, T. T. 2002. Fluvsim: A Program for Object-Based Stochastic Modeling of Fluvial Depositional Systems. *Computers & Geosciences* **28** (4): 525-535.

Deutsch, C. V. and Wang, L. 1996. Hierarchical Object-Based Stochastic Modeling of Fluvial Reservoirs. *Mathematical Geology* **28** (7): 857-880.

Dorn, O. and Villegas, R. 2008. History Matching of Petroleum Reservoirs Using a Level Set Technique. *Inverse Problems* **24** (3), 035015.

Dubrule, O. 1998. *Geostatistics in Petroleum Geology*. Tulsa, OK: Continuing Education Course Note Series, The American Association of Petroleum Geologists.

Egeland, T., Georgsen F., Knarud R., et al. 1993. Multifacies Modelling of Fluvial Reservoirs. Paper SPE 26502 presented at SPE Annual Technical Conference and Exhibition, Houston, Texas, 3-6 October.

Ehlig-Economides, C. A. 1992. Computation of Test Area of Investigation in Nonradial Geometries. Paper SPE 25020 presented at the European Petroleum Conference, Cannes, France, 16-18 November.

Freeman, C. M., Moridis, G., Ilk, D., et al. 2009. A Numerical Study of Performance for Tight Gas and Shale Gas Reservoir Systems. Paper SPE 124961 presented at SPE Annual Technical Conference and Exhibition, New Orleans, Louisiana, 4-7 October.

Green, P. J. 1995. Reversible Jump Markov Chain Monte Carlo Computation and Beyesian Model Determination. *Biometrika* **82** (4): 711-732.

Gringarten, A. C. 1984. Interpretation of Tests in Fissured and Multilayered Reservoirs With Double-Porosity Behavior: Theory and Practice. *Journal of Petroleum Technology* **36** (4): 549-564.

Gringarten, A. C. 2010. Practical Use of Well Test Deconvolution. Paper SPE 134534 presented at SPE Annual Technical Conference and Exhibition, Florence, Italy, 19-22 September.

Haldorsen, H. H. and Damsleth, E. 1990. Stochastic Modelling. *Journal of Petroleum Technology* **42** (4): 404-412.

Hastings, W. K. 1970. Monte Carlo Sampling Methods Using Markov Chains and Their Applications. *Biometrika* **57** (1): 97-109.

Holditch, S. A. 2006. Tight Gas Sands. *Journal of Petroleum Technology* **58** (6): 86-93.

Jafarpour, B. and McLaughlin, D. B. 2008. History Matching with an Ensemble Kalman Filter and Discrete Cosine Transform. *Computational Geosciences* **12** (2): 227-244.

Jafarpour, B. and McLaughlin, D. B. 2009. Reservoir Characterization with the Discrete Cosine Transform Part 1: Parameterization Part 2: History Matching. *SPE Journal* **14** (1): 182-201. SPE-106453-PA.

Jain, A. K. 1989. *Fundamentals of Digital Image Processing*, Englewood Cliffs, New Jersey: Information and System Sciences Series, Prentice Hall.

Kang, S., Datta-Gupta, A. and Lee, W. J. 2011. Impact of Natural Fractures in Drainage Volume Calculations and Optimal Well Placement in Tight Gas Reservoirs. Paper SPE 144338 presented at North American Unconventional Gas Conference and Exhibition, The Woodlands, Texas, 14-16 June.

Karlsen, K. H., Lie, K.-A. and Risebro, N. H. 2000. A Fast Marching Method for Reservoir Simulation. *Computational Geosciences* **4** (2): 185-206.

Karrenbach, M. 2000. Combining Eikonal Solutions with Full Wave Form Modeling. Paper presented at SEG Annual Meeting, Calgary, Alberta, 6-11 August.

Kim, J. U., Datta-Gupta, A., Brower, R. et al. 2009. Calibration of High-Resolution Reservoir Models using Transient Pressure Data. Paper SPE 124834 presented at SPE Annual Technical Conference and Exhibition, New Orleans, Louisiana, 4-7 October.

Kline, M. and Kay, I. W. 1965, *Electromagnetic Theory and Geometrical Optics*. New

York: Pure and Applied Mathematics series, John Wiley and Sons.

Koltermann, C.E. and Gorelick, S. M. 1996. Heterogeneity in Sedimentary Deposits: A Review of Structure-Imitating, Process-Imitating, and Descriptive Approaches. *Water Resour. Res.* **32** (9): 2617-2658.

Kuchuk, F. J. 2009. Radius of Investigation for Reservoir Estimation from Pressure Transient Well Tests. Paper SPE 120515 presented at SPE Middle East Oil and Gas Show and Conference, Bahrain, Bahrain, 15-18 March.

Lorentzen, R. J., Flornes, K. M., and Naevdal, G. 2012. History Matching Channelized Reservoirs Using the Ensemble Kalman Filter. *SPE Journal* **17** (1): 137-151. SPE-14020-PA.

Lee, W. J. 1982. *Well Testing*. Richardson, Texas: Textbook Series, SPE.

Lee, W. J. and Hopkins, C. W. 1994. Characterization of Tight Reservoirs. *Journal of Petroleum Technology* **46** (11): 956-964.

Lie, K.-A. and Juanes, R. 2005. A Front-tracking Method for the Simulation of Three-phase Flow in Porous Media. *Computational Geosciences* **9** (1): 29-59.

Ma, X., Al-Harbi, M., Datta-Gupta, A. et al. 2008. An Efficient Two-Stage Sampling Method for Uncertainty Quantification in History Matching Geological Models. *SPE Journal* **13** (1): 77-87. SPE-102476-PA.

Metropolis, N., Rosenbluth, A. W., Rosenbluth, M. N., et al. 1953. Equation of State Calculations by Fast Computing Machines. *J. Chem. Phys.* **21** (6): 1087-1092.

Mondal, A., Efendiev, Y., Mallick, B., et al. 2010. Bayesian Uncertainty Quantification for Flows in Heterogeneous Porous Media Using Reversible Jump Markov Chain

Monte Carlo Methods. *Advances in Water Resources* **33** (3): 241-256.

Moreno, D. L., Aanonsen, S. I., Evensen, G., et al. 2008. Channel Facies Estimation Based on Gaussian Perturbations in the EnKF. 11th European Conference on the Mathematics of Oil Recovery, Bergen, Norway, 08 September.

Nielsen, L. K., Li, H., Tai, X.-C., et al. 2009. Reservoir Description Using a Binary Level Set Model. *Computing and Visualization in Science* **13** (1): 41-58.

Nordbotten, J. M., Celia, M. A., and Bachu, S. 2004. Analytical Solutions for Leakage Rates through Abandoned Wells. *Water Resour. Res.* **40** (4), W04204.

Osher, S. J. and Fedkiw, R. P. 2002. *Level Set Methods and Dynamic Implicit Surfaces*. New York: Springer.

Osher, S. J. and Sethian, J. A. 1988. Fronts Propagating with Curvature-Dependent Speed: Algorithms Based on Hamilton-Jacobi Formulations. *J. Comput. Phys.* **79** (1): 12-49.

Popovici, A. M. and Sethian, J. A. 1998. Three-dimensional Travel-time Computation Using the Fast Marching Method. In *Mathematical Methods in Geophysical Imaging V: Proceedings of SPIE*, 20-21 July 1998, San Diego, California, ed. S. Hassanzadeh, Vol. 3453, 82-93. Bellingham, Washington: SPIE.

Prodanovic, M., Bryant, S. L. and Karpyn, Z. T. 2010. Investigating Matrix-Fracture Transfer via a Level Set Method for Drainage and Imbibition. *SPE Journal* **15** (1): 125-136. SPE-116110-PA.

Raghavan, R. 1993. *Well Test Analysis*. Englewood Cliffs, New Jersey: Petroleum Engineering series, Prentice Hall.

Remy, N., Boucher, A. and Wu, J. 2009. *Applied Geostatistics with SGeMS*. New York City: Cambridge University Press.

Scheidt, C. and Caers J. K. 2009. Representing Spatial Uncertainty Using Distances and Kernels. *Mathematical Geosciences* **41**(4): 397-419.

Sehbi, B. S., Kang, S. and Datta-Gupta, A. 2011. Optimizing Fracture Stages and Completions in Horizontal Wells in Tight Gas Reservoirs Using Drainage Volume Calculations. Paper SPE 144365 presented at North American Unconventional Gas Conference and Exhibition, The Woodlands, Texas, 14-16 June.

Sethian, J. A. 1999. *Level Set Methods and Fast Marching Methods*. New York City: Cambridge University Press.

Sethian, J. A. and Vladimirsky A. 2000. Fast methods for the Eikonal and related Hamilton-Jacobi Equations on Unstructured Meshes. *Proc. Natl. Acad. Sci. USA* **97** (11): 5699-5703.

Song B., Economides, M. J. and Ehlig-Economides, C. 2011. Design of Multiple Transverse Fracture Horizontal Wells in Shale Gas Reservoirs. Paper SPE 140555 presented at SPE Hydraulic Fracturing Technology Conference, The Woodlands, Texas, 24-26 January.

Strebelle, S. B. and Journel, A. G. 2001. Reservoir Modeling Using Multiple-Point Statistics. Paper SPE 71324 presented at the SPE Annual Technical Conference and Exhibition, New Orleans, Louisiana, 30 September-3 October.

Sun Y. and Fomel S. 1998. Fast-marching Eikonal Solver in the Tetragonal Coordinates.

Paper presented at SEG Annual Meeting, New Orleans, Louisiana, 13-18 September.

Vasco, D., Keers, H. and Karasaki, K. 2000. Estimation of Reservoir Properties using Transient Pressure Data: An Asymptotic Approach. *Water Resour. Res.* **36** (12): 3447-3465.

Virieux, J., Flores-Luna, C. and Gilbert, D. 1994. Asymptotic Theory for Diffusive Electromagnetic Imaging. *Geophysics J. Int.* **119** (3): 857-868.

Watanabe, S., Datta-Gupta A., Efendiev Y. R., et al. 2009. A Hybrid Ensemble Kalman Filter With Coarse Scale Constraint for Nonlinear Dynamics. Paper SPE 124826 presented at SPE Annual Technical Conference and Exhibition, New Orleans, Louisiana, 4-7 October.

Weber, K. J. 1982. Influence of Common Sedimentary Structures on Fluid Flow in Reservoir Models. *Journal of Petroleum Technology* **34** (3): 665-672.

Yin, J., Park, H. Y., Datta-Gupta, A., et al. 2010. A Hierarchical Streamline-Assisted History Matching Approach With Global and Local Parameter Updates. Paper SPE 132642 presented at SPE Western Regional Meeting, Anaheim, California, 27-29 May.

Yin, J., Xie, J., Datta-Gupta, A., et al. 2011. Improved Characterization and Performance Assessment of Shale Gas Wells by Integrating Stimulated Reservoir Volume and Production Data. Paper SPE 148969 presented at SPE Eastern Regional Meeting, Columbus, Ohio, 17-19 August.

VITA

Name: Jiang Xie

Address: TAMU Mailstop 3116
701 Richardson Building
College Station, Texas 77843

Email: jiang.xie@pe.tamu.edu

Education: Bachelor of Science, Polymer Science & Engineering
University of Science & Technology of China, Hefei, China
June 2005

Master of Science, Petroleum Engineering
Texas A&M University, College Station, Texas
December 2008

Doctor of Philosophy, Petroleum Engineering
Texas A&M University, College Station, Texas
August 2012